Thermal Modeling of Short Pulse Collimated Radiation in a Participating Medium

A THESIS SUBMITTED IN FULFILLMENT OF THE REQUIREMENT FOR THE DEGREE OF

Doctor of Philosophy

IN

MECHANICAL ENGINEERING

BY

BIRANCHI NARAYANA PADHI

National Institute of Technology, Rourkela-769008

Odisha, India

2012

Dedicated to

My

Parents

Dr. A K Satapathy
Associate Professor
Department of Mechanical Engineering
National Institute of Technology, Rourkela
Odisha, India

CERTIFICATE

Date:

This is to certify that the revised thesis entitled "***Thermal modeling short pulse collimated radiation in a participating medium"*** being submitted by Mr. Biranchi Narayana Padhi, bearing Roll No: 50703005, for the award of the degree of DOCTOR OF PHILOSOPHY of the National Institute of Technology, Rourkela, Odisha, is a record of bonafide research work carried out by him under my supervision. Mr. Biranchi Narayana Padhi has worked for more than four and half years on the above problem at the Department of Mechanical Engineering, National Institute of Technology, Rourkela and this has reached the standard fulfilling the requirements and the regulation relating to the degree. The results embodied in this thesis, in full or part, have not been submitted to any other University or Institution for the award of any degree or diploma.

Prof. A K Satapathy

ACKNOWLEDGEMENTS

That author is highly indebted to the thesis supervisor Dr. A. K. Satapathy, for his invaluable encouragement, helpful suggestions and supervision at the critical stage of this investigation. His willingness to devote time and attention amidst numerous responsibilities is gratefully acknowledged. Above all, his patience and optimistic attitude could lead to complete this work.

The author also wishes to express his gratitude to Dr. S. K. Mahapatra and Dr. P. Rath, Professor in Mechanical Engineering Department, I.I.T., Bhubaneswar for their unconditional support for many fruitful discussions that was held with them especially during the initial stages of this work, formulation of the problem and implementation of finite volume method.

Also thankful to all the faculty members and staff of Mechanical Engineering Department for their direct and indirect help in carry out this research work.

The author also expresses his gratitude for the loving support, cooperation and sacrifice that came from his better-half, junior Padhi and family.

Biranchi Narayana Padhi

ABSTRACT

In most traditional engineering applications, such as in the thermal analysis of boilers, furnaces, internal combustion engines, etc., as temporal variations in thermal quantities of interest are much slower than the time scale associated with the propagation of radiation, the transient term from the radiative transfer equation is usually neglected. The rapid progress in the field of short pulse laser in a participating medium has lead to some interesting applications such as materials processing, optical tomography, remote sensing, laser micro-surgery etc. The temporal radiative signals from a medium irradiated by short pulse lasers offer more useful information which reflects the internal structure and properties of the medium than that by the continuous light sources. The time scales of such applications are usually in the order of 10^{-12} to 10^{-15} seconds. Therefore, the consideration of the transient term in the radiation transport equation is necessary. To understand the physical phenomena involved in this complicated transport process, two cases are considered such as 1) one dimensional model and 2) a two dimensional model. The models assume a participating medium bounded by diffusely emitting and reflecting boundaries, one of the boundaries is irradiated with a short pulse laser beam. The gray wall assumption resembles more to the practical application as compared to the simplified assumption of black wall. Due to reflective characteristics of the gray boundary surface, the temporal spread changes significantly by the multiple reflections and partial transmissions at the surfaces, this draws attention to the present problem considered. The finite volume method is applied to solve the transient radiative transfer equation governing the above said physical phenomena. The fully implicit scheme is used to

discretize the transient term. In the proposed approach, one does not have to split the intensity into diffused and collimated part unlike the case with other existing methods like DTM, DOM, and REM etc. Intensity of radiation can directly be evaluated by solving the governing transient radiative transfer equation. The proposed methodology is compared with other existing methods. The effects of optical thickness, scattering albedo, emissivity, and linear anisotropic scattering on the transmitted and reflected signals are studied. The performance of two different spatial schemes: STEP and CLAM also have been tested. It is seen that the CLAM scheme yields results to a greater accuracy in case of two dimensional problems and, hence, correctly predicts the speed of photon whereas STEP scheme overpredicts the same.

Key words:

Transient radiative transfer, Short pulse laser, Finite volume method, STEP and CLAM.

CONTENTS

List of Figures

List of Tables

Nomenclature

a anisotropy factor

A area

c the speed of radiation intensity

D_{cx} direction cosine in x-direction

D_{cy} direction cosine in y-direction

D_{cz} direction cosine in z-direction

G irradiation

I radiation intensity

k absorption coefficient

$\hat{n}$ unit outward normal vector

q radiative heat flux

s distance

S source term in radiative transfer equation

t time

t_c cut-off period

t_p pulse width

V volume

x,y,z space coordinates

Greek symbols

Δt time step

ϕ azimuthal angle

Φ scattering phase function

Ω solid angle

β extinction coefficient

ε emissivity

θ polar angle

ρ reflectivity

σ_s scattering coefficient

τ optical thickness

ω scattering albedo

Ψ_T transmittance

Ψ_R reflectance

Superscripts

l and l' index for the discrete direction

* non-dimensional quantities

o value from previous time step

~ normalized value

Subscripts

b black body

c collimated

D downstream

f face

m modified

P node

P^* value from previous iteration

U	upstream
e, w, s, n	respective direction at face of the control volume
E, W, S, N	respective direction at node of the control volume

Abbreviations

CDM	Collapsed Dimension Method
CLAM	Curved Line Advection Method
CMCFVM	Combine Monte Carlo and Finite Volume Method
CVFEM	Control Volume Finite Element Method
DEA	Direct Exchange Area
DOM	Discrete Ordinates Method
DRESOR	Distribution of Ratios of Energy Scattered by the medium Or Reflected by the boundary surface
DTM	Discrete Transfer Method
FEM	Finite Element Method
FVM	Finite Volume Method
GEAM	Generalized Exchange Area Methods
LBM	Lattice Boltzmann Method
MCDM	Modified Collapsed Dimension Method
MCM	Monte Carlo Method
MDA	Modified Differential Approximation
MDTM	Modified Revised Discrete Transfer Method
MNDOM	Modified New Discrete Ordinates Method
RTE	Radiative Transfer Equation
RDTM	Revised Discrete Transfer Method

RDOM	Revised Discrete Ordinates Method
REM	Radiation Element Method
RMC	Reverse Monte Carlo method
TEA	Total Exchange Area

Chapter-1

Introduction

1.1. Back ground

Radiative heat transfer is an important mode in high-temperature systems. Thermal radiation is important in many engineering applications and its analysis is difficult in the presence of a participating medium because of absorption, emission and scattering. Thermal radiation being electromagnetic waves, propagates at the speed of light. In most traditional engineering applications, such as in the thermal analysis of boilers, furnaces, internal combustion engines etc., as temporal variations in thermal quantities of interest are much slower than the time scale associated with the propagation of thermal radiation, the transient term from the radiative transfer equation is neglected, i.e. radiation is assumed to be an instantaneous (steady-state) process.

The main objective of the present thesis is to study the energy transfer by means of radiation. Therefore, the basic phenomenology of radiative heat transfer has been studied. However, considering the nature of the equation that describes such energy transfer, this work is focused on the numerical methods which help taking radiation into account, for both transparent and participating media. For this purpose, Chapter 1 contains an introduction to radiative energy transfer, and the basic equations that govern radiative transfer are discussed. A discussion is also given on when this mode of energy transfer should be considered. In this chapter all of the magnitudes and concepts used throughout this work are also defined. It ends with a brief description of some approximate methods to take radiation into account. Here onwards the radiative energy transfer is referred as the variation of the energy of any system due to absorption or emission of electromagnetic waves. From a physical point of view, such electromagnetic waves can be understood as a group of massless particles that propagate at the speed of light. The

amount of energy carried by each of these particles is inversely proportional to the wavelength of its associated wave. Radiation heat transfer has been, probably, the last mode of energy transfer to be widely taken into account by the community of numerical scientists. The reason is mainly the complicated nature of the radiative transfer equation, which will be discussed later. This equation determines the intensity radiation field, a magnitude used to perform radiative energy balances over volumes and surfaces. In its general form, the radiative transfer equation involves both differentiation and integration, and therefore a complete solution is available only for a few simplified situations.

Plenty of tests have been performed to the numerical code that resulted from the elaboration of this thesis. Its results have been compared to other existing numerical methods, published in several specialized journals, or directly to available analytical solutions. According to the results obtained, the objectives proposed in this thesis have been satisfied. It is becoming possible to create and observe thermophysical phenomenon at increasingly shorter time scales due to the rapid progress in technology. One such phenomenon of interest is the propagation of light through a participating medium subjected to different boundary conditions.

The years passed, and the computers got faster and better. Different numerical methods to solve the radiative transfer equation were formulated. These include the Discrete Transfer Method, the Discrete Ordinates Method (DOM), and some of its variants, Finite Volume Methods, the REM^2 method, the Galerkin Finite element method, the Lattice Boltzmann Method (LBM); most recently researchers adapted the DRESOR method. These methods are all capable of handling radiation in transparent and participating gray media.

Chapter 1 Introduction

There has been an increased interest to create and observe thermophysical phenomenon at increasingly shorter time scale regime. One such phenomenon of interest, which is the topic of discussion of this work, is the propagation of light through a participating medium. In spite of achieving success in generating short pulse lasers, there exists a need to refine the models to analyze their propagation through scattering absorbing media. The transient radiative transfer equation is one approach to analyze such phenomenon.

Traditional engineering analysis of transport of thermal radiation, or photons through scattering media inevitably use the assumptions to simplify the transient term, such as the time derivative, in the transport analysis, even though radiation propagation vary significantly with time. This is valid for most of the engineering applications of thermal radiation because the imposed temporal variations are relatively slow when compared to those associated with the speed of propagation of radiation. With the creation of short pulse lasers and their rapid deployment in a variety of engineering applications, the traditional radiative transfer formulation cannot be used to analyze their propagation through a participating medium. In such applications the characteristic time of the problem is comparable to the characteristic length divided by the speed of light. For example, the speed of light in vacuum is 0.3 millimeter per picoseconds or 0.3 micrometer per femtosecond and therefore corresponding to the duration of a 1 picoseconds pulse the penetration distance is only 0.3 millimeter or for a 100 femtosecond pulse only 30 micrometer. The transient term in the radiative transfer usually neglected, is of the same order of magnitude as the spatial derivative in such situations, and must be considered.

Ultra-short pulsed lasers are used in many applications such as micro-machining, removal

of contaminated particles, ablation of polymers, remote sensing of the atmosphere, combustion chambers and other environments which involve interaction of the laser beam with scattering and absorbing particles of different sizes. Optical tomography is also an application of short pulse lasers interacting with scattering absorbing tissues which is of great scientific and engineering importance. This technology holds promise of providing the information, both physiological and morphological, about the living tissues and organs without any adverse side effects such as those associated with the X-rays. The advantages of the short pulse laser probing techniques over conventional very large pulse width (or steady state) radiation sources are primarily due to the additional information conveyed by the temporal variation of the observed signal. When conventional large pulse width sources are utilized in conjunction with detection at larger time scales compared to that of short pulse lasers, the information available is the magnitude of the net attenuation and the angular distribution of the transmitted or reflected signal. When the source is shut off, the measured signal vanishes virtually instantaneously in relation to the time scale of measurement. In contrast, for very short pulses the observed signal has a distinct temporal shape, and the shape is a function of the medium properties.

However, since an exact analytical solution to the highly nonlinear integro-differential radiative transfer equation (RTE) is nearly impossible to find, an efficient tool to deal with multi-dimensional radiative heat transfer is in strong demand to analyze various thermal problems. Numerical computations of radiation based on conventional methods such as the zonal method, the Monte Carlo method (MCM), etc. prove to be laborious and very time consuming. For this reason, numerous investigations are currently being carried out worldwide to assess computationally efficient methods. Treatment of radiative transport in the multidimensional geometry is difficult mainly because of the three extra

independent variables namely the polar angle, the azimuthal angle and the wavelength. Since there is no way out to get rid of the physical dimensions of the geometry and the wavelength of radiation, all numerical models, except the zonal method and the MCM, deal with different types of discretization schemes to make radiation less and less dependent on angular dimensions. The various methods differ primarily in the angular discretization schemes and the use of either the differential form or the integral form of the radiative transfer equation.

1.2. Radiative Heat Transfer

Radiative energy transfer is referred as the variation of the energy of any system due to absorption or emission of electromagnetic waves. From a physical point of view, such electromagnetic waves can be understood as a group of massless particles that propagate at the speed of light c. Each of these particles carries an amount of energy, inversely proportional to the wavelength of its associated wave. A single photon represents a plane wave; therefore we are forced to assume that it propagates along a straight path. Because of this, we can think of a system loosing energy by emitting a number of photons, or gaining energy by absorbing them. Each photon has a well-defined polarization state, an internal degree of freedom, which is important in calculating properties such as the fraction of incident energy that is reflected by a medium. However, thermal radiation is not polarized on average, and therefore the polarization of the photons is ignored hereinafter.

Radiation heat transfer presents a number of unique characteristics. First of all, the amount of radiative heat transfer does not depend on linear differences of temperature,

but on the difference of the fourth power of the temperature. This fact implies that, at high temperatures, radiative energy transfer should be taken into account, particularly if large differences in temperature exist. Furthermore, it is the only one form of energy transfer in vacuum.

The photon density is defined as the number of photons, with wavelength between λ and $\lambda + d\lambda$, crossing an area dA perpendicular to the photon direction $\hat{s}$, within a solid angle $d\Omega$, per unit time dt and per unit wavelength $d\lambda$. It is more useful to consider the energy density I instead of the photon density. The energy density is simply the number of photons multiplied by the energy of each photon. The energy density is usually named intensity radiation field, and its physical meaning is therefore

$$I(r,\hat{s},\lambda)=\frac{Energy\ of\ wavelength\,\lambda\ through\ an\ area\ normal\ to\,\hat{s}}{dA\,d\Omega\,d\lambda\,dt} \tag{1.1}$$

From this definition is clear that, for a fixed point and wavelength, the intensity radiation field is a function defined over the unit sphere, and therefore is not a conventional scalar field, such as the temperature. With the definition of the intensity radiation field on mind, the total energy that crosses a surface perpendicular to a given unit vector $\hat{n}$, per unit time and area, is readily obtained as

$$q(r,\hat{n})=\int_0^\infty d\,\lambda \int_{4\pi} d\Omega(\hat{n}\cdot\hat{s})I(r,\hat{s},\lambda) \tag{1.2}$$

where the $(\hat{n}.\hat{s})$ factor appears since I is defined as energy through the propagation direction $\hat{s}$.

1.3. Surface properties

Each surface will radiate a certain amount of energy due to its temperature. Such emitted energy, which will depend on the properties of the surface, its temperature, the radiation wavelength, the direction of emission, leads to the definition of the emissivity of a surface. As conventional, we can use the black body as a reference to define the surface properties of real bodies. Therefore, if the surface is at temperature *T*, the emissivity is defined as

$$\varepsilon = \frac{I_{emitted}(T, \lambda, \hat{s})}{I_b(T, \lambda)} \tag{1.3}$$

where the temperature, wavelength, and incident direction dependence, have been dropped for the sake of clarity. As the black body is defined as the perfect radiation absorber, by the Kirchhoff's law, there is no body capable of emitting more radiation energy than a black body for any given temperature. Therefore, the emissivity ε will be between zero and one. On the other hand, when an electromagnetic wave incidents on a surface, the interaction between this incident wave and the elements of the surface result on a fraction of the energy of the wave being reflected, while the remaining fraction will be absorbed (or transmitted) within the material. These fractions may very well depend on the incident angle and the wavelength of the original wave. Specifically, we can define

$$\rho = \frac{I_{reflected}}{I_{incoming}} \; ; \alpha = \frac{I_{absorbed}}{I_{incoming}} ; \; \tau = \frac{I_{transmitted}}{I_{incoming}} \tag{1.4}$$

again, the temperature, wavelength, and incident direction dependence, have been dropped. The coefficients ρ, α and τ are the reflectivity, absorptivity and transmissivity of

the surface respectively. As the wave is either reflected or absorbed or transmitted, it is clear that we must have $\rho + \alpha + \tau = 1$ if the energy is to be conserved.

1.4. Radiative Heat Transfer Equations

The equations governing the transport of radiant energy, boundary conditions, scattering phase function and other related quantities are as follows:

Radiative Transfer Equation (RTE)

The RTE for a gray medium can be written as

$$\frac{1}{c}\frac{\partial I(r,\hat{s},t)}{\partial t}+\frac{\partial I(r,\hat{s},t)}{\partial s}=-k(r)I(r,\hat{s},t)-\sigma_s(r)I(r,\hat{s},t)+k(r)I_b + \frac{\sigma_s(r)}{4\pi}\int_{4\pi} I(r,\hat{s}',t)\Phi(r,\hat{s}',\hat{s},t)d\Omega' \tag{1.5}$$

where $c = ds/dt$ is the speed with which the radiation intensity propagates.

$$\frac{1}{c}\frac{\partial I(r,\hat{s},t)}{\partial t}+\frac{\partial I(r,\hat{s},t)}{\partial s}=-\beta I(r,\hat{s},t)+k(r)I_b + \frac{\sigma_s(r)}{4\pi}\int_{4\pi} I(r,\hat{s}',t)\Phi(r,\hat{s}',\hat{s},t)d\Omega' \tag{1.6}$$

where the terms on the left hand side represents radiation intensity gradient with respect to time and space. On the right hand side, the first term indicates the attenuation of radiation intensity due to absorption in the direction of travel and outscattering from the direction of travel. The second and third term represent the augmentation part due to emission from the medium and inscattering from all other directions.

Boundary condition

The radiation intensity leaving an opaque diffuse surface contains emitted and reflected energy. This can be written as

$$I(r,\hat{s},t) = \varepsilon(r) I_b(r,t) + \frac{1-\varepsilon(r)}{\pi} \int_{\hat{s}'.\hat{n}\langle 0} I(r,\hat{s}',t)\left|\hat{s}'\cdot\hat{n}\right| d\Omega' \tag{1.7}$$

The above equation provides the boundary intensity for the RTE.

Scattering phase function

The scattering phase function Φ in the RTE describes how the radiation energy is scattered by a participating medium. Scattering can be classified into two categories such as isotropic and anisotropic scattering. Isotropic scattering indicates energy scattered equally into all directions whereas anisotropic scattering can be forward and backward scattering. Scattering phase function satisfy

$$\int_{4\pi} \Phi(\hat{s}',\hat{s}) d\Omega' = 4\pi \tag{1.8}$$

Radiation heat transfer relations

The total incident radiation is defined as

$$G(r,t) = \int I(r,\hat{s},t) d\Omega \tag{1.9}$$

The radiative heat flux in any direction *s* is defined as

$$q_s = \int_{2\pi} I(r,\hat{n},t)(\hat{n}\cdot\hat{s}) d\Omega \tag{1.10}$$

where $\hat{s}$ is the unit vector pointing in the *s* direction.

The divergence of the radiative heat flux is

$$\nabla.q = k\left[4\pi I_b(r,t) - G(r,t)\right] \tag{1.11}$$

In combined mode of heat transfer as well as in radiation dominated process, the divergence of radiative heat flux plays a vital role. In the absence of a heat source/sink, a system is in radiative equilibrium if other modes of heat transfer are negligible. Under such conditions $\nabla.q = 0$ and the temperature of the medium can be obtained from Eq. (1.11).

1.5. The Finite-Volume Method

The finite volume method for radiation heat transfer presented in the literature has formulated the discretization equation by integration over both spatial control volume and angular control (solid) angle. For the purpose of this discussion, spatial discretization is deferred and only angular discretization is considered. A typical control (solid) angle is shown in Fig. 1.1.

Integrating the RTE over a control angle (Fig. 1.1) gives

$$\int_{\Delta\Omega^l}\int_{\Delta V}\int_{\Delta t^*}\frac{\partial I^l}{\partial t^*}dt^*dV\,d\Omega + \frac{1}{\beta}\int_{\Delta\Omega^l}\int_{\Delta V}\int_{\Delta t^*}\frac{\partial I^l}{\partial s}dt^*dV\,d\Omega = \int_{\Delta\Omega^l}\int_{\Delta V}\int_{\Delta t^*}\left(-\beta_m^l I^l + S_m^l\right)dt^*dV\,d\Omega \tag{1.12}$$

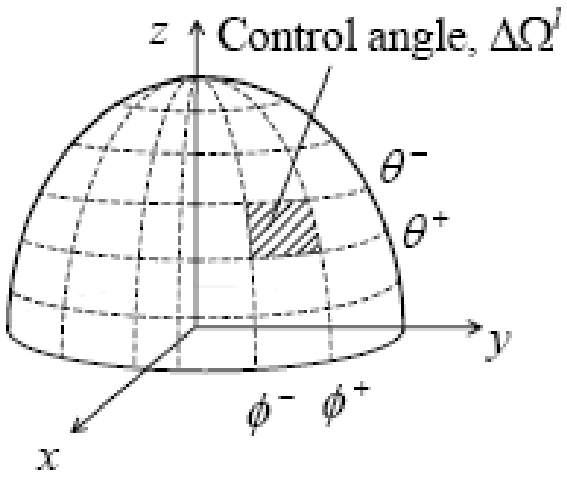

Fig.1.1 The control angle.

The discretization equation is formulated by integrating the RTE over a discrete solid angle. In the finite volume method, the magnitude of the radiant intensity is assumed to be uniform over a control angle. Radiation is allowed to travel in all directions within a solid angle.

1.6. Domain discretization

The numerical method described here is based on the control volume approach. Discretization equations are formulated by integrating the RTE over control volumes and control (solid) angles. Control volumes and control angles are subdivisions of the spatial and angular spaces respectively. The coordinate system is shown in Fig. 1.2. The next subsections describe these subdivisions.

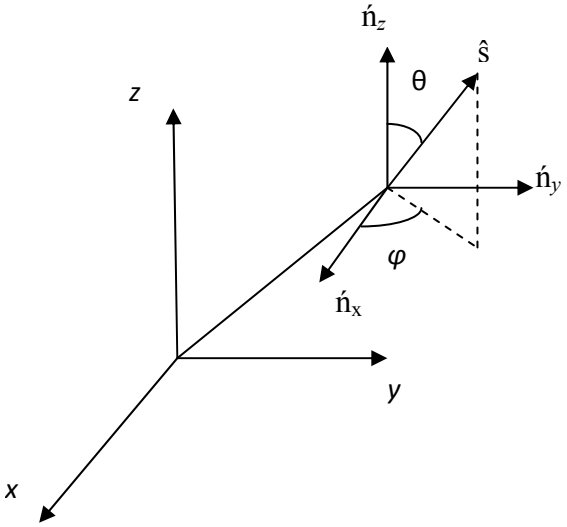

Fig.1.2 The coordinate system.

The control volume boundaries (dashed lines) are drawn first. Grid points are then placed at the geometric centers of the control volumes as represented in Fig. 1.3. Similar to the spatial discretization, the angular space is discretized by placing control (solid) angle boundaries throughout the 4π solid angle.

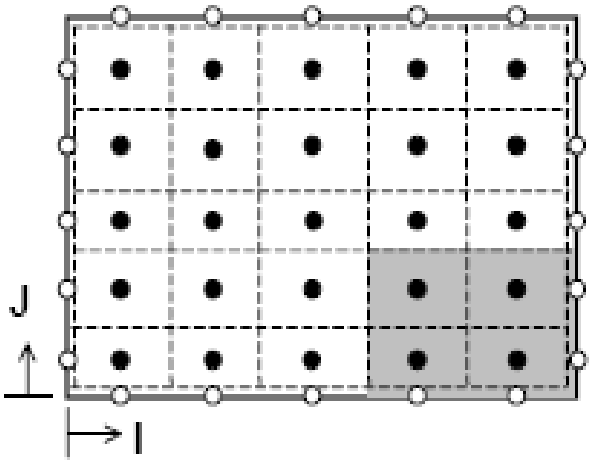

Fig.1.3 The control volume grid.

The simplest angular discretization is to divide the angular space into $N_\theta \times N_\phi$ control angles with equally spaced $\Delta\theta$ and $\Delta\phi$. The size of these control angles can be adjusted to capture the physics of the problem at hand. For example, collimated incidence can be

captured by designing a control angle with small $\Delta\theta$ and $\Delta\phi$. The finite volume discretization results in a set of algebraic equations with the radiant intensities as the unknowns. An iterative method is used to solve the resulting set of equations. Within each iteration, marching order can be employed to efficiently solve the set of equations.

1.7. Spatial differencing schemes

The STEP and CLAM schemes used in the discretization equations in the present work are presented in this section. Chai et al. (1994) presented a study on spatial differencing schemes for radiation heat transfer. The study indicates that control volume boundary intensity should be calculated by tracing a beam to an appropriate "upstream" location where the intensity is known or can be approximated. A few "more accurate" spatial differencing schemes are discussed in this section. Most "more accurate" spatial differencing schemes are formulated as the STEP scheme with additional source or sink terms. The additional source or sink terms can be negative. This can lead to negative intensities. Physically, intensity of radiation is an always-positive variable. Therefore, negative intensity may be physically unrealistic. The discretization equation should not allow the possibility of negative intensity as a solution. The always-positive variable treatment of Patankar (1991) can be used to eliminate this possibility.

Higher-order resolution schemes like the CLAM scheme express the dependent variable (the radiation intensity in the present case) at a cell face "f" as a function of its values at three neighboring grid nodes, two upstream and one downstream from the cell face. These are denoted by the subscripts U, C and D as shown in Fig. 1.4, and are referred to

as upstream, central and downstream grid nodes, respectively. Figure 1.4 represents two-dimensional control volumes for the sake of clarity.

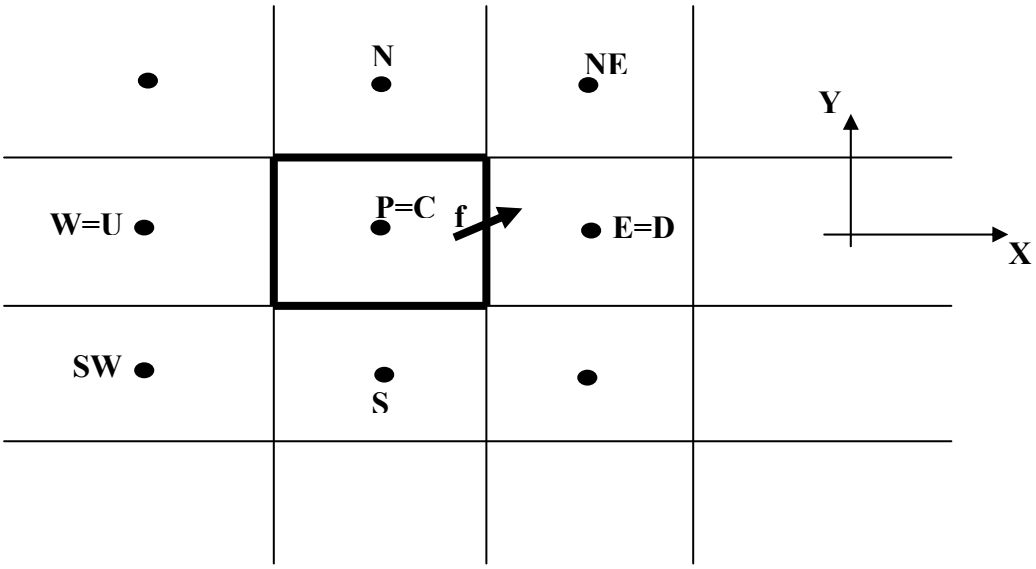

Fig.1.4 Typical control volume for CLAM scheme. The radiation intensity at the east cell face is computed from its values at upstream (U), central (C) and downstream (D) grid nodes in High order Resolution schemes.

According to this formulation, normalized radiation intensity $\tilde{I}$ and a normalized coordinate $\tilde{x}$ are defined as

$$\tilde{I}_f = \frac{\left(\tilde{x}_C^2 - \tilde{x}_f\right)}{\tilde{x}_C\left(\tilde{x}_C - 1\right)}\tilde{I}_C + \frac{\left(\tilde{x}_f - \tilde{x}_C\right)}{\tilde{x}_C\left(\tilde{x}_C - 1\right)}\tilde{I}_C^2 \qquad \text{for } 0 < \tilde{I}_C < 1 \qquad (1.13)$$

$$\tilde{I}_f = \tilde{I}_C \qquad \text{elsewhere} \qquad (1.14)$$

1.8. Objectives

With the advancement in technology and computational facilities available, the short pulse laser has made its way into many diversified field of engineering and bio-medical applications. A fundamental understanding of thermophysical phenomenon associated with the ultra short pulse laser transport is crucial for further advancement of the technology in different applications. The objective of the present work is to study the unique feature involved during the interaction of short pulse lasers with a participating medium. This work outlines the formulation of the transient radiative heat transfer through the participating media and discusses the need for developing methods for predicting and evaluating transient radiative transfer. The transient radiative transfer equation has been solved for one-dimensional and two dimensional problems to predict the transmitted flux and reflective flux of the medium. The time dependent reflection and transmission can be correlated to the optical properties of the medium. The complete transient radiative transfer equation is solved using finite volume method taking two different spatial differencing schemes: STEP and CLAM.

The significance of this research is that it examines the theoretical and numerical modeling of transient radiation transport of short pulse laser through an anisotropically scattering participating medium with diffusely reflecting boundaries.

Chapter-2

Literature Review

2.1. One-Dimensional Steady-State Problem

Kim et al. (1991) had applied the S-N discrete ordinates method to analyze radiative heat transfer in nongray gases. Spectral correlation between the terms in the equation of transfer was considered for black or nearly nonreflecting walls. Formulations to apply the S-N method using a narrow-band or the exponential wide-band model were presented. The computational speed of the gray-band approximation was obtained at the expense of accuracy in the internal fluxes and radiative source distributions. A new, normalized variable and space formulation (NVSF) methodology was developed by Darwish and Moukalled (1994), where spatial parameters were introduced so as to extend the applicability of the NVF methodology to non-uniformly discretized domains. Furthermore, the required conditions for accuracy and boundedness of convective schemes on nonuniform grids were also derived. Computational results show substantial improvement in accuracy when using the NVSF methodology with third-order high-resolution schemes. A thermal and optical one-dimensional numerical analysis of semi-transparent single and multilayer thin films on a transparent semi-infinite glass substrate, irradiated by a laser source, was presented by Bianco et al. (2001), using classical conductive Fourier hypothesis. Four different typical pulse shapes were compared at the same energy amount: a rectangular on-off shape, a symmetric triangular shape, a Gaussian shape, an asymmetric triangular Weibull profile. Altaç (2002) proposed the SK_N (Synthetic Kernel) approximation for solving radiative transfer problems in linearly anisotropically scattering homogeneous and inhomogeneous participating plane-parallel medium. The cause of the inaccuracies present in DOM for solving radiation transfer in

absorbing, emitting, anisotropically scattering hollow cylinders with reflecting boundaries with spatially varying absorption and scattering coefficients was identified and the correct solutions obtained using DOM S_6 were provided by Altaç (2002). A new explicit matrix relation for the calculation of the total exchange areas (TEA) in emitting, absorbing and anisotropically scattering semi-transparent medium bounded by emitting, absorbing and anisotropically reflecting walls had been established by Goyhénèche and Sacadura (2002).

A revised discrete ordinates method (RDOM) was developed by Liu et al. (2002) to overcome the normalized condition problem, in which a renormalizing factor was added into the numerical quadrature of inscattering term. The RDOM was used to solve the radiative transfer problem in one-dimensional anisotropically scattering media with complex phase function. The results show the RDOM can overcome the false scattering resulted from the numerical quadrature of in-scattering term and largely improve the accuracy of solution of the radiative transfer equation as compared to the CDOM. Mishra and Prasad (2002) extended the usage of the collapsed dimension method (CDM) for solving radiative heat transfer problems in an anisotropically scattering gray planar medium inside one-dimensional Cartesian enclosure. Modest(2003) discussed various implementations of the backward Monte Carlo method, allowing efficient Monte Carlo simulations for problems with arbitrary radiation sources, including small collimated beams, point sources, etc. in media of arbitrary optical thickness.

The ray tracing technique was used by Tan et al. (2003, 2004) to determine the radiative equilibrium temperature field as well as the temperature and heat flux fields of coupled radiation–conduction for two types of sinusoidal refractive index distributions. The

advantage of the method was that it only needs to disperse spatial position, but not the solid angle. According to analyzed results of linear and nonlinear scattering, they found that the ratio of two dimensionless heat fluxes with two different scattering phase functions was a monotone function of optical thickness. To avoid the complicated computation of ray trajectories, a finite element formulation was developed by Liu (2005). A general formulation of the discrete transfer method was provided to analyze radiative heat transfer problems in a participating medium subjected to collimated radiation by Sarma et al. (2005). Results were obtained for different angles of incidence of the collimated radiation. Analysis of radiative heat transfer in a plane-parallel participating medium subjected to diffuse and/or collimated radiation had been studied by Singh and Mishra (2007) using three popular methods in radiative heat transfer, viz. the discrete transfer method (DTM), the discrete ordinate method (DOM) and the finite volume method (FVM). They concluded that the FVM was computationally the most efficient. The DRESOR method was formulated by Cheng and Zhou (2007) to study the radiative heat transfer process in an isotropically scattering layer exposed to collimated radiation.

Several higher order resolution schemes were applied by Coelho and Aelenei (2008) to the spatial discretization of a hybrid finite volume/finite element method for the solution of the RTE in enclosures with a gray medium, and compared with the STEP scheme. The results revealed an interaction between spatial and angular discretization errors, and show that the higher order resolution schemes yield improved accuracy over the STEP scheme if the angular discretization error is small. The ultra spherical-polynomials approximation or the $P^{(\lambda)}_N$ method was obtained by Yilmazer and Kocar (2008) incorporating all approximations that employ ultraspherical polynomials into a unified form and was

applied to the radiative transfer problem in plane-parallel, absorbing, emitting, non-isothermal, gray medium with linearly anisotropic scattering. Jiang (2009) proposed a vector form of generalized exchange area methods (GEAM), which was found to be very efficient for handling the anisotropic scattering and reflection and also the computational time was decreased by an order as compared to that for computing isotropic radiation by conventional EAM.

2.2. One-Dimensional Transient Problem

Hasegawa et al. (1991) had analyzed the slabs contained either (i) two types of scattering particles in a solution or (ii) one type of particle with pigment added to the solution to trace the paths of the rays incident using the Monte Carlo method. Temporal analyses of the transmittance have illustrated that the differences in the optical density among the slabs having different absorption coefficients with the same scattering coefficient vary linearly with time. Also, their gradients have been shown to be proportional to the differences in the absorption coefficients, thus verifying the microscopic Beer-Lambert law in highly scattering media when temporally resolved measurement was used. The unsteady heat transfer characteristics in a semi-transparent liquid layer exposed to diffused and/or the collimated radiation was elucidated theoretically and experimentally by Itaya et al. (1985). A computational and experimental investigation was reported by Brewster and Yamda (1995) regarding the feasibility of determining optical properties of turbid media from picosecond (PS) time-resolved light scattering measurements in conjunction with diffusion theory predictions, Monte Carlo simulations and other appropriate optical measurements. The findings were verified using PS time-resolved

transmission measurements on aqueous latex particle suspensions. It was also found that the albedo criterion for application of diffusion theory to time-dependent scattering may be much less restrictive than is usually reported (weak absorption or albedo near one is not necessary).

The problem of estimating the optical signal for an oceanographic lidar was taken up by Mitra and Churnside (1999) and used the discrete ordinates method to obtain the time-dependent from the one-dimensional transient radiative transfer equation. Here the optical signal that was available to the receiver was calculated, rather than the receiver output, to reduce the number of parameters. The effects of albedo of a uniform water column were investigated. The effects of a school of fish in the water were also investigated for various school depths, thicknesses and densities. The attenuation of a lidar signal is found to be greater than the diffuse attenuation coefficient at low albedo and close to it at higher albedo. The presence of fish in the water was found to have a significant effect on the signal at low to moderate albedo, but not at higher albedo. Mitra and Kumar (1999) examined the transport of short light pulses through scattering–absorbing media through different approximate mathematical models. They predicted that optical signal characteristics are significantly influenced by the various models considered, such as P_N expansion, two-flux and discrete ordinates. Results of some of the models asymptotically approach those of direct numerical simulation if the order of approximation is increased. In this study they emphasized the importance of model selection in analyzing short-pulse laser applications such as optical tomography and remote sensing and highlight the parameters, such as wave speed, that must be examined before a model is adopted for analysis. The integral equation in terms of angle-distance integration was developed by Wu (2000) for transient radiative transfer in an absorbing and isotropically scattering

planar medium with pulse irradiation. The exact integral equation was solved by an adaptation of the quadrature method. Accurate results for the time-resolved hemispherical reflectivity and transmissivity of the slab were presented. An isotropic scaling formulation is evaluated for transient radiative transfer in a one-dimensional planar slab subject to collimated and/or diffuse irradiation by Guo and Kumar (2000). The Monte Carlo method was used to implement the equivalent scattering and exact simulations of the transient short-pulse radiation transport through forward and backward anisotropic scattering planar media. The scaled equivalent isotropic scattering results are compared with predictions of anisotropic scattering in various problems. They revealed that the equivalent isotropic scaling law is not appropriate for backward-scattering media in transient radiative transfer. Even for an optically diffuse medium, the differences in temporal transmittance and reflectance profiles between predictions of backward anisotropic scattering and equivalent isotropic scattering were large.

A time-dependent Monte Carlo method is developed for modeling the transient radiative transfer within absorbing and scattering media by Hsu (2001), Tan and Hsu (2001). The development was based on a rigorous analysis of the wave propagation process inside the participating media. The physical significance of their integral formulation was the consideration of the time-dependent domain of computation, which is different from the domain disturbed by radiation (i.e., the wave front envelope). The spatial and temporal incident radiation and radiative flux distributions were presented for different boundary conditions and for uniform and nonuniform property distribution. They had shown that the solutions of reflecting boundary condition exhibit distinctive behavior from that of the non-reflecting boundary. Wong et al. (2002) considered the most versatile MC approach in solving the RTE in a plane-parallel, absorbing and isotropically scattering medium

subjected to a collimated light source. The collimated light source was assumed to be an impulse function impinged instantaneously on the upper boundary of the medium. Time-dependent as well as steady-state cases are considered. Three FORTRAN codes were developed and compared in terms of speed of convergence and statistical accuracy. Wu and Ou (2002) had applied the modified differential approximation (MDA) and the modified $P_{1/3}$ approximation ($MP_{1/3}A$) as well to transient radiative transfer in a scattering planar medium exposed to collimated pulse irradiation. Their results show that the temporal distribution of the transmissivity obtained by the MDA contains a small protuberance or an abrupt slope change, which decreases with the decrease of the scattering albedo. They concluded that the results obtained by the $MP_{1/3}A$ were more accurate than those obtained by the MDA for most of the cases considered, because the $MP_{1/3}A$ corrects the propagation speed of the transmitted radiation.

In the last few decades, there has been an exponential growth in the research area of transient radiative transfer associated with the short pulse laser in participating media. Traditional analysis of radiation transfer usually neglects the transient effect of light propagation due to the large speed of light compared to the local time and length scales. With the rapid progress on ultrashort pulse laser, the transient radiative transfer in absorbing and scattering media has attracted increased attention. The temporal radiative signals from a medium irradiated by ultra short pulses offer more useful information which reflects the internal structure and properties of media than that by the continuous light sources. Chai (2003) presented a finite-volume method to calculate transient radiative transfer in an one-dimensional slab. The fully implicit scheme was used to discretize the transient term. The STEP and CLAM spatial differencing schemes were used in this study. The capabilities of the procedure were then examined using three

different test problems. In these test problems, one of the walls was subjected to a single-pulse collimated beam and a repeated-pulse collimated beam. The effects of the two spatial differencing schemes were discussed. Application of the discrete transfer method was extended to solve transient radiative transport problems with a participating medium. Rath et al. (2003) considered a one-dimensional gray planar absorbing and anisotropically scattering medium. The incident boundary of the medium was subjected to pulse-laser irradiation, while the other boundary was cold. Reverse or backward Monte Carlo (RMC) was considered by Lu and Hsu (2004) as an alternative approach as against the conventional (or forward) Monte Carlo method because of the long computational time it takes for the convergence when solutions are only needed at certain locations and time. It was shown that as tracking of the bundles that do not reach a particular detector was not needed, RMC method takes up much less computation time than the conventional MC method. In the situation where detailed information of radiative transport across the media is needed the RMC may not be appropriate. RMC algorithm is most suitable for diagnostic applications where inverse analysis was required, e.g. optical imaging and remote sensing. The results of non-emitting, absorbing and anisotropically scattering media subjected to an ultra short light pulse irradiation were compared with the forward Monte Carlo and discrete ordinates methods results.

Katika and Pilon (2006) presented the modified method of characteristics for simulating multidimensional transient radiative transfer in emitting, absorbing and scattering media. The method was based on the method of characteristics that follows photons along their path lines. The method makes use of a fixed set of points and, unlike the conventional method of characteristics, it follows the photons backward in space. It was concluded that the scheme is fast and was able to capture the sharp discontinuities associated with the

propagation of a radiation front in transient radiation transport. A general formulation of the governing transient radiative transfer equation applicable to a three-dimensional Cartesian enclosure has been presented by Mishra et al. (2006). To solve the transient radiative transfer equation, formulations had been presented for the three commonly used methods in the study of radiative heat transfer, viz. the discrete transfer method, the discrete ordinate method and the finite volume method. To show the uniformity in the formulations in the three methods, the intensity directions and the angular quadrature schemes for computing the incident radiation and heat flux had been taken the same. The problem of an absorbing and scattering planar layer irradiated with a square short-pulse laser having pulse-width of the order of a femtosecond was considered and the effects of the medium properties such as the extinction coefficient, the scattering albedo and the anisotropy factor and the laser properties such as the pulse-width and the angle of incidence on the transmittance and the reflectance signals had been studied for all the three methods. The discrete ordinate method was found to be computationally the most efficient method.

An et al. (2007) developed a finite element model, which is based on the discrete ordinates method and least-squares variational principle, to simulate short-pulse light radiative transfer in homogeneous and nonhomogeneous media. They concluded that the reflected signals can imply the break of optical properties profile and their location. Moreover, the investigation for uniqueness of temporal reflected and transmitted signals indicate that neither of these two kinds of signals can be solely taken as experimental measurements to predict the optical properties of medium. They should be measured simultaneously in the optical imaging application. Guo and Kumar (2007) formulated the radiation element method to solve transient radiative transfer with light radiation

propagation effect in participating media with inhomogeneous property. The sensitivity of the method against element size, ray emission number and time increment size was examined. The transient effect of radiation propagation is essential in short-pulse laser radiation transport when the input pulse width is not considerably larger than the system radiation propagation time. The transient characteristics of radiative transfer were investigated in the media subject to collimated laser irradiation and/or diffuse irradiation with temporal Gaussian and/or square profiles. From their study it was revealed that the inhomogeneous profile of extinction coefficient of the medium affects strongly the transient radiative flux divergence inside the medium. A discontinuous finite element method based on the discrete ordinates equation was extended by Liu and Liu (2007) to solve transient radiative transfer problems in absorbing, emitting and scattering media. The fully implicit scheme was used to discretize the transient term. By comparison, it was shown that the discontinuous finite element method is efficient, accurate, stable and can be used for solving transient radiative transfer problems in participating media. The continuity at interelement boundaries was relaxed in discontinuous finite element discretization, which makes the discontinuous finite element method able to predict the correct propagation speed within medium and accurately capture the sharp drop in the incident radiation and the radiative heat flux at the penetration front. Okutucu and Yener (2006), Okutucu and Yener (2007) and Okutucu et al. (2007) demonstrated the Laguerre–Galerkin method for the solution of radiative transfer in a one-dimensional absorbing and isotropically scattering medium with short-pulse irradiation on one of its boundaries. The time-dependent radiative intensity was expanded in a series of Laguerre polynomials with time as the argument. The transient transmittance and reflectance of the medium were evaluated for various values of the optical thickness, scattering albedo and pulse duration.

They concluded that the Laguerre–Galerkin method is not only easier to implement and more efficient but also yields more accurate results compared to the direct application of the Galerkin method. An assessment was made of the Galerkin technique as an effective method of solution for transient radiative transfer problems in participating media.

2.3. Two-Dimensional Steady-State Problem

The integral equation for radiative transfer in a two-dimensional rectangular scattering medium exposed to diffuse radiation was solved numerically by Crosbie and Schrenker (1984) removing the singularity. This method yielded accurate results except at very large optical thicknesses. A method was presented for extending these results to the problem of a strongly anisotropic scattering phase function which was made up of a spike in the forward direction superimposed on an isotropic phase function. Radiative heat transfer in a two dimensional rectangular enclosure with gray medium and internal heat generation was solved by generating a point allocation technique in which unknown temperature profiles were expressed as polynomials. Analytical solutions were developed in the optically thin limit. Both the optical thickness and the enclosure geometry are demonstrated to have strong effects on the temperature distribution within the medium (Yuen and Ho, 1985). The differential approximation was extended by Condiff (1987) to account for anisotropic scattering in invariant three-dimensional form. Radiative heat transfer in two-dimensional enclosures was studied by Kim and Lee (1988) using the S-N discrete ordinates method. They concluded that phase function anisotropy plays a significant role in the radiation heat transfer when the boundary condition is nonsymmetrical, but it is not important for symmetric environments. Using optical

interaction coefficients typical of mammalian soft tissues in the red and near infrared regions of the spectrum, calculations of fluence-depth distributions, effective penetration depths and diffuse reflectance from two models of radiative transfer, diffusion theory and Monte Carlo simulation were compared by Flock et al. (1989) for a semi-infinite medium. The predictions from diffusion theory are shown to be increasingly inaccurate as the albedo tends to zero and/or the average cosine of scatter tends to unity. Kim and Lee (1990) found that the isotropic scaling approximation predicted accurately the radiative flux and the average incident radiation for the isothermal emission problem and for most diffuse incidence problems. For the collimated incidence problem, the isotropic scaling solutions were acceptable only for weakly scattering media. For large scattering albedo the error in the isotropic scaling was appreciable for the diffuse incidence problem and unacceptably large for the collimated incidence problem. Liu et al. (1992) used the P_1-approximation method, along with the Eddington phase function approximation, to study radiative heat transfer in absorbing-emitting-scattering media. It was established that the asymmetry factor of the scattering phase function plays an important role in radiative transfer.

Chui et al. (1992) initially shown that the finite volume method can be implemented to solve three-dimensional radiation problems in cylindrical enclosures. The medium considered was participating and both isotropic and nonisotropic scattering were included. For the special case of axisymmetric radiation, a mapping is described that yields a complete solution by solving the intensity in a single azimuthal direction. The method was seen to rapidly converge to the solution of the radiation transfer equation as the spatial and directional grid was refined. Results from the solution of axisymmetric bench mark problems show that the method was stable, accurate and computationally

efficient. Chai et al. (1994a and 1994b) presented a finite volume method which can be used to model transparent, absorbing-emitting and anisotropically scattering media. They also demonstrated a procedure to capture collimated beam. Wu and Wu (1997) applied the integral equation method to study radiative transfer in a two-dimensional cylindrical medium exposed to collimated radiation. To overcome the wiggling behavior of FVM , Baek et al. (2000) proposed a combined procedure of the Monte Carlo and finite volume method (CMCFVM) for solving radiative heat transfer with an isolated boundary heat source. The CMCFVM was later on extended to two-dimensional irregular geometry by Byun (2004). The radiative heat transfer in a complex two-dimensional enclosure with obstacles with participating medium was investigated by Kim et al. (2001) and they derived the finite-volume method (FVM) for radiation using the unstructured grid system. A general discretization equation was formulated by introducing the directional weight and the STEP scheme for spatial differencing. Also it was revealed that the wiggling behavior occurring in the blocked-off FVM was not produced by the unstructured FVM. The ray effects of the finite volume method (FVM) or discrete ordinates method (DOM) were known to show the non-physical oscillations usually observed in the solution of radiative heat transfer on a boundary. This wiggling behavior was caused by the finite discretization of the continuous control angle.

Radiative heat transfer in a finite axisymmetrical cylindrical enclosure exposed to collimated radiation was solved by a novel method by Hsu et al. (1999). Integrated intensity and radiative heat flux were presented in homogeneous and nonhomogeneous scattering media exposed to both uniform and Gaussian distributions of normal collimated incident radiation. The effects of aspect ratio, different incident radiation and anisotropic scattering phase function as well as nonhomogeneous property distribution

were discussed. In order to eliminate the ray effect, an adaptive angular quadrature scheme was described and applied.

The radiation element method by ray emission method, REM^2, had been formulated by Guo and Maruyama (2001) to predict radiative heat transfer in three-dimensional arbitrary participating media with nongray and anisotropically scattering properties surrounded by opaque surfaces. As a numerical example, the method was applied to predict radiative heat transfer in a boiler model with nonisothermal combustion gas and carbon particles and diffuse surface wall. Elsasser narrow-band model as well as exponential wide-band model was adopted to consider the spectral character of CO_2 and H_2O gases. Sakami et al. (2001) extended the modified discrete ordinates method to analyze absorbing, emitting and isotropically or anisotropically scattering media within an enclosure of arbitrary geometry. Results confirmed that the proposed method was a good general remedy for anomalies caused by the ray effect due to the geometry. Thomson et al. (2001) developed an adaptive and scalable alternative to the finite element and finite volume methods to solve the steady multi-dimensional radiative transport equation.

Effect of scattering on radiative heat transfer in two- dimensional rectangular media was studied by Jinbo et al. (2003) using the finite-volume method. Furthermore, relative errors caused by the approximation that linear and nonlinear anisotropic scattering media was simplified to isotropic scattering media also studied. Joseph et al. (2003) extended a structured radiative heat transfer code based on the standard discrete ordinates method to unstructured meshes in order to be coupled with a CFD code. The code had been specially written for unstructured grids using tetrahedrical cells, by trying to avoid complex

adaptations that were time consuming. The mesh influence was studied for different cases. A complete genuinely multidimensional discretization in two-dimensional discrete ordinates method was formulated by Ismail (2004) to solve radiative heat transfer in a rectangular enclosure composed of diffusely emitting and reflecting boundaries and containing homogeneous media that absorbs, emits and scatters radiation.

Radiative integral transfer equations for a rectangular participating and isotropically scattering inhomogeneous medium are solved numerically for the incident energy and the net partial heat fluxes using the method of ‘‘subtraction of singularity’’. All the relevant single (surface integrals) and double integrals (volume integrals) are carried out analytically by Altaç and Tekkalmaz (2004) to reduce the computation time and numerical integration errors. The resulting systems of linear equations are solved iteratively. A benchmark problem was chosen as a rectangular inhomogeneous cold participating medium which is subject to externally uniform diffuse radiation on the bottom surface. Solutions for linearly and quadratically varying scattering albedos are provided. Trivic et al. (2004) developed a new mathematical model based on the coupling of (i) finite volume method for the solution of radiative transfer equation with (ii) Mie equations for the evaluation of scattering phase function for radiative heat transfer of particulate media with anisotropic scattering for two-dimensional rectangular enclosure. The new model was applied to the solid particles of coal and ash and a series of two-dimensional predictions are performed. The effects of particle size parameter and of scattering albedo on radiative heat flux and on incident radiation were analyzed. It was found that the model developed is reliable and very accurate and thus suitable for extension towards: (i) three-dimensional geometries, (ii) mixtures of non-gray gases with particles as well as for (iii) incorporation in computational fluid dynamics codes.

An et al. (2005) proposed a finite element method (FEM) for simulation of radiative heat transfer in absorbing, emitting and anisotropic scattering media. This simulation was developed on the basis of discrete ordinates method and finite element theory. Unstructured triangular element grids were employed in spatial discretization while azimuthal discretization strategy was used in the angular discretization. Two efficient iterative solvers were employed to solve the sparse equations of FEM. Some typical two-dimensional problems are used to verify the method. A two-dimensional scheme using the finite-volume method was proposed to solve the radiative transfer equation for axisymmetric radiative transfer by Tian and Chiu (2005).

Kowsary and Mahan (2006) presented an exact analytical method for determination of emissive as well as absorptive performance of spherical cavities having diffuse-specular reflective walls. The method presented utilizes a novel coordinate transformation technique, which provides convenient means for setting up the governing radiant exchange integral equations. These equations were then solved by the usual iterative method devised for the Fredholm integral equation of the second kind. The suggested coordinate transformation was also utilized for determination of directional absorptivity of a fully specular spherical cavity when collimated radiation enters through its mouth from a specified direction. Pourshaghaghy et al. (2006) attempted an inverse radiative design problem in which the objective was to determine the spatial distribution of heat source strengths which produces a desired temperature and heat flux distribution on the design surface. The furnace whose walls are diffuse-gray is assumed to be filled with an absorbing, emitting and scattering medium. Radiative heat flux calculations are accomplished by means of the modified discrete transfer method (MDTM) using the correction factors. For inverse design calculations the Conjugate Gradient Method (CGM)

is employed, in which the sensitivity coefficients were defined and used as needed by the algorithm.

A blocked-off region procedure was implemented with the collapsed dimension method (CDM) to deal with radiative transport problems in irregular geometries by Talukdar (2006). He concluded that, it is an alternative than to write an algorithm in curvilinear coordinate for irregular geometries which found to be complicated for a ray-tracing method like the CDM. Mishra et al. (2006) proposed the MCDM, where the time consuming procedures of ray tracing and source term evaluation are not required, as a result of which the method becomes computationally efficient. For the same level of accuracy, MCDM has been found faster than the CDM and the DOM.

Hassanzadeh and Raithby (2008) had applied the finite-volume method to the second-order radiative transfer equation, to study its accuracy and solution cost for two simple two-dimensional problems. The second-order equation leads to results that were accurate and bounded, but the iterative solution of the equations was expensive, especially for weakly participating media. The high cost was mainly due to the elliptic character of the second-order equation and the lack of diagonal dominance of the algebraic equations. Ferretti (2010) introduced the wavelet function which makes it possible to study the radiative transfer through a nongray medium with an arbitrary distribution of the absorption coefficient.

Coelho and Carvalho (1997) examined the non-conservative behavior of the discrete transfer method and a conservative formulation was proposed and evaluated. Coelho (2002) refined the two main shortcomings, namely ray effects and numerical smearing

from which the discrete ordinates method for the solution of the radiative heat transfer equation suffers, applying bounded and skewed high-order resolution schemes (CLAM, MUSCL and SMART). Calculations were performed for two and three-dimensional enclosures with transparent, emitting–absorbing and emitting, absorbing, scattering media. One of the walls of the enclosure was hot, while the others were cold. The results demonstrated that the bounded high-order schemes were more accurate, regardless of the radiative properties of the medium. A drawback of the skewed schemes is their higher computational requirements, associated with an increased number of iterations required for convergence. Coelho (2004) proposed a new version of discrete ordinates method to overcome the same shortcomings and concluded that the modified new DOM (MNDOM) yields accurate solutions even for coarse spatial and angular discretizations. Coelho and Aelenei (2008) applied several higher order resolution schemes to the spatial discretization of a hybrid finite volume/finite element method for the solution of the RTE in enclosures with a gray medium and compared with the STEP scheme. They revealed that an interaction between spatial and angular discretization errors and shown that the higher order resolution schemes yield improved accuracy over the STEP scheme if the angular discretization error was small.

2.4. Two-Dimensional Transient Problem

Flock et al. (1989) experimentally measured the fluence-depth distributions and the diffuse reflectance of 633 nm light in liquid media with optical properties similar to soft tissues. Except at extremely high albedo, the experimental data and the Monte Carlo results agree well for the depth dependence of the fluence as a function of incident light

beam diameter and optical absorption and scattering, and for the dependence of the diffuse reflectance on the albedo. The absolute experimental values for the fluence must be renormalized by a factor which varies with the albedo in order to match the model values, and the possible sources of this discrepancy were discussed. A mathematical description of light propagation in terms of radiative transfer was developed by Patterson et al. (1991). The application of the two-flux and diffusion models to tissue optics was discussed in some detail. Mitra et al. (1997) formulated two-dimensional transient radiation transport through a scattering–absorbing medium. The P_1 approximation in a Cartesian coordinate system was invoked to simplify the transient radiative transfer equation. A boundary-driven radiative problem was considered in which the radiation intensities at some areas on a surface were modeled as boundary conditions and maintained at constant values in all angular directions. Pfefer et al. (2000) investigated the effects of laser irradiation with a wavelength of 532 nm and pulse duration of 10 ms on whole blood in vitro. The progression of effects with increasing radiant exposure from evaporation to coagulation-induced light scattering to aggregated coagulum formation to ablation was described. The Monte Carlo technique was used by Guo et al. (2000) to simulate the two-dimensional transient radiative heat transfer in scattering and absorbing media. The influences of medium dimensions, anisotropic scattering characteristics, incident pulse width and spatial and temporal Gaussian distributions, and the effect of Fresnel reflection resulting from refractive index changes at the boundaries were discussed. It was found that the temporal distribution shape and spread of the predicted transmissivity and reflectivity were significantly influenced by the incident pulse width and the dimensions of the media. Forward scattering increases the magnitude of maximum transmissivity and reduces the transmitted pulse width. Neglecting the

boundary reflection resulted in overestimated transmissivity and reflectivity and shortens the transmitted pulse width. The discrete-ordinates method was formulated by Guo and Kumar (2001) to solve transient radiative transfer with the incorporation of a transient term in the transfer equation in two-dimensional rectangular enclosures containing absorbing, emitting and anisotropically scattering media subject to diffuse and/or collimated laser irradiation. Short-pulsed laser interaction and propagation in a turbid medium with high scattering albedo were studied. The imaging of an inhomogeneous zone inside a turbid medium was demonstrated. Wu (2001) analyzed the transient radiative transfer in a two-dimensional finite cylindrical medium with collimated pulse irradiation and a large mean free path for scattering. Highly accurate solutions of integral equation for transient radiative transfer revealed that the radiative energy of the medium core was less than the radiative energy of the medium boundary, after the attenuated pulse irradiation had passed through the medium. It was found that influence of the decrease rate of radiative energy with the passage of time was larger than that of the extinction decay of the radiative intensity along a propagation path for transient radiative transfer in a two- dimensional medium with large mean free path for scattering. It is also concluded that the scattering coefficient and geometric size were the major factors determining the spatial distribution type of scattered radiation energy at large time and the temporal evolution of the spatial distribution type of radiation energy.

The time-dependent discrete ordinates method was used with the higher order upwind piecewise parabolic interpolation scheme to analyze the ultra-short light pulse propagation in an anisotropically scattering rectangular medium by Sakami (2002). Tzou et al. (2002) extended the hot-electron blasting model to describe the ultrafast deformation in thin metal films during the sub-picosecond to picosecond domain. Method

of lines is used to solve the coupled field equations describing ultrafast deformation in the picosecond domain. Beck et al. (2003) in their investigations showed that spatially resolved diffuse reflectance in combination with total diffuse remission provides a valuable method to determine tissue optical properties in vivo. Li and Kumar (2003) developed the discrete ordinate method to incorporate transient radiation heat transfer in tissue welding and soldering with use of ultrafast lasers. The tissue was assumed to be an axially symmetric cylinder. The temporal distribution of radiative energy inside the tissue as well as the radiative heat flux along the tissue surface was obtained. Comparisons were performed between laser welding and laser soldering. The use of solder was found to substantially enhance the radiation energy absorption in upper solder-stained tissue region but the surface radiative heat flux. A detailed formulation of the radiative transport problem using the finite volume method and discrete ordinate method was presented by Chai and Rath (2003).

Chai (2004) presented a finite volume method to calculate transient radiative transfer in two-dimensional irregularly shaped enclosures. The fully implicit scheme was used to discretize the transient term. The STEP and CLAM spatial differencing schemes were used in this study. Trivedi et al. (2005) used a time-resolved technique to detect tumors/inhomogeneities in tissues by measuring transmitted and reflected scattered temporal optical signals when a short pulse laser source is incident on tissue phantoms. An et al. (2006) developed a finite element model, which is based on the discrete ordinates method and least-square variational principle, to simulate the transient radiative transfer in absorbing and scattering media. A discontinuous finite element method based on the discrete ordinates equation was extended by Liu and Liu (2007) to solve transient radiative transfer problems in absorbing, emitting and scattering media. They concluded

that the discontinuous finite element method was efficient, accurate, stable and can be used for solving transient radiative transfer problems in participating media. Because the continuity at interelement boundaries was relaxed in discontinuous finite element discretization, field variable considered was discontinuous across the element boundaries. This feature makes the discontinuous finite element method able to predict the correct propagation speed within medium and accurately capture the sharp drop in the incident radiation and the radiative heat flux at the penetration front.

The transport of a train of short-pulse radiation through a two-dimensional rectangular participating medium consisting of local inhomogeneities was investigated by Muthukumaran and Mishra (2008). Heat flux distributions inside the participating medium containing square shaped local inhomogeneity were studied using the finite-volume method with a collimated beam of step temporal profile and of multiple pulses. For many clinical light applications, such as photodynamic therapy (PDT), the therapeutic effect strongly depends on the light dose in a certain tissue depth. A measure for the attenuation and penetration of light in tissue is the optical penetration depth, which is derived from the tissue's optical properties at a certain wavelength. Therefore, in vivo measurements to determine the optical properties were performed of the bladder wall and brain tissue on patients undergoing photodynamic therapy. The tip of a 400 μm bare fiber was placed in contact with the investigated tissue, either during open surgery (brain) or through the working channel of a cystoscope (bladder wall). Light of the wavelengths 420-450 nm, 532 nm, and 635 nm was coupled alternately into the fiber. The diffuse backscattered light was detected, spatially resolved by means of a CCD camera. Additionally, the total diffuse reflectance of the tissue site was determined, by relating the white light spectra remitted from the tissue to that of a reflectance standard. These two

independent measurements were fitted with Monte Carlo simulations. Thus, the reduced scattering and absorption coefficient could be obtained and the optical penetration depth was derived. Jaunich et al. (2008) analyzed the temperature distributions and heat affected zone in skin tissue medium when irradiated with either a collimated or a focused laser beam from a short pulse laser source. Experiments were performed on multi-layer tissue phantoms simulating skin tissue with embedded inhomogeneities simulating subsurface tumors and as well as on freshly excised mouse skin tissue samples. Two types of lasers have been used in this study – namely a Q-switched pulsed 1064 nm Nd:YAG short pulse laser having a pulse width of 200 ns and a 1552 nm diode short pulsed laser having a pulse width of 1.3 ps. The experimental measurements demonstrated that converging laser beam focused directly at the subsurface location can produce desired high temperature at that location compared to that produced by collimated laser beam for the same laser parameters. Finally the ablated tissue removal was characterized using histological studies as a function of laser parameters.

Jiao and Guo (2009) developed a time-dependent thermal interaction in a skin tissue cylinder subjected to the irradiation of a train of short laser pulses. The ultrafast radiation heat transfer of the focused beam was simulated by the transient discrete ordinates method. The numerical scattering caused by spatial discretization in finite volume method was addressed by Zhang and Tan (2009). They had considered different numerical schemes based on an analysis of the generation process of numerical scattering. The integral equation formulation for transient radiative transfer in two-dimensional cylindrical non-homogeneous absorbing and linearly anisotropically scattering media with collimated pulse irradiation was presented by Wu and Wu (2010). The integral equations were solved by the quadrature method. The effects of spatially variable

properties on transient radiative transfer were investigated for various optical sizes and extinction coefficient distributions.

2.5. Three-Dimensional Problem

Henson and Malalasekera (1997) presented the modified formulations of the discrete transfer and Monte Carlo methods for the prediction of radiative heat transfer in three-dimensional nonhomogeneous participating media. They found that the average deviation between the two methods is less than 1.2% for both the boundary surface flux and the divergence of radiative flux or gas emissive power within the enclosed, isotropically scattering media. Maruyama and Aihara (1997) analysed the radiation heat transfer between absorbing, emitting and scattering media and specular surfaces with arbitrary three-dimensional configurations, using the Radiation Element Method by Ray Emission Model (REM^2). Guo and Maruyama (1999) investigated the radiative heat transfer in three-dimensional nonhomogeneous participating medium using REM^2 method. The anisotropic scattering phase function was dealt with the scaling technique based on delta function approximation. Radiative heat transfer in three-dimensional inhomogeneous, non-gray and anisotropically scattering participating media was investigated by using REM. The ray effects and the influences of radiation element division and spectral discretisation were examined by Guo (2000).

The finite-volume method (FVM) and the discrete ordinate method (DOM) are implemented by Kim and Huh (1999), to assess their capability to predict radiative heat transfer in a three-dimensional enclosure. They concluded that the FVM performs better than the DOM in optically thin media, while they show comparable accuracy in optically

thick media. Cha and Song (2000) applied the DOIM in a general grid system in three-dimensional problems. They had shown that the DOIM is a potential powerful tool for radiation analysis. A new angular discretisation scheme was presented by Kim (2000) known as FT_n of the finite volume method in three dimensional radiative transfer. The FT_n FVM was applied to absorbing, emitting and anisotropically scattering media with variable optical thickness in a rectangular enclosure. They concluded that the FTn FVM performs better than the discrete ordinate method (DOM) and the FVM with N × N uniform angular discretisation except near the optically thick diffusion limit.

A three-dimensional Monte Carlo simulation of transient radiative transfer is performed by Guo (2002) for short pulse laser transport in scattering and absorbing media. The refractive index of the scattering particles was found to strongly influence the prediction of transmitted pulse shape. The temporal shape of the transmittance was very weakly influenced by the output detector angle for a diffuse medium. Scaled isotropic scattering modeling was shown to be insufficient in transient three-dimensional radiative transfer for early times. Tan (2002) studied the transient radiative transfer by an integral equation model in a rectangular volume with absorbing and isotropic scattering medium. Diffuse irradiation enters at one boundary surface and the other five boundaries were cold and black surfaces. The spatial and temporal distributions of the integrated intensity and radiative flux were presented for different radiative property distributions.

Jeong et al. (2003) examined the tumor cells which were more sensitive to temperature increase than normal tissue. They used a combination of an 805-nm laser and in-situ indocyanine green (ICG) solutions in treating rat tumors. Multiple beams were also used to irradiate the tumor. They observed that when the tumor was free of ICG, the

temperature increase of the tumor was less significant under the laser irradiation with a power density of 0.33 W/cm^2; tumor tissue at a depth of 1 cm only experienced a 7°C increase in temperature. However, when the tumor contained ICG solution, the temperature at 1-cm depth experienced more than 15°C-temperature increase. Furthermore, when one fiber was used, the edge of the tumor experienced less impact by the laser beam, while multiple beams resulted in an almost uniform temperature increase over the entire tumor. Joseph et al. (2003) extended a structured radiative heat transfer code based on the standard discrete ordinates method to unstructured meshes in order to be coupled with a CFD code. The mesh influence was studied for different cases. Cui and Li (2005) presented a discontinuous finite element method for the numerical solution of internal thermal radiation problems in three-dimensional (3D) geometries using an unstructured mesh of mixed elements. Different domain discretization methods were presented and a new angular space discretization was also given. Liu et al. (2003) shown that when the open boundary locates in the high-temperature zone and the temperature gradient is large, the error resulted from the open boundary to be treated as a black wall with local temperature may be very large and cannot be omitted. In order to get the reasonable numerical results, the open boundary needs to be set up far from the interesting zone more than 1.0 optical thickness if the open boundary of computational domain is treated as a black wall with local temperature.

Talukdar et al. (2005) implemented the finite volume method of radiation in non-orthogonal curvilinear coordinates for complex three-dimensional problems in order to use it for combined heat transfer problems in connection with CFD codes and also to handle irregular structure with a body-fitted structured grid. They considered both radiative and non-radiative equilibrium situations along with an absorbing, emitting and

scattering medium. Talukdar et al. (2007) extended the application of block structured grid with the finite volume method (FVM) to conduction and radiation heat transfer in cylindrical enclosures. Results of temperature, radiative heat flux and total heat flux distributions were presented for different optical thicknesses, scattering albedos, emissivities and conduction–radiation parameters. A three-dimensional algorithm for the treatment of radiative heat transfer in emitting, absorbing and scattering media was developed by Grissa et al. (2007). The approach was based on the utilization of control volume finite element method (CVFEM) which was applied for the first time to 3D radiative heat transfer in participating media.

A two-step procedure for the computation of radiative heat transfer with anisotropic scattering and reflection was presented by Jiang (2008). It was shown that the method gives more accurate solution than the isotropic scaling for the heat transfer in anisotropically scattering media. An original model and code for three-dimensional radiation of anisotropically scattering gray media was developed by Trivic and Amon (2008) where radiative transfer equation (RTE) was solved by finite volume method (FVM) and scattering phase function (SPF) was defined by Mie Equations (ME). The effects of scattering albedo and wall reflectivity on the radiative heat flux were presented. It was found that the developed three-dimensional model, where FVM was coupled with ME, was reliable and accurate. An efficient numerical inverse radiation analysis based on

the backward Monte Carlo (BMC) method was presented by Wang et al. (2008) to determine the three-dimensional temperature distribution in a large rectangular enclosure containing the participating medium, using radiative intensities in the visible range received by charge-coupled device (CCD) cameras.

From the exhaustive literature survey, it is revealed that the radiative heat transfer equation has been considered as the governing equation for a numerous situations. Many engineering applications in which the participating medium is assumed to be subjected to steady radiation and walls of the enclosures are black. In the last few decades with the progress in technology, there is an exponential growth in the research area of transient radiative transfer with the interaction of short pulse laser in participating media. The commonly used methods to solve the transient radiative transfer equation, to cite a few are like MC method, Integral equation solution, REM, DTM, DOM, FEM and FVM etc. But it is found that the majority of them are based on the most simplified assumption of black wall, whereas the reflective wall assumption resembles more to the practical applications. When the boundary surface becomes reflective, then the temporal spread changes significantly by the multiple reflections and partial transmissions at the surfaces. Hence the motive behind the study is to focus on the unique features of the situation when a short pulse laser interacts with a participating medium bounded by reflective boundaries. Different optical properties related to tissues are available in Jaunich et al. (2008). They conducted experimental work on multi-layer tissue phantoms simulating skin tissue with embedded inhomogeneities simulating subsurface tumors and as well as on freshly excised mouse skin tissue samples. If the bio-medical applications are considered, then the medium will be more scattering than absorbing. Therefore, in the present work, the variations in optical properties are considered in a wide range so as to be applicable for different engineering applications.

Chapter-3

One-dimensional Problem Formulation

3.1. One-Dimensional Problem Formulation

The physical case under consideration is a one dimensional anisotropically scattering and absorbing medium of length L having azimuthal symmetry and constant properties (Fig.3.1a). The equation of transient radiative transfer in the case considered may be expressed as (Modest, 2003)

$$\frac{1}{c}\frac{\partial I^l}{\partial t}+\frac{\partial I^l}{\partial s}=-kI^l-\sigma_s I^l+kI_b+\frac{\sigma_s}{4\pi}\int_{4\pi} I^{l'}\Phi(l'\rightarrow l)d\Omega^{l'} \tag{3.1}$$

The first two terms on the right hand side, which are negative, accounts for the decrease in the intensity of radiation in the given direction, either because it is absorbed by the medium (with an absorption coefficient k) or because it is scattered onto another direction (with a scattering coefficient σ_s). The third term has positive sign, therefore implying an increase in the intensity of radiation. This term is due to thermal emission from the medium. It is zero only if the temperature is zero, or the absorption coefficient is zero. It may be noticed that the proportionality coefficient is the same absorption coefficient appearing in the first term. This holds under the assumption of local thermodynamic equilibrium (see, for instance, Modest (2003) section 9.2). The fourth term on right hand side contributes only if the medium scatters radiation. We should take into account that any photon, propagating along a direction given by *l'*, may be redirected to the analyzed direction *l*. We define the function $\Phi(l',l)$ to be 4π times the probability of such redirection occurring. Then we integrate to consider all possible directions *l'*. The

function $\Phi(l',l)$ is known as the scattering phase function. It has to be normalized, in a way that

$$\int_{4\pi} \Phi\left(\hat{s}^{l'},\hat{s}^{l}\right)d\Omega^{l'} = 4\pi \tag{3.2}$$

where this time the phase function is integrated over the second argument. This equation merely states that the incoming photon should be scattered into some other direction.

However, the interaction between radiation and matter is more complicated than that, and it is indeed possible for a scattered photon to vary its energy. This can be taken into account by allowing the phase function to depend on the incoming and outgoing photon wavelengths. The usual approximation for problems related to heat transfer is to consider elastic scattering that is, to take a phase function of the form used in Eq. (3.1), thus ignoring the energy change of a scattered photon. Moreover, it is assumed that the phase function depends only on the relative orientation of the two directions *l* and *l'*, that is, of the scalar product $\left(\hat{s}^{l'}\cdot\hat{s}^{l}\right)=\cos\theta$.

The scattering phase function can be represented as a series in terms of Legendre's polynomial as follows:

$$\Phi\left(\hat{s}',\hat{s}\right)=1+\sum_{m=1}^{M} a_m P_m\left(\hat{s}'\cdot s\right) \tag{3.3}$$

For linear anisotropic condition $M = 1$, hence, the above equation becomes

$$\Phi\left(\hat{s}',\hat{s}\right)=1+a_1 P_1\left(\hat{s}'\cdot\hat{s}\right)=1+a_1\left(\hat{s}'\cdot\hat{s}\right) \tag{3.4}$$

since, $P_1\left(\hat{s}'\cdot\hat{s}\right)=\left(\hat{s}'\cdot\hat{s}\right)$.

Therefore, linear anisotropic scattering the phase function for 1-D problem can be expressed as follows

$$\Phi\left(\hat{s}^{l'} \to \hat{s}^{l}\right) = 1 + a\cos\theta^{l}\cos\theta^{l'} \tag{3.5}$$

The average scattering phase function is given by

$$\Phi^{l'l} = \frac{\int_{\Delta\Omega^{l'}} \Phi\left(\hat{s}' \cdot \hat{s}\right) d\Omega^{l'}}{\Delta\Omega^{l'}} \tag{3.6}$$

Now substituting the value from Eq. (3.4) and integrating, we get

$$\Phi^{l'l} = \frac{\Delta\Omega^{l'} + \frac{a\cos\theta}{4}\left(\cos 2\theta_1' - \cos 2\theta_2'\right)}{\Delta\Omega^{l'}} \tag{3.7}$$

The radiation intensity leaving a gray surface that emits and reflects energy diffusely, can be written as

$$I^{l} = \varepsilon I_b + \frac{1-\varepsilon}{\pi} \int_{\hat{s}'.\hat{n}<0} I^{l'} \left|\hat{s}' \cdot \hat{n}\right| d\Omega^{l'} \tag{3.8}$$

Equation (3.8) provides the boundary intensity for the TRTE. The first term on the right side represents the thermal contribution of the surface. This term may depend on the outgoing direction through the emissivity coefficient. The second term takes into account the diffuse contribution of the reflected intensity and hence all incoming directions should be considered. This is why the integral is carried out over the incoming directions to the surface. This boundary equation works only for directions such that $\left(\hat{s}' \cdot \hat{n}\right) > 0$.

The north boundary at $z = L$ as shown in Fig.3.1 (a) is irradiated normally with a short-pulse laser beam. The radiation intensity incident on the boundary for a square pulse or a Gaussian pulse with finite temporal width can be expressed as follows.

Square pulse (Fig.3.1 (b)):

$$I(L,\Omega_c,t) = q_c \times \left[H(t) - H(t-t_p)\right]\delta(\theta-\theta_0)\delta(\phi-\phi_0) \tag{3.9}$$

where δ is the Dirac delta function and H(t) is the Heaviside function.

Gaussian pulse (Fig.3.1 (c)):

$$I(L,\Omega_c,t) = q_c \times \exp\left[-4\ln 2\left(\frac{t-t_c}{t_p}\right)^2\right]\delta(\theta-\theta_0)\delta(\phi-\phi_0) \qquad 0 < t < 2t_c \tag{3.10}$$

$$I(L,\Omega_c,t) = 0 \qquad t \geq 2t_c \tag{3.11}$$

The temporal pulse shape described in Eqs. (3.10) and (3.11) is a truncated Gaussian distribution with the maximum at $t = t_c$ and the half maximum at $t = t_c \pm t_p/2$. The factor 4 ln 2 is required in Eq. (3.10) to ensure that $I(0, \theta, t_c \pm t_p/2) = q_c \delta(\theta-\theta_0)/2$, as required by the definition of the full-width at half-maximum (FWHM) t_p for the pulse shape.

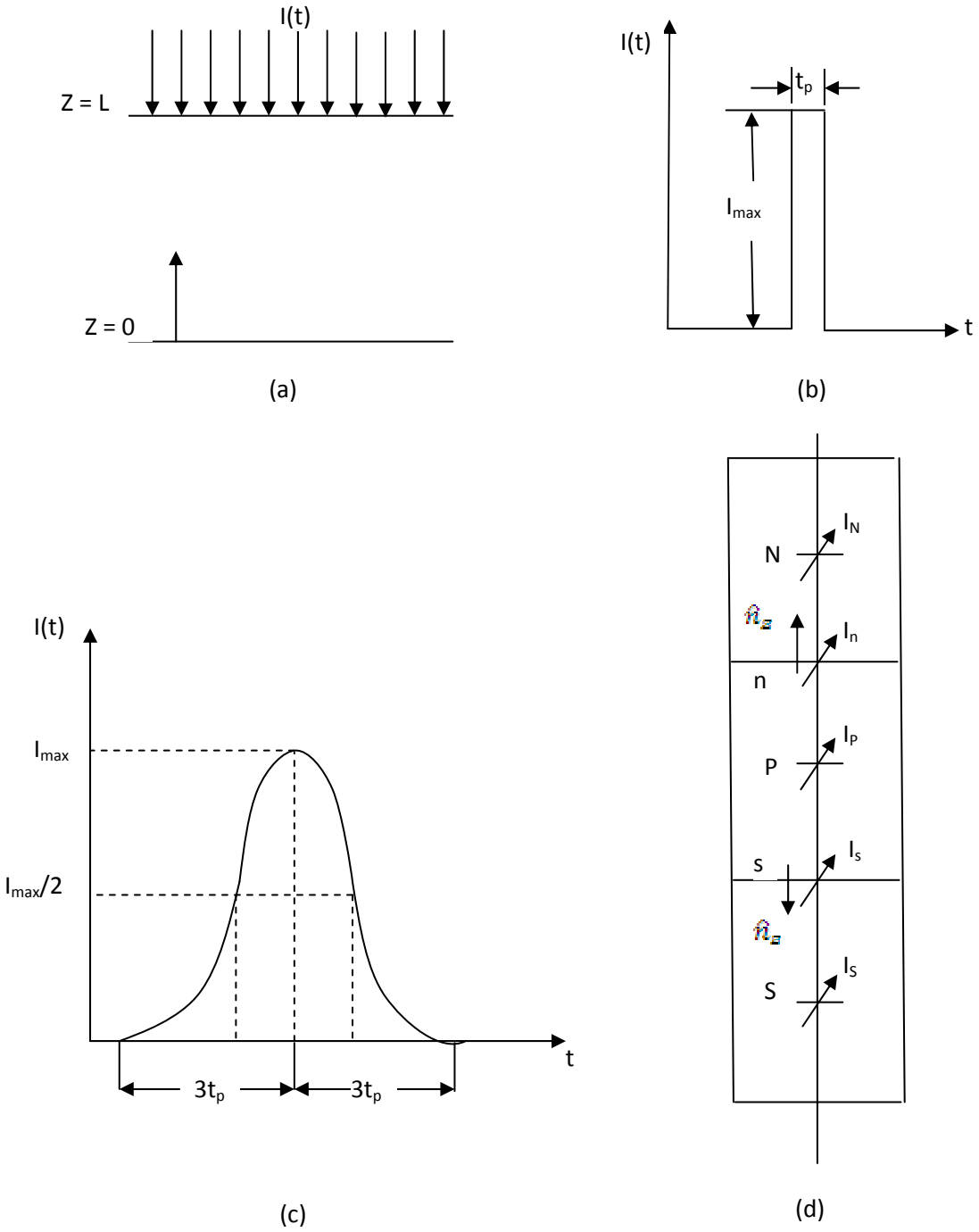

Fig.3.1 (a) Computational Domain (b) Square profile (c) Gaussian Profile (d) Control Volume.

The radiative transfer equation is sometimes written by changing the geometrical length variable l by the optical depth (or thickness) τ, defined by $d\tau = \beta\, ds$, where $\beta = k + \sigma_s$ is the extinction coefficient. The optical thickness is defined in a differential fashion, since the extinction coefficient may depend on l, for instance for a non-isothermal medium. The use of the non-dimensional optical depth is useful, since approximations to the RTE exist for the limits of large or small optical thickness. On the other hand, a large absorption coefficient is meaningless until the size of the domain under consideration is given. In the terms of these variables, the RTE becomes

$$\frac{1}{\beta c}\frac{\partial I^l}{\partial t}+\frac{1}{\beta}\frac{\partial I^l}{\partial s}=-I^l+(1-\omega)I_b+\frac{\omega}{4\pi}\sum_{l'=l}^{M}I^l\Phi^{l'l}\Delta\Omega^{l'} \tag{3.12}$$

where $\omega = \sigma_s / \beta$ is known as the scattering albedo, a measure of the relative significance of absorption and scattering. Here the optical thickness is dimensionless and therefore the above equation can be thought as being non-dimensional.

3.2. Formulation of the Discretization Equation

Equation (3.1) in non-dimensional form can be written with linear anisotropy as

$$\frac{1}{\beta c}\frac{\partial I^l}{\partial t}+\frac{1}{\beta}\frac{\partial I^l}{\partial s}=-I^l+(1-\omega)I_b+\frac{\omega}{4\pi}\sum_{l'=l}^{M}I^l\Phi^{l'l}\Delta\Omega^{l'} \tag{3.13}$$

Now the linearised TRTE can be written as, $\frac{1}{\beta c}\frac{\partial I^l}{\partial t}+\frac{1}{\beta}\frac{\partial I^l}{\partial s}=-\beta_m^l I^l+S_m^l$ (3.14)

where the modified extinction coefficient is

$$\beta_m^l = 1 - \frac{\omega}{4\pi} a \cos\theta^l \cos\theta^l \Delta\Omega^l - \frac{\omega}{4\pi}\Delta\Omega^l \tag{3.15}$$

and the modified source function is

$$S_m^l = (1-\omega) I_b + \left\{ \frac{\omega}{4\pi} \sum_{\substack{l'=1 \\ l' \neq l}}^{M} I^{l'} \Delta\Omega^{l'} + a\cos\theta \sum_{\substack{l'=1 \\ l' \neq l}}^{M} I^{l'} \cos\theta^{l'} \Delta\Omega^{l'} \right\} \tag{3.16}$$

Upon integration over a typical one-dimensional control volume and a control angle within a specified time step, the TRTE becomes

$$\int_{\Delta\Omega^l} \int_{\Delta V} \int_{\Delta t^*} \frac{\partial I^l}{\partial t^*} dt^* dV\, d\Omega + \frac{1}{\beta} \int_{\Delta\Omega^l} \int_{\Delta V} \int_{\Delta t^*} \frac{\partial I^l}{\partial s} dt^* dV\, d\Omega = \int_{\Delta\Omega^l} \int_{\Delta V} \int_{\Delta t^*} \left(-\beta_m^l I^l + S_m^l \right) dt^* dV\, d\Omega \tag{3.17}$$

Applying divergence theorem to the 2nd term on the left hand side of Eq. (3.17) the TRTE simplifies to

$$\begin{aligned} \int_{\Delta\Omega^l} \int_{\Delta V} \int_{\Delta t^*} \frac{\partial I^l}{\partial t^*} dt^* dV\, d\Omega \; + \; \frac{1}{\beta} \int_{\Delta\Omega^l} \int_{\Delta t^*} \int_{\Delta A} I^l \left(s^l \cdot \hat{n} \right) dA dt^* d\Omega \\ = \int_{\Delta\Omega^l} \int_{\Delta V} \int_{\Delta t^*} \left(-\beta_m^l I^l + S_m^l \right) dt^* dV\, d\Omega \end{aligned} \tag{3.18}$$

where $\hat{n}$ is the unit outward normal vector. The first term in the left hand side represents the change of radiation intensity with time; the second term represents the inflow and outflow of radiant energy across the faces of the control volume. The term on the right side accounts for the attenuation and augmentation of energy within a control volume and control angle. In the finite volume method, the magnitude of intensity is assumed to be

constant over the control volume and a control angle. Under these assumptions and using the fully-implicit scheme, Eq. (3.18) can be written as

$$\left(I_P^l - I_P^{l0}\right)\Delta V\Delta\Omega^l + \frac{1}{\beta}\sum_{i=1}^{4} I_i^l \Delta A_i \Delta t^* \int_{\Delta\Omega^l}\left(\hat{s}\cdot\hat{n}\right)d\Omega^l = \left(-\beta_m^l I_P^l + S_m^l\right)\Delta V\Delta\Omega^l\Delta t^* \tag{3.19}$$

where I_P^{l0} and I_P^l are the nodal intensities at the start and at the end of the time step respectively. On further simplification, for a control volume and a control angle, Eq. (3.19) becomes

$$\frac{\left(I_P^l - I_P^{l0}\right)\Delta V\Delta\Omega^l}{\Delta t^*} + \frac{\left(I_n^l - I_s^l\right)\Delta A_z D_{cz}^l}{\beta} = \left(-\beta_{m,P}^l I_P^l + S_{m,P}^l\right)\Delta V\Delta\Omega^l \tag{3.20}$$

where, $D_{czn}^l = \int\left(\hat{s}\cdot\hat{n}_z\right)d\Omega^l = -D_{czs}^l = D_{cz}^l$, $\Delta\Omega^l = \int_{\Delta\Omega'} d\Omega$, $\Delta A_{zn} = \Delta A_{zs}$.

To relate the boundary intensities to the nodal intensities, two spatial difference schemes: STEP and CLAM are used.

3.3. Formulation using STEP scheme

In the STEP (first order) or upwind scheme the downstream boundary intensities are set equal to the upstream nodal intensities (Fig.3.1 (d)).

$$I_n^l = I_P^l \ , \ I_s^l = I_S^l \tag{3.21}$$

Applying the STEP scheme, Eq. (3.20) becomes

$$\left[\frac{\Delta A_z D_{cz}^l}{\beta}+\beta_{m,P}^l \Delta V \Delta\Omega^l+\frac{\Delta V \Delta\Omega^l}{\Delta t^*}\right] I_P^l=\left(\frac{\Delta V \Delta\Omega^l}{\Delta t^*}\right) I_P^{l0} + \frac{\Delta A_z D_{cz}^l I_S^l}{\beta}+S_{m,P}^l \Delta V \Delta\Omega^l \tag{3.22}$$

The standard form of the discretization equation in control volume formulation is

$$a_P I_P = a_P^0 I_P^0 + \sum a_{nb} I_{nb} + b \tag{3.23}$$

So the final discretization equation for the nodal intensities for the $D_{cz}^l > 0$ conditions can be written as

$$a_P^l I_P^l = a_P^{l0} I_P^{l0} + a_S^l I_S^l + b^l \tag{3.24}$$

where, $a_P^{l0}=\dfrac{\Delta V \Delta\Omega^l}{\Delta t^*}$, $a_S^l=\dfrac{\Delta A_z D_{cz}^l}{\beta}$, $a_P^l=\left[\dfrac{\Delta A_z D_{cz}^l}{\beta}+\beta_{mP}^l \Delta V \Delta\Omega^l+\dfrac{\Delta V \Delta\Omega^l}{\Delta t^*}\right]$

$$b^l = S_{mP}^l \Delta V \Delta\Omega^l$$

3.4. Formulation using CLAM scheme

Higher order (Second order) resolution CLAM (Coelho, 2002) scheme expresses the dependent variables (the radiative intensity in the present case) at a cell face "f" as a function of its values present at three neighboring grid nodes (two upstream and one downstream) from the cell face. In the present problem the relations are as follows:

For the north face (Fig.3.1d)

$$\tilde{I}_n = \frac{\left(\tilde{z}_P^2 - \tilde{z}_n\right)}{\tilde{z}_P\left(\tilde{z}_P - 1\right)}\tilde{I}_P + \frac{\left(\tilde{z}_n - \tilde{z}_P\right)}{\tilde{z}_P\left(\tilde{z}_P - 1\right)}\tilde{I}_P^2 \tag{3.25}$$

$$I_n = I_P + S_{Cn^+} + S_{Pn^+} I_P \tag{3.26}$$

$$\text{where, } \tilde{z}_P = \frac{z_P - z_S}{z_N - z_S} = 0.5\,,\ \tilde{z}_n = \frac{z_n - z_S}{z_N - z_S} = 0.75 \tag{3.27}$$

$$S_{Cn^+} = I_N\left(\frac{I_P - I_S}{I_N - I_S}\right),\ S_{Pn^+} = -\left(\frac{I_P - I_S}{I_N - I_S}\right) \tag{3.28}$$

For the south face,

$$\tilde{I}_s = \frac{\left(\tilde{z}_S^2 - \tilde{z}_s\right)}{\tilde{z}_S\left(\tilde{z}_S - 1\right)}\tilde{I}_S + \frac{\left(\tilde{z}_s - \tilde{z}_S\right)}{\tilde{z}_S\left(\tilde{z}_S - 1\right)}\tilde{I}_S^2 \tag{3.29}$$

$$I_s = I_S + S_{Cs^+} + S_{Ps^+} I_P \tag{3.30}$$

where

$$\tilde{z}_S = \frac{z_S - z_{SS}}{z_P - z_{SS}} = 0.5\ ,\ S_{Cs^+} = -I_S\left(\frac{I_S - I_{SS}}{I_P - I_{SS}}\right) \tag{3.31}$$

$$\tilde{z}_s = \frac{z_s - z_{SS}}{z_P - z_{SS}} = 0.75\ ,\ S_{Ps^+} = \left(\frac{I_S - I_{SS}}{I_P - I_{SS}}\right) \tag{3.32}$$

After substituting the boundary intensities in terms of nodal intensities, we may end up with negative intensity which is physically not acceptable. To avoid such unrealistic

situation during the iteration procedure an overall positive variable treatment mentioned in Patankar (1991) is adopted. After the treatment, the discretization equation becomes

$$\left[\left[D_{cz}+D_{cz}\left(\frac{S_{cn^+}-S_{cs^+}}{I^l_{P^*}}\right)\right]\times\left(\frac{1}{\beta}\right)+\beta_m\Delta V\Delta\Omega+\frac{\Delta V\Delta\Omega}{\Delta t^*}\right]I^l_P=D_{cz}\left(\frac{I_S}{\beta}\right)- D_{cz}\left(S_{Pn^+}-S_{Ps^+}\right)I^l_{P^*}+S_{mP}\Delta V\Delta\Omega+\frac{\Delta V\Delta\Omega}{\Delta t^*}I^{lo}_P \tag{3.33}$$

where $I^l_{P^*}$ is the intensity in a given direction 'l' at a node point 'P' from the previous iteration. Gauss-Seidel iterative method is used to solve the resulting set of algebraic equations with the radiation intensities as the unknowns within each time step. The solution process adopts a marching procedure to solve the set of algebraic equations. All computations are carried out using the code generated using MS FORTRAN 90.

3.5. Algorithm FLOW CHART

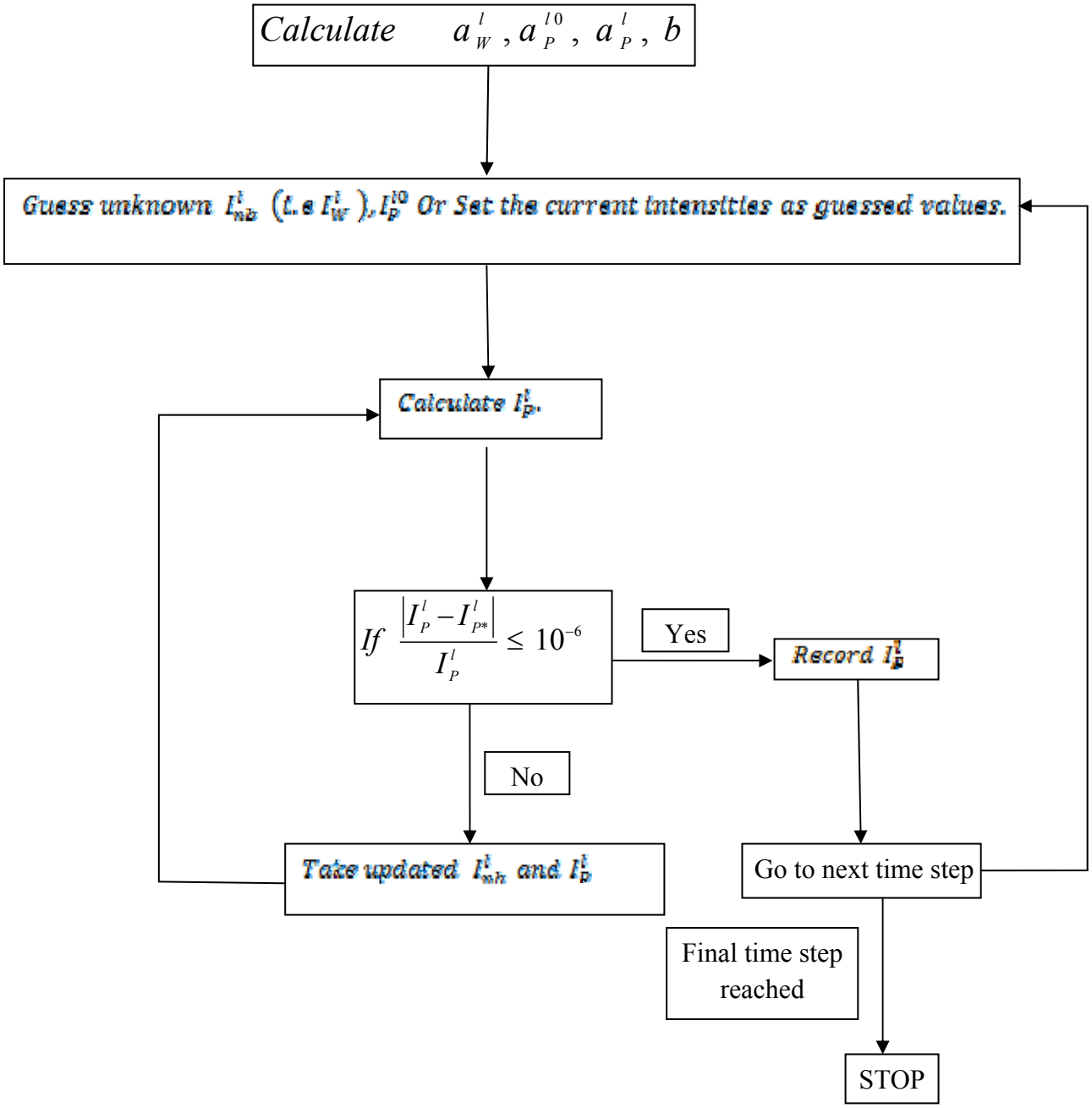

For 1-D Problem : $I_P^l = \dfrac{a_P^{l0} I_P^{l0} + a_W^l I_W^l + b}{a_P^l}$

For 2-D Problem : $I_P^l = \dfrac{a_P^{l0} I_P^{l0} + a_W^l I_W^l + a_S^l I_S^l + b}{a_P^l}$

Chapter-4

Results and Discussion

(One-Dimensional Problem)

4.1. Introduction

In the study of radiative transfer caused by a short-pulse laser irradiation, the time dependent transmittance and reflectance signals are the two quantities that can provide specific information about the medium. Transmittance is defined as the net radiative heat flux emerging out of the medium due to transmission and with reference to a planar medium (Fig. 3.1a), it is the net radiative heat flux at the bottom boundary (z = 0.0). Reflectance is the net radiative heat flux at the boundary which is subjected to the laser irradiation and, in the present case, it is the reflected heat flux at the top boundary ($z = L$). In this chapter the numerical results for the transmitted flux and reflected flux for a planar participating medium subjected to short pulse collimated radiation are discussed. The finite volume method is considered to evaluate the propagation of radiation intensity through a participating medium bounded by one-dimensional geometry and also different spatial differencing schemes are applied to enhance the accuracy of the solution. The collimated intensity of radiation travels with a speed of light through the medium. The effects of different properties like optical and geometrical properties are also analyzed. Both isotropic scattering and linearly anisotropic scattering medium (with forward scattering and backward scattering) are considered.

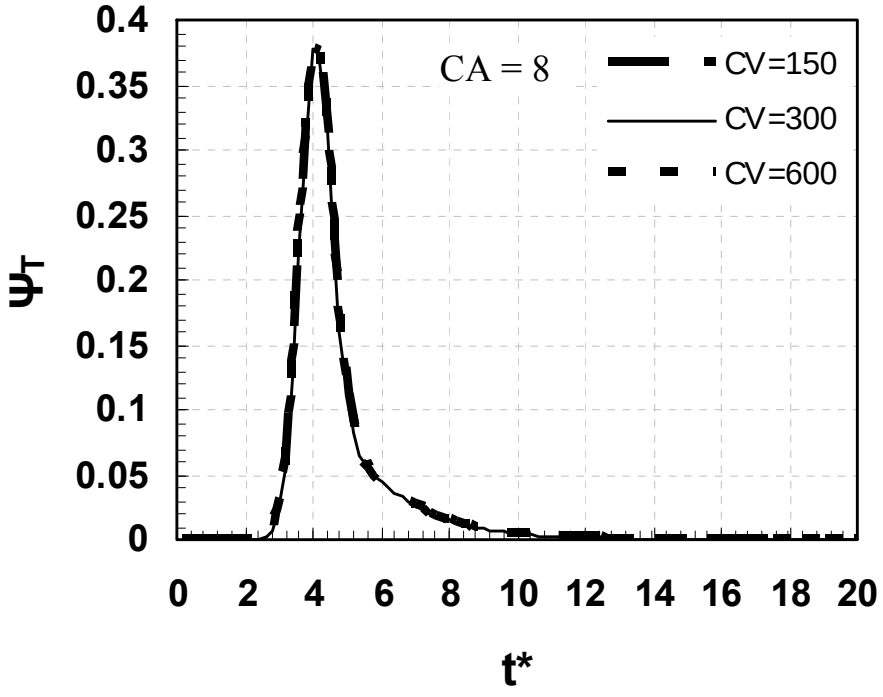

Fig. 4.1 Grid independence test for control volume.

4.2. Grid independence test

A grid independent test was conducted with different spatial and angular grid sizes. It is observed that further refinement to the grid size of 300 control volumes and 8 control angles results in negligible change in the transmittance value as seen from Figs. (4.1) and (4.2). Although it is not shown, a time independent test is also conducted for each grid size and it is found that beyond the dimensionless time step size of 0.01 ($\Delta t^* = 0.01$), there is negligible change in the results. Henceforth, the above grid size and time step size are used for further presentation of results.

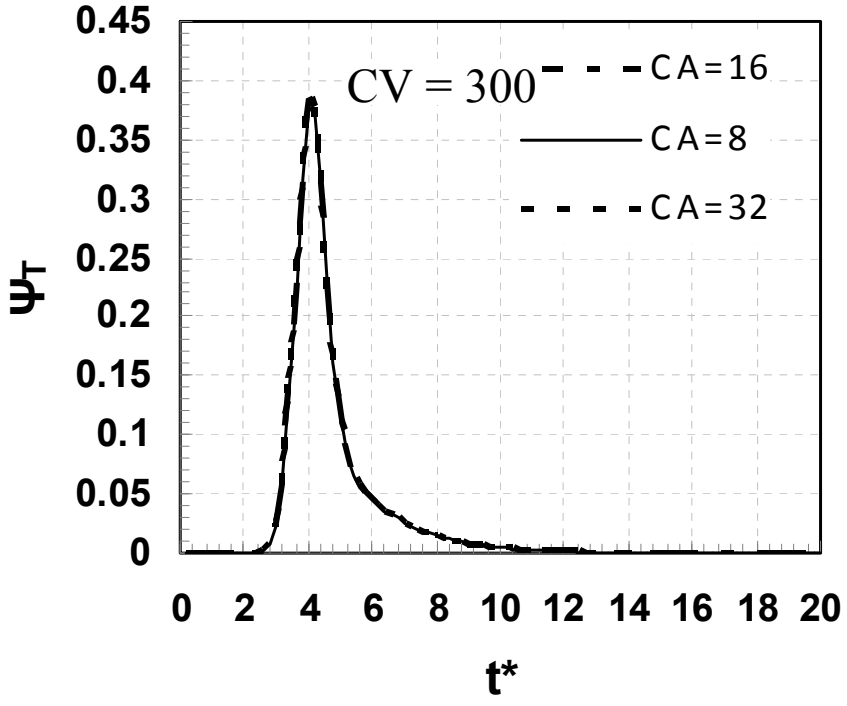

Fig. 4.2 Grid independence test for control angle.

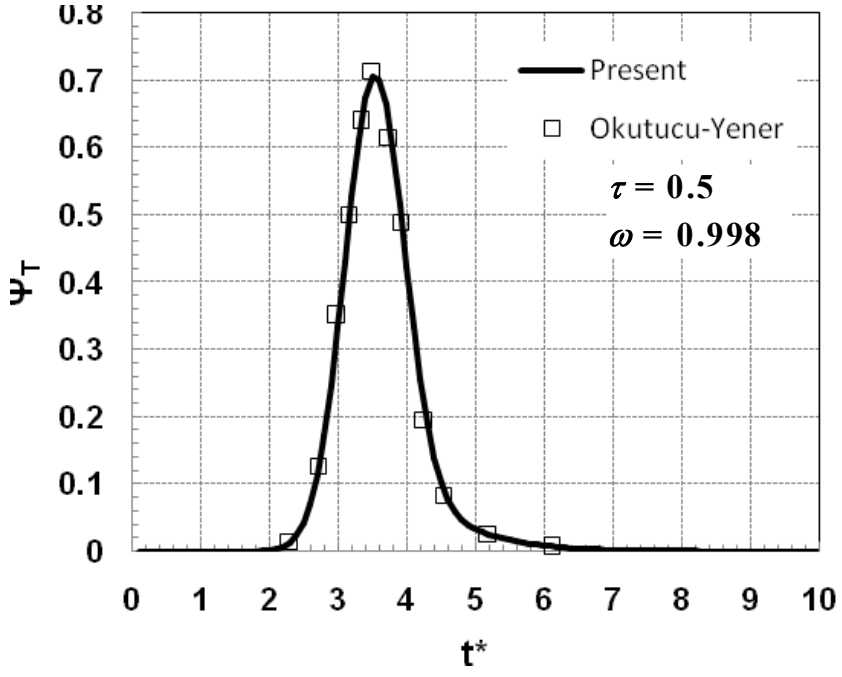

Fig. 4.3 (a) Comparison of transmittance in a scattering medium subjected to Gaussian pulse collimation.

4.3. Validation

The proposed methodology is validated with available existing solutions of Okutucu and Yener (2006) and Sakami et al. (2000), as shown in Figs. 4.3(a), (b), (c), (d). Figures 4.3(a) and (b) show the comparison with Galerkin based finite element method (Okutucu and Yener, 2006) for isotropic scattering medium subjected to Gaussian pulse collimation and the medium optical thickness as $\tau = 0.5$. The pulse width of the collimated beam is taken as unity ($t_p = 1$).

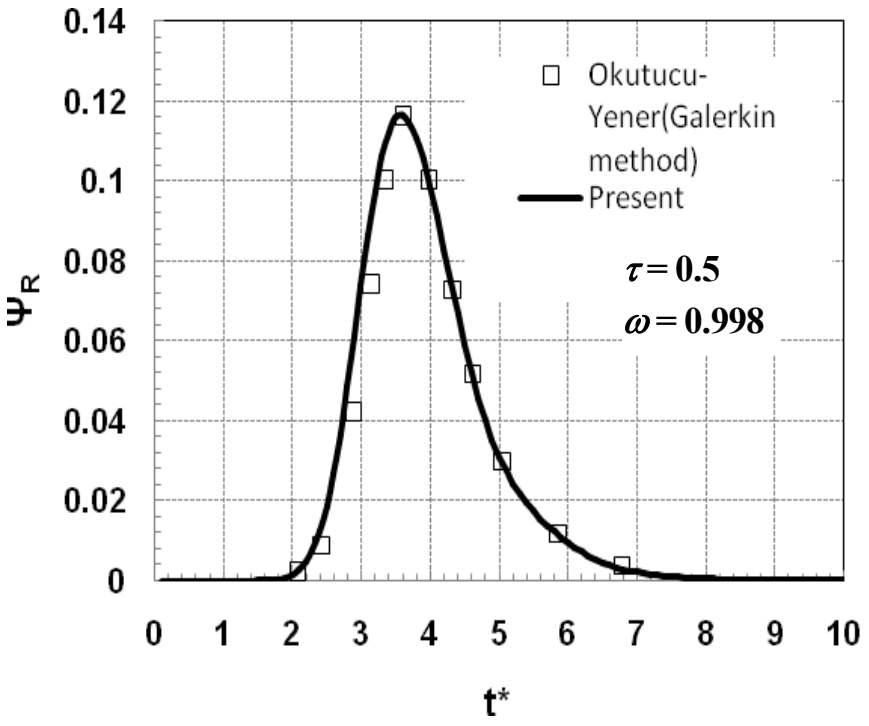

Fig. 4.3 (b) Comparison of reflectance in a scattering medium subjected to gaussian pulse collimation.

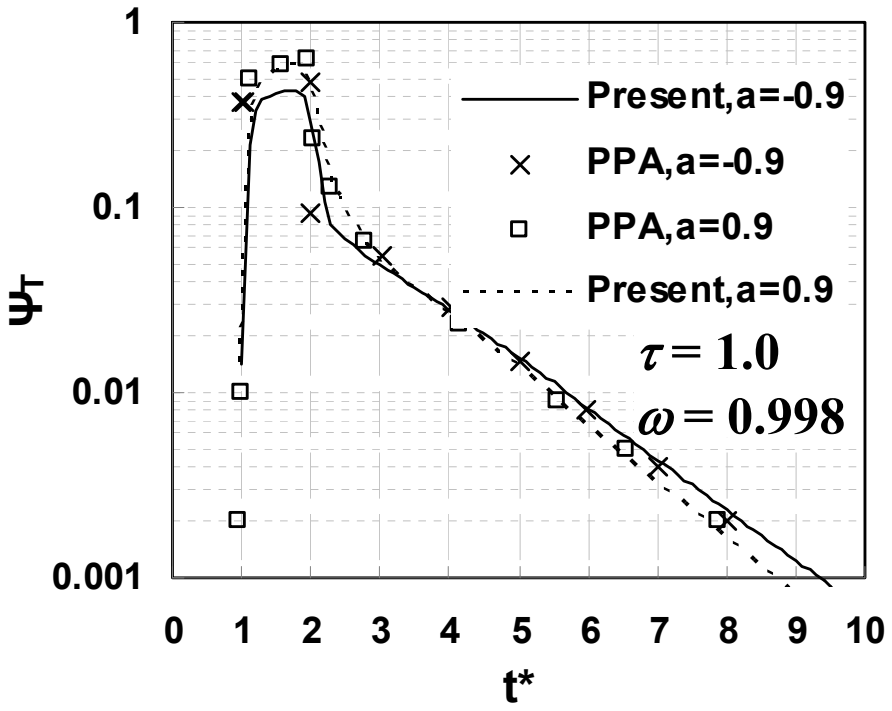

Fig. 4.3 (c) Comparison of transmittance in a scattering medium subjected to square pulse collimation.

Figures 4.3(c) and (d) shows the comparison of transmittance and reflectance with PPA method (Sakami et al., 2000) for linear anisotropic scattering medium when one of the boundaries is subjected to a square pulse collimation and the medium optical thickness as $\tau = 1.0$ and the scattering albedo is taken as $\omega = 0.998$ for both the cases. It is found that for both the cases, results obtained from the present method are in good agreement with the existing approaches.

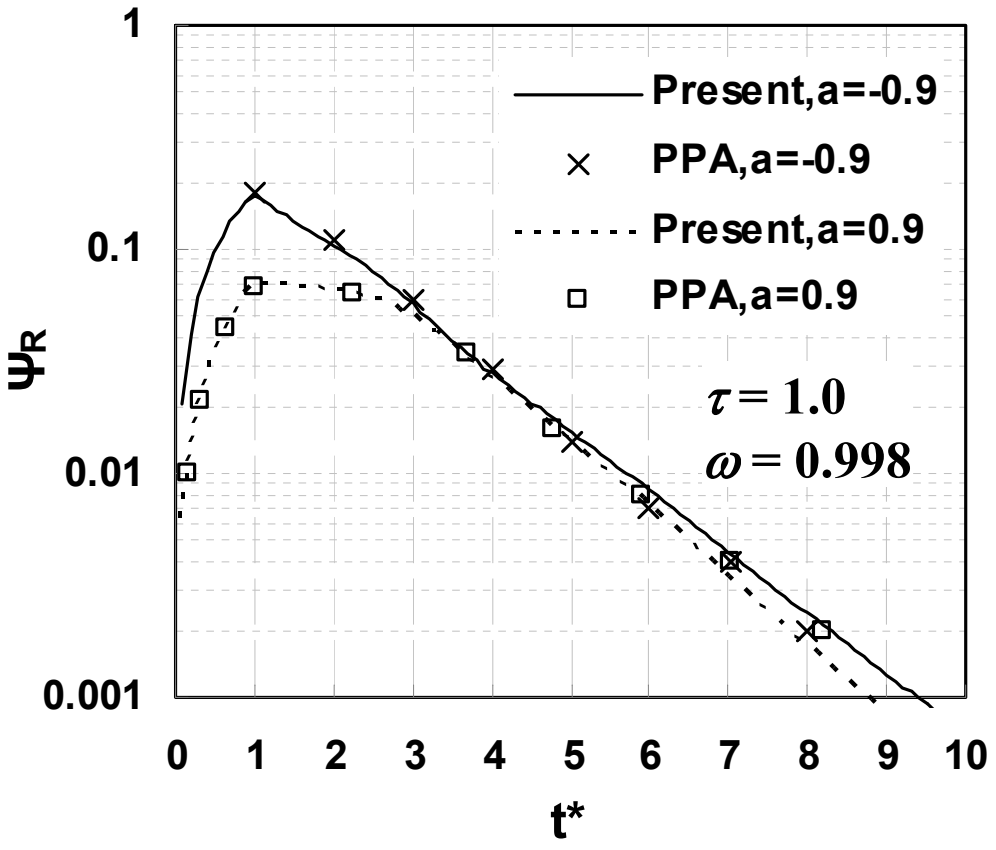

Fig. 4.3 (d) Comparison of reflectance in a scattering medium subjected to square pulse collimation.

4.4. Effects of anisotropy

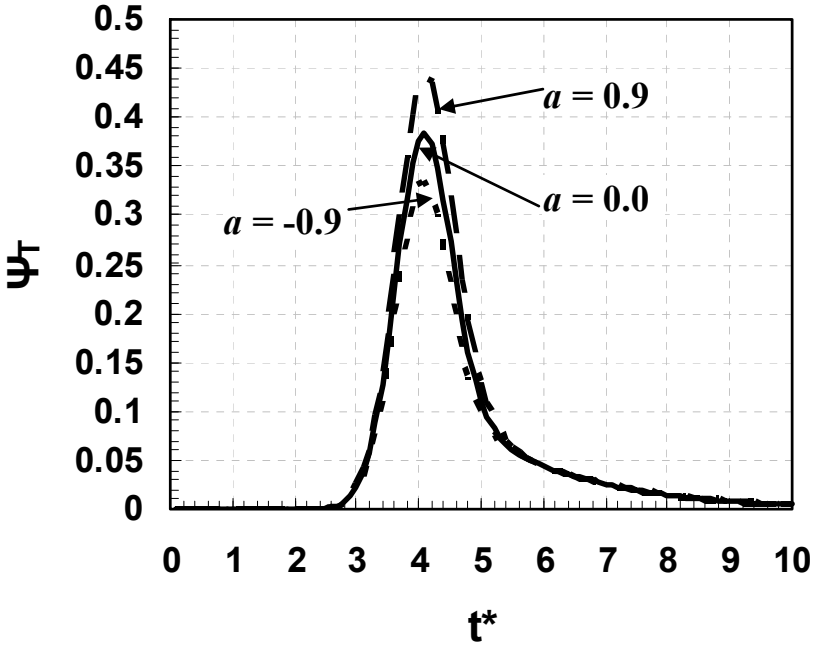

Fig. 4.4 (a) Effect of anisotropy on transmittance for ε_s = 0.8, τ = 1.0 and ω = 1.0.

Figures 4.4(a) and (b) show the influence of anisotropic scattering on the temporal variation of transmittance and reflectance. As expected, the transmission of radiation is found to be stronger in a forward scattering medium compared to the reflectance as seen from Fig. 4.4 (a). It is revealed from the reflectance curve (Fig. 4.4 b), there are two maxima in case of forward and isotropic scattering medium and it disappears as the medium becomes backward scattering. This is due to the effect of the gray wall. The reflected flux from opposite gray wall gets added to the reflectance which causes multiple maxima to appear.

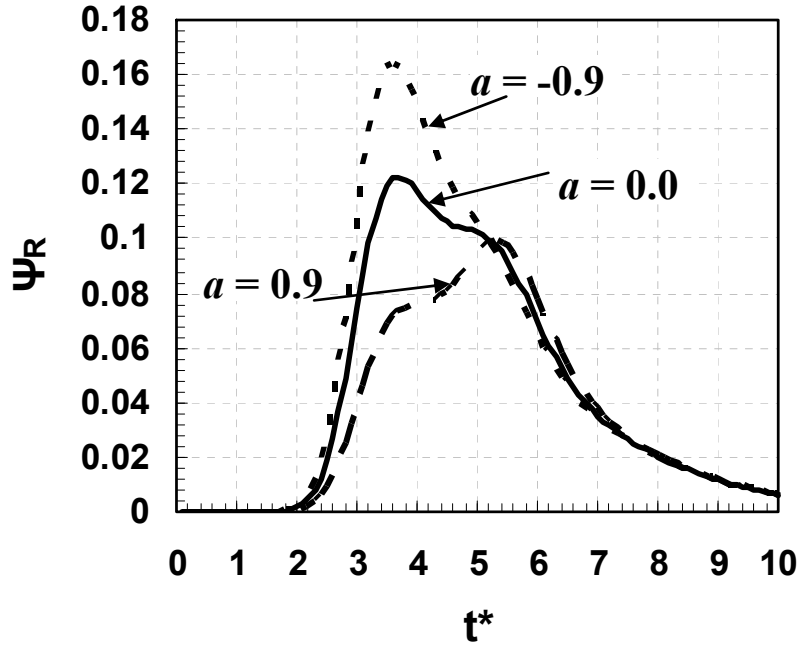

Fig. 4.4 (b) Effect of anisotropy on reflectance for ε_s = 0.8, τ = 1.0 and ω = 1.0.

The reflected flux starts reducing once the pulse is switched off and, as a combined effect of the flux reflected from the opposite gray wall and back scattered flux, the reflected flux once again reaches to the second maxima. Forward scattering enhances the maximum value of the transmittance peaks, whereas the maximum value of reflectance is augmented by backward scattering. The observations from the figures obey the isotropic scaling rule, which states that forward scattering can be scaled into isotropic scattering with a smaller scattering coefficient and backward scattering can be modeled by isotropic scattering with an increased scattering coefficient.

4.5. Effects of pulse profile

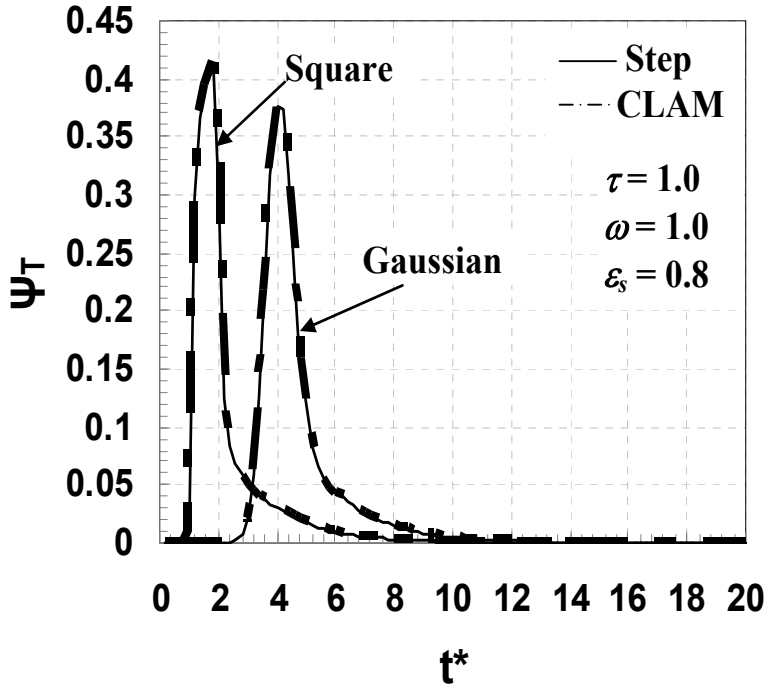

Fig. 4.5 (a) Effect of pulse profile on transmittance for ε_s = 0.8, τ = 1.0 and ω = 1.0.

The effect of pulse profile is shown in Figs. 4.5 (a) and (b). It is observed that, even though there is a little change in maximum value of transmittance as well as reflectance, the temporal width is broadened in case of Gaussian pulse due to the distribution given by Eqs (3.10) and (3.11) as expected. Due to the cumulative effect of the back scattered flux and reflected flux from the opposite gray wall, the reflected flux reaches the second maxima for both the pulses. Because of the nature of the Gaussian pulse the transmitted flux reduces smoothly as compared to that of the square pulse after the pulse is switched off. There is a sharp rise in both transmittance as well as in reflectance curve in case of square profile while it is not so for the Gaussian pulse.

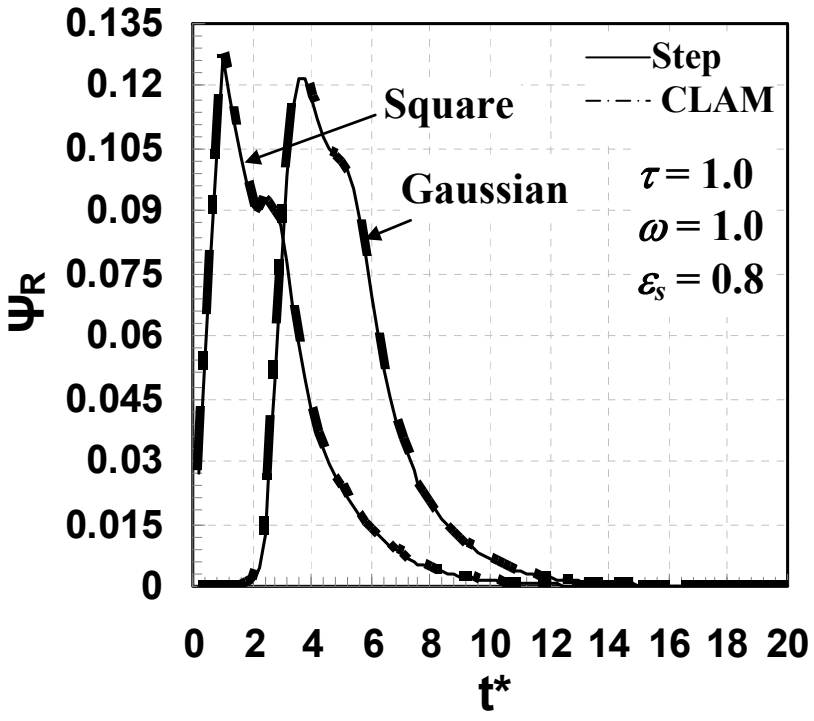

Fig. 4.5 (b) Effect of pulse profile on reflectance for ε_s = 0.8, τ = 1.0 and ω = 1.0.

4.6. Effects of optical thickness

Here the effects of optical thickness on transmittance and reflectance are discussed. Figs. 4.6 (a) and (b) reflect the nature of variation for transmittance and reflectance when the optical thickness is increased from 0.25 to 1. From Fig. 4.6(a) it can be observed that the magnitude of transmittance reduces as the optical thickness increases from 0.25 to 1. The interesting feature here is that the signal continues to give information for a longer duration for higher optical thickness values as compared to lower values of optical thickness because of more interaction between the medium and irradiation.

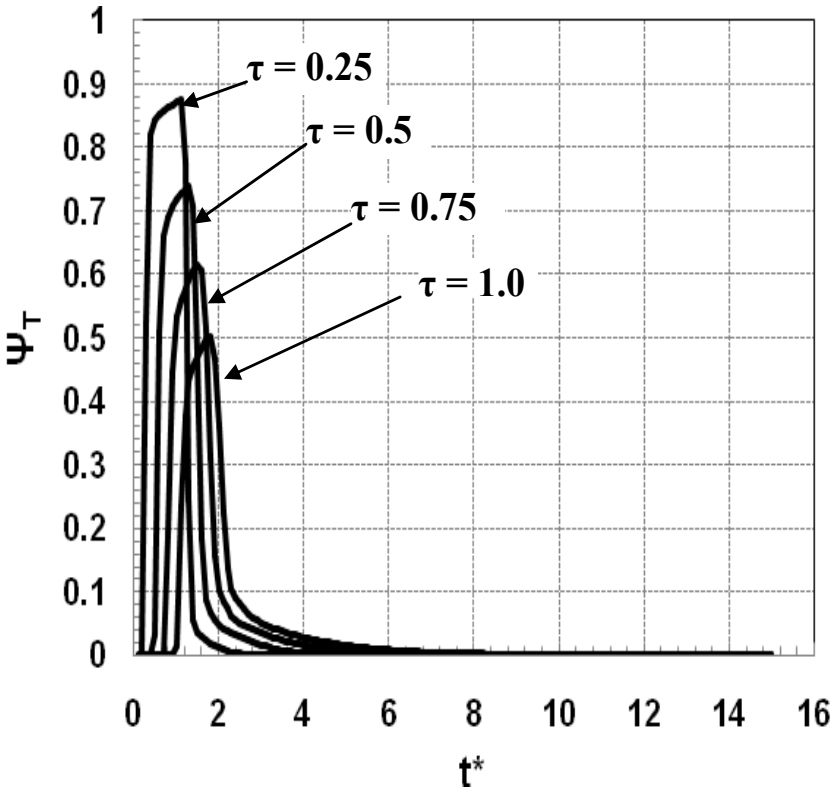

Fig 4.6(a).Effect of optical thickness on transmittance for black wall and ω=1.0.

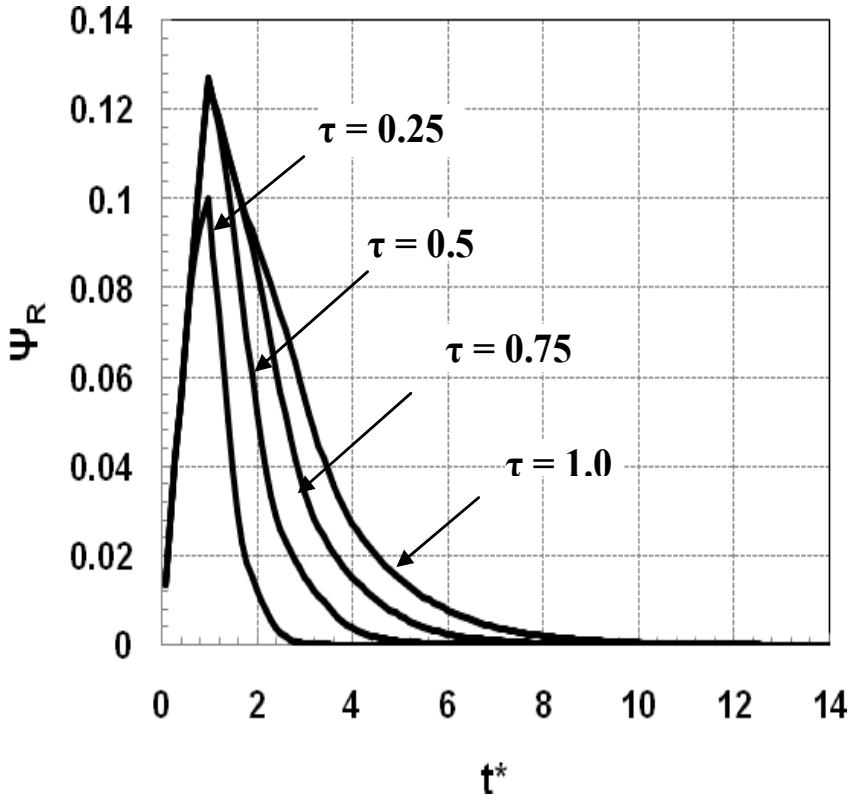

Fig. 4.6(b) Effect of optical thickness on reflectance for black wall and ω=1.0.

Figures 4.7 (a) and (b) present the influence of optical thickness on transmittance when the boundary wall is gray. As expected, the magnitude is reduced with increase in the optical thickness. When the medium is strongly forward scattering, the peak value of transmittance increases significantly. After the pulse left, transmittance signal will tend to leave the medium much faster when the optical thickness of the medium is small. For larger optical thickness, the medium and collimated beam interact with each other for a longer duration which results in the reduction of peak values in both isotropic and anisotropic scattering medium. But when compared between the isotropic and anisotropic scattering, the peak value in the later case gains more since the contribution from the medium is more in the direction of propagation.

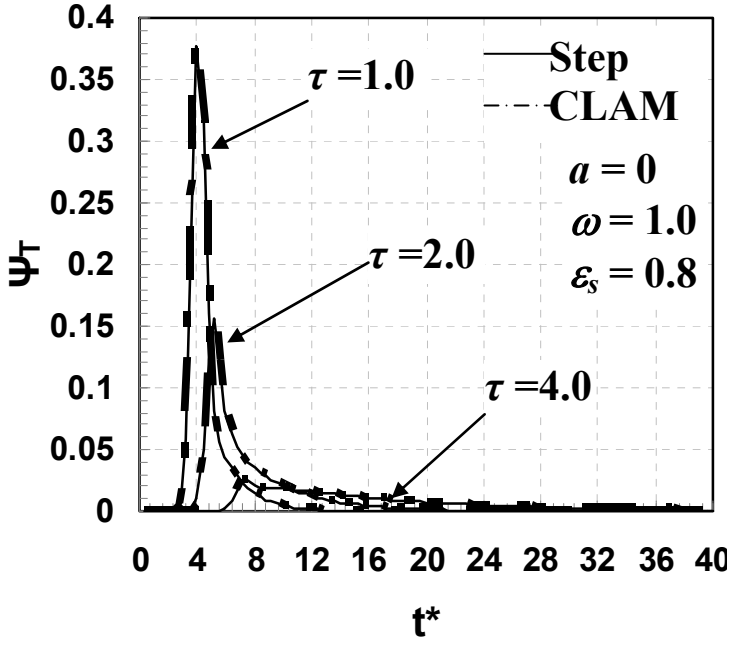

Fig. 4.7 (a) Effect of optical thickness on transmittance with ε_s = 0.8 and ω = 1.0 for a = 0.0.

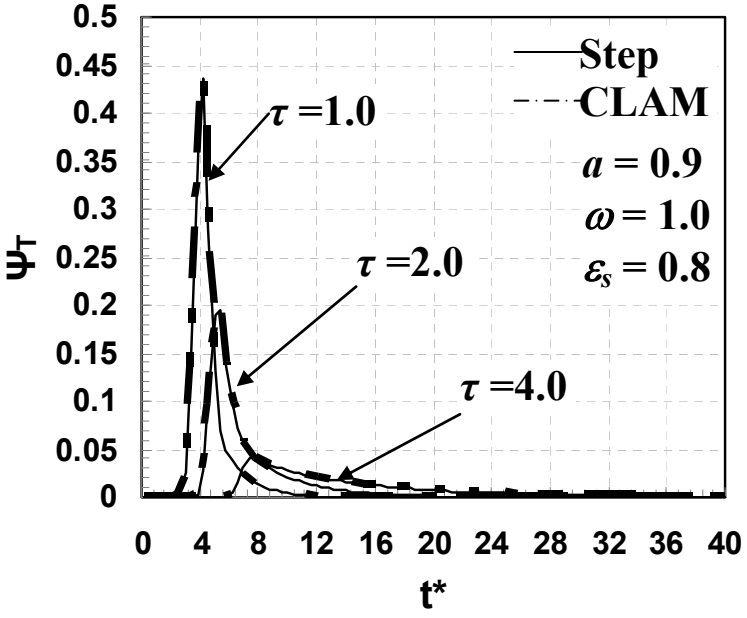

Fig. 4.7 (b) Effect of optical thickness on transmittance with ε_s = 0.8 and ω = 1.0 for a = 0.9.

4.7. Effects of scattering albedo

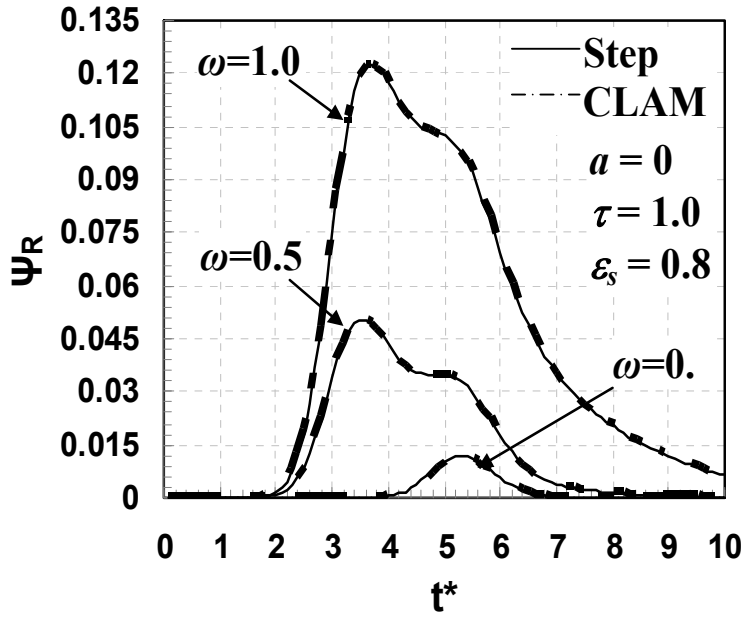

Fig. 4.8 (a) Effect of scattering albedo on reflectance with ε_s = 0.8 and τ = 1.0 for a = 0.0.

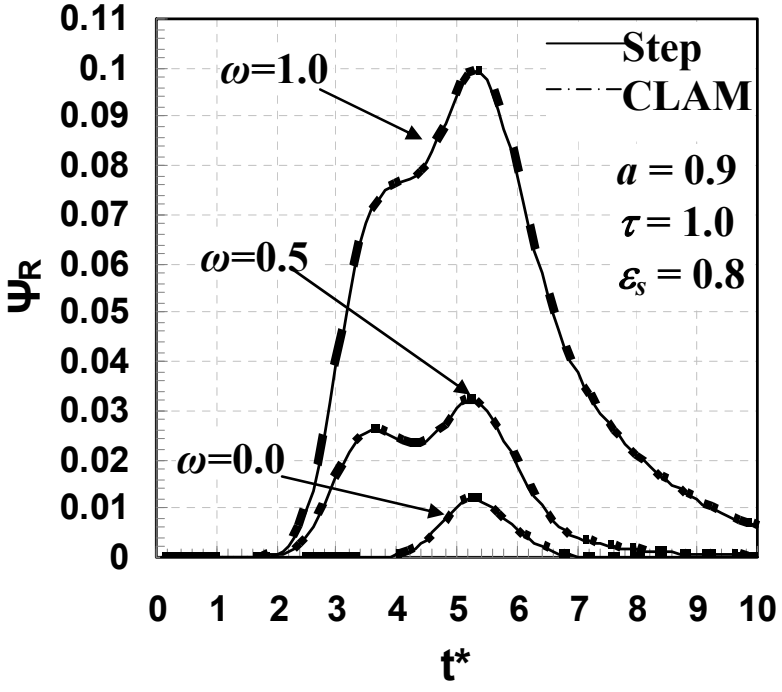

Fig. 4.8 (b) Effect of scattering albedo on reflectance with ε_s = 0.8 and τ = 1.0 for a = 0.9.

It is seen from Figs. 4.8 (a) and (b) that when the scattering is absent (pure absorption medium), multiple peaks of reflected flux are absent. It can be seen from the Figs. 4.8(a) and (b), a reverse trend is persisting in case of reflectance for the anisotropic scattering medium. While the radiation back propagates from the opposite wall, even though the medium is forward scattering, the peak value decreases as compared to the isotropic scattering medium. This happens because the scattering from the medium opposes the radiation while it travels from opposite wall to the top wall of incidence. From Figs. 4.8 (a) and (b), few interesting features are observed considering the net effect of the scattering albedo and gray wall. The interesting revealing of the observation is that the multiple maxima disappear when the scattering albedo approaches to either zero or one. This is because, when the scattering albedo is very low, then emissivity plays the dominant role and for higher scattering albedo, the scattering effect takes the lead role.

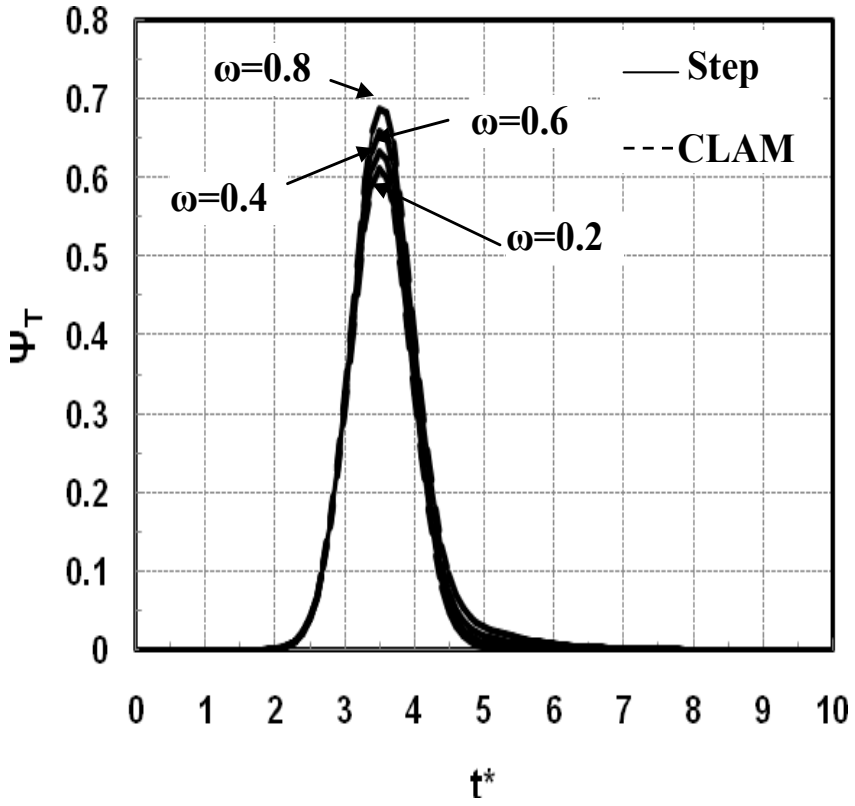

Fig. 4.9 (a) Effect of scattering albedo on transmittance for $\tau = 0.5$ and $\varepsilon_s = 0.8$.

From the Figs. 4.9(a), 4.10(a) and 4.11(a) it is observed that the transmittance decreases with increased optical thickness. While the irradiation propagates through the medium, it gets attenuated more and more due to absorption with decreased value of scattering albedo for all optical thicknesses. Therefore, the transmittance decreases for lower scattering albedos. The change in peak value becomes significant as the scattering albedo increases with increasing optical thickness. For higher values of optical thickness, the transmittance signal prevails for a longer period of time and also as the scattering albedo increases the effect further becomes cumulative. As the scattering albedo increases, change in the pattern of the curve is almost similar for all optical thicknesses till it attains the peak value, but thereafter they are separated as their slope (change of transmittance with time) increases with increased optical thickness. It is observed from the graphs that

the STEP scheme underpredicts the transmittance as the optical thickness increases. CLAM scheme also gives the similar results.

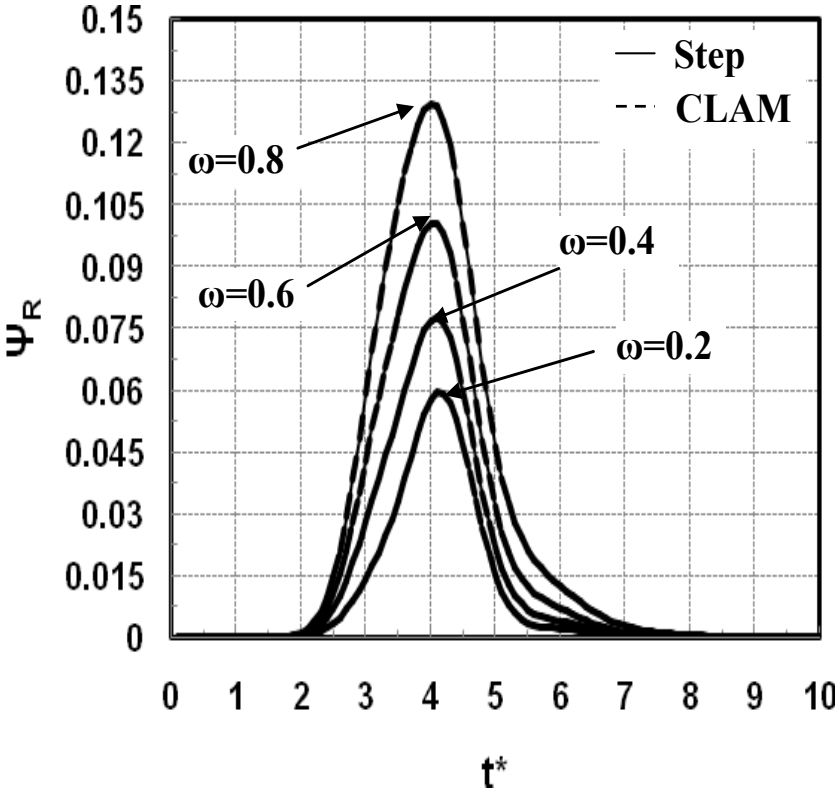

Fig. 4.9 (b) Effect of scattering albedo on reflectance for $\tau = 0.5$ and $\varepsilon_s = 0.8$.

As the optical thickness increases, the change in the peak value of reflectance becomes insignificant as seen from Figs. 4.9(b), 4.10(b) and 4.11(b). The reflectance increases as the scattering albedo increases. Two maxima are observed when $\tau = 1$ (indicating the effect of emissivity of the boundary wall), but when the optical thickness is increased the second maxima disappears (which reflects that the effect of optical thickness dominates the effect of emissivity). Unlike the transmittance, the reflectance is well captured by both the schemes when the pulse is switched off. Initially the STEP scheme underpredicts the reflectance for all optical thicknesses.

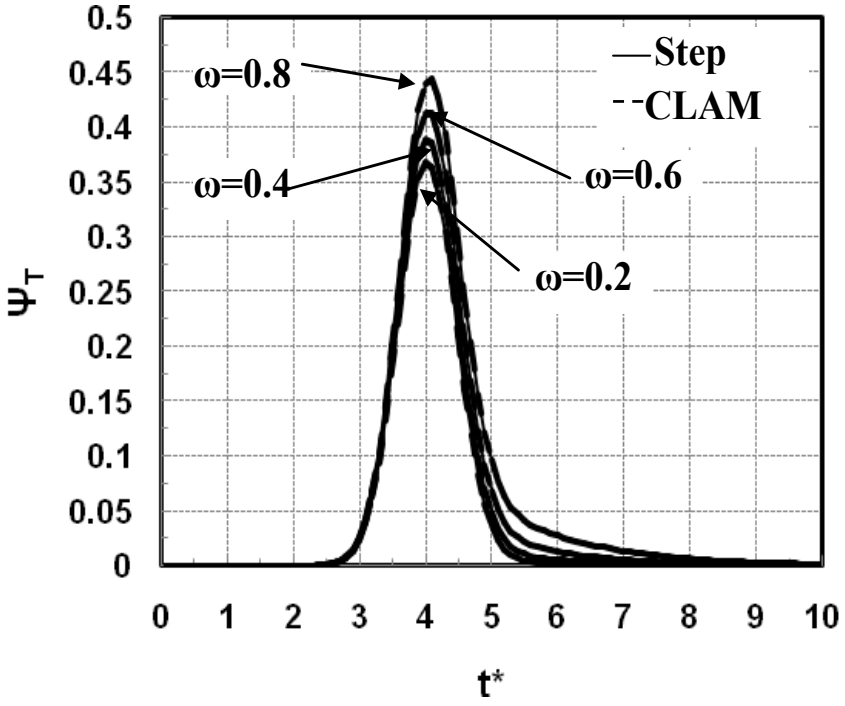

Fig. 4.10 (a) Effect of scattering albedo on transmittance for $\tau = 1.0$ and $\varepsilon_s = 0.8$.

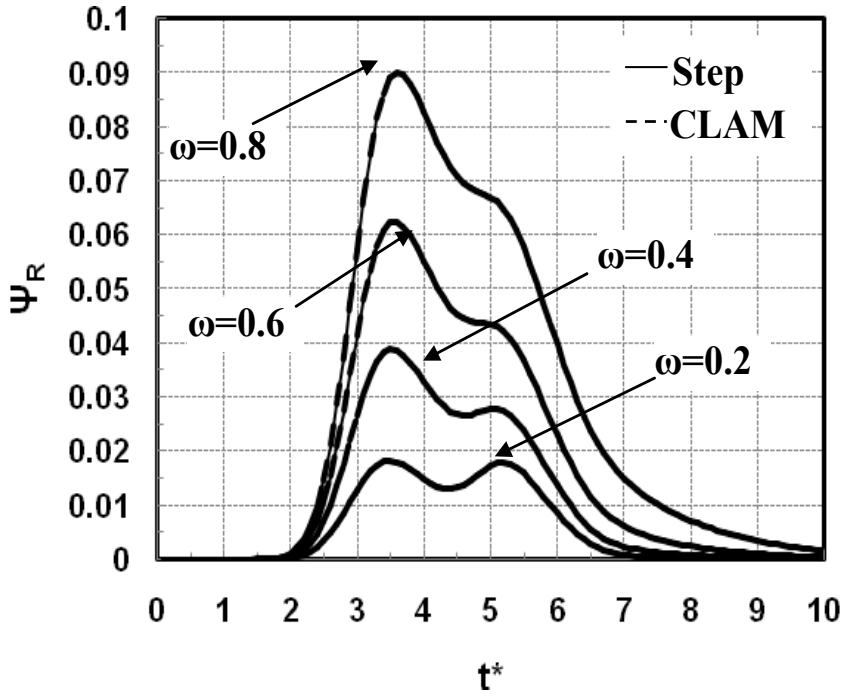

Fig. 4.10 (b) Effect of scattering albedo on reflectance for $\tau = 1.0$ and $\varepsilon_s = 0.8$.

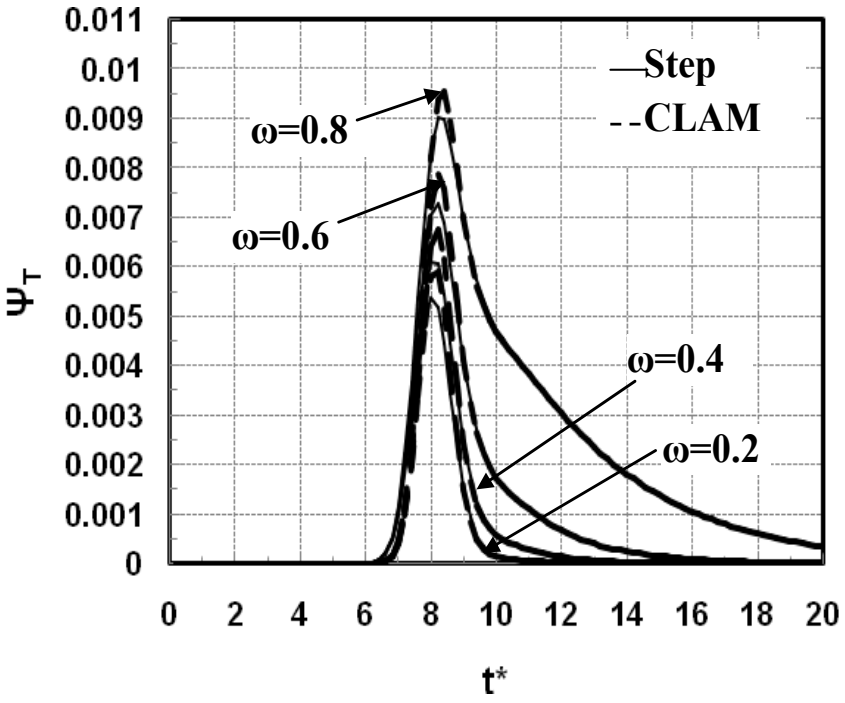

Fig. 4.11 (a) Effect of scattering albedo on transmittance for $\tau = 5.0$ and $\varepsilon_s = 0.8$.

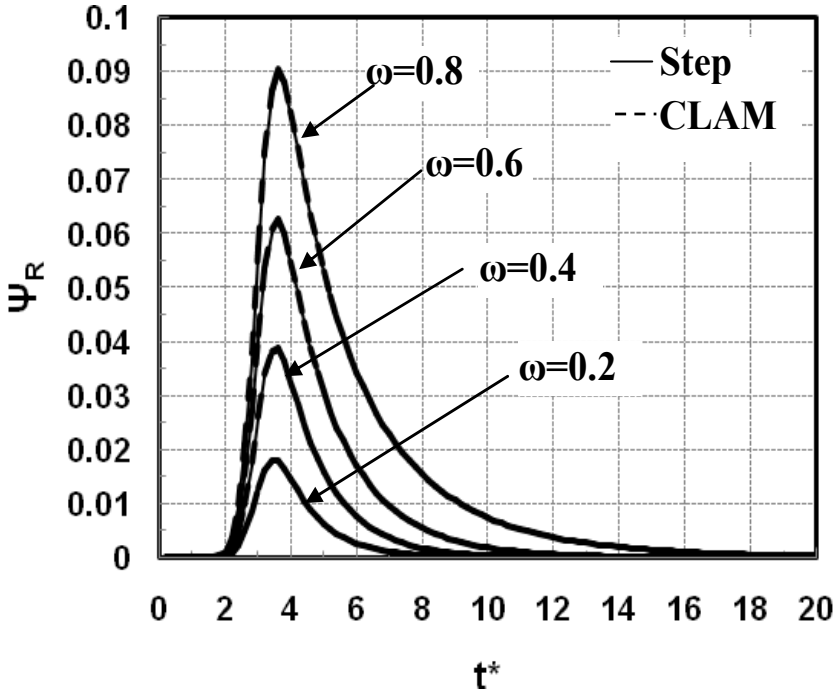

Fig. 4.11 (b) Effect of scattering albedo on reflectance for $\tau = 5.0$ and $\varepsilon_s = 0.8$.

4.8. Effects of emissivity

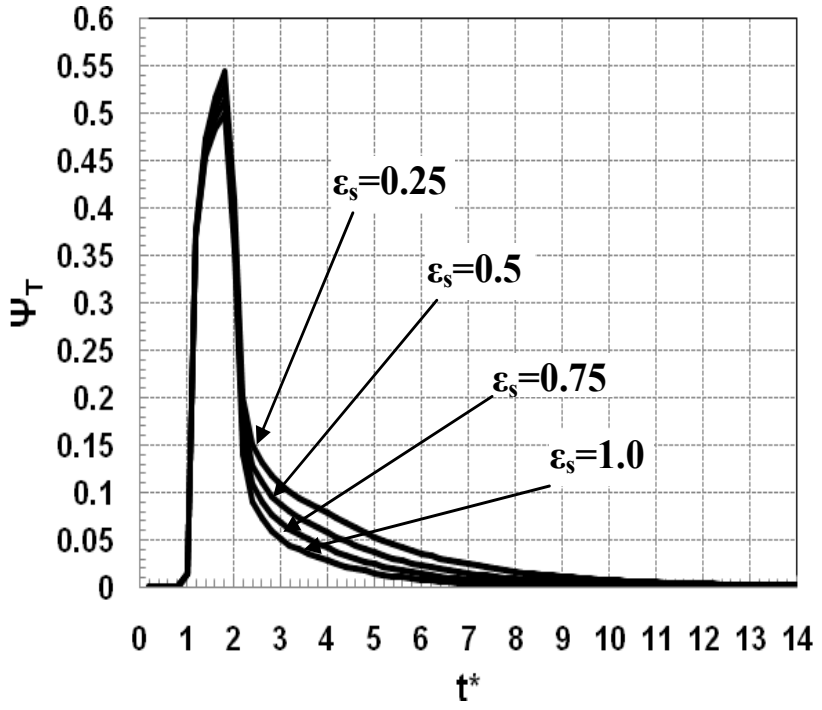

Fig. 4.12(a) Effect of emissivity on transmittance for τ = 1.0 and ω = 1.0 for square pulse.

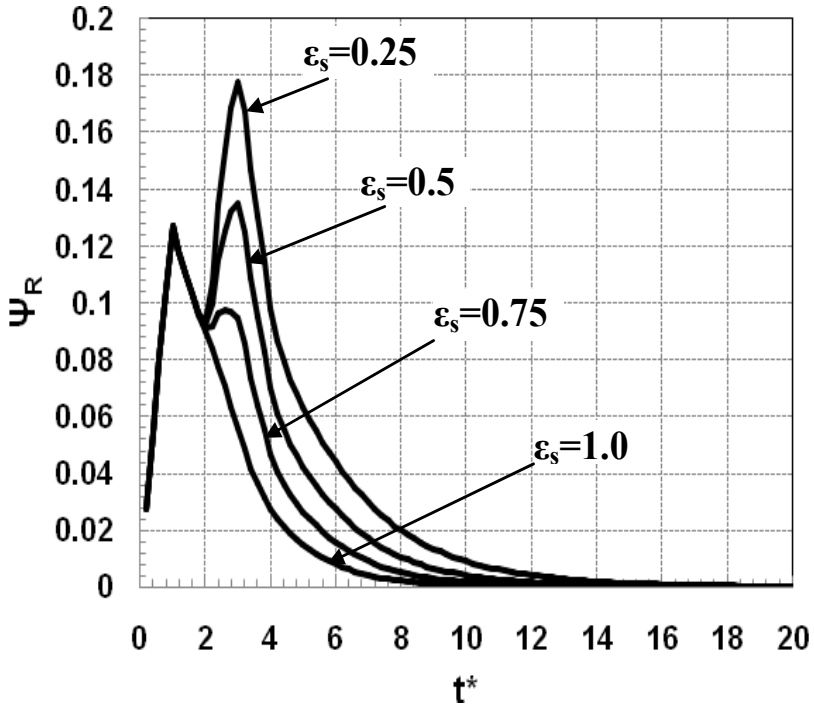

Fig. 4.12(b) Effect of emissivity on reflectance for τ = 1.0 and ω = 1.0 for square pulse.

Figure 4.12 (a) depicts that there is no significant change in the peak value of transmittance for different emissivities. The reflectance increases sharply for all emissivities and then reduces before increasing to reach the second peak as seen from Fig. 4.12 (b). As the value of emissivity reduced, more reflection is caused at the south boundary which gets added to the back scattering and this results in two maxima as observed from Fig. 4.12 (b). One of them disappears, as the emissivity increases. As seen from Fig. 4.12 (a), the transmittance persists for longer time with smaller value of emissivity. The effect of emissivity on transmittance and reflectance is not significant for higher values of optical thickness.

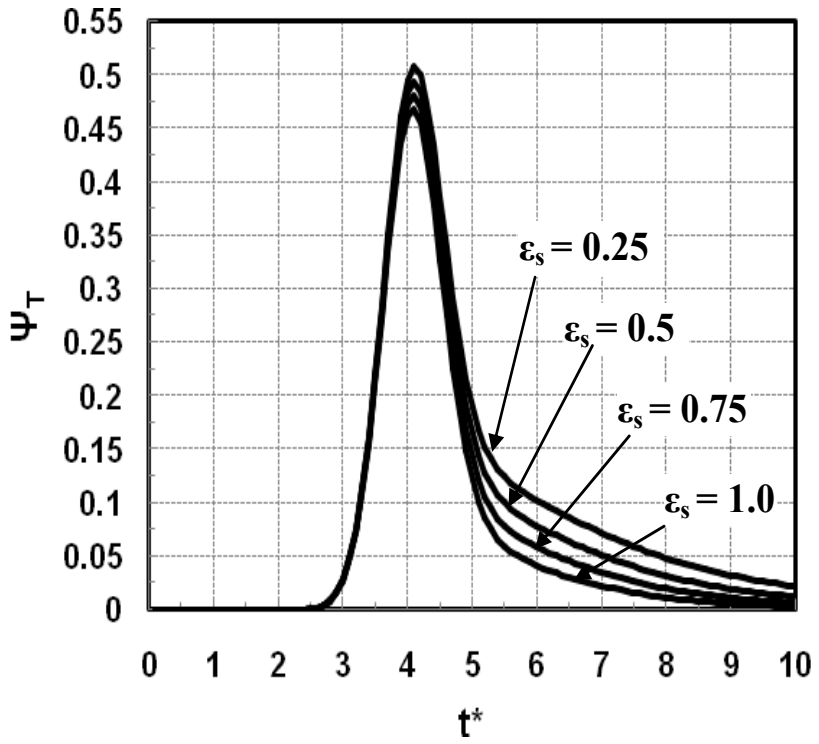

Fig. 4.13 (a) Effect of emissivity on transmittance for $\tau = 1.0$ and $\omega = 1.0$ for Gaussian pulse.

Figures 4.13(a) and (b) show the influence of gray south wall and other black walls on transmittance and reflectance, when the pulse is a Gaussian pulse. It is seen from Fig.4.13 (a) that, even though there is marginal change in the peak value of transmittance, the signal remains for longer duration as the emissivity of the south wall decreases since there is more interaction between the reflected flux from wall and the medium.

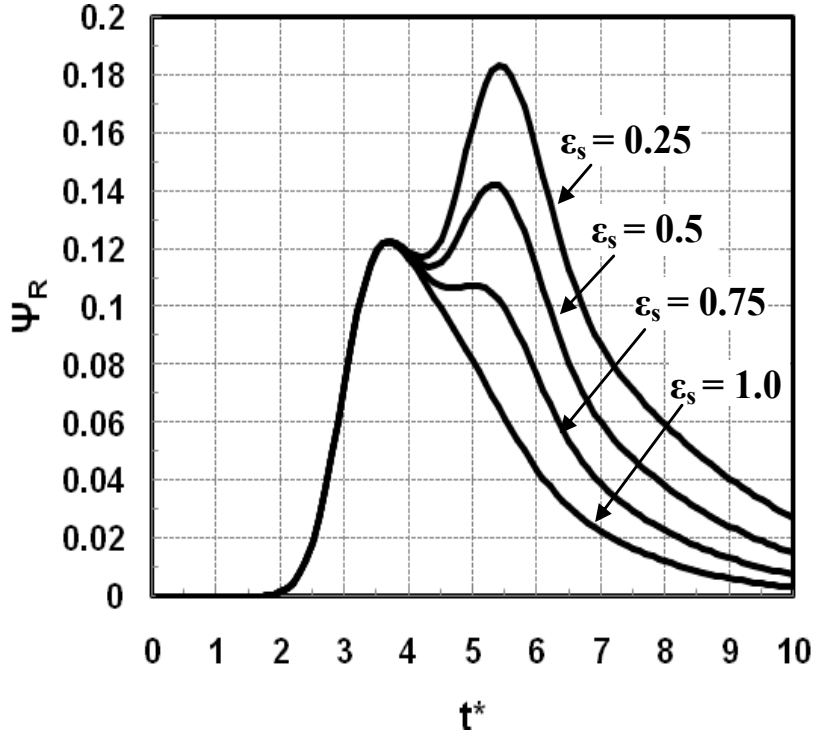

Fig. 4.13 (b) Effect of emissivity on reflectance for τ =1.0 and ω = 1.0 for Gaussian pulse.

Chapter-5

Two-dimensional Problem Formulation

5.1. Two-Dimensional Problem Formulation

The physical case (Fig.5.1 (a)) under consideration is a two-dimensional anisotropically scattering and absorbing medium of dimension $L \times L$ with constant properties. The transient radiative transfer equation (TRTE) in the above case considered may be expressed as (Modest, 2003)

$$\frac{1}{c}\frac{\partial I^l}{\partial t}+\frac{\partial I^l}{\partial s}=-kI^l-\sigma_s I^l+kI_b+\frac{\sigma_s}{4\pi}\int_{4\pi} I^{l'}\Phi(l'\rightarrow l)d\Omega^{l'} \tag{5.1}$$

As mentioned earlier, the scattering phase function obeys the following condition

$$\int_{4\pi}\Phi\left(\hat{s}^{l'},\hat{s}^{l}\right)d\Omega^{l'}=4\pi \tag{5.2}$$

In the finite volume method this is approximated as

$$\int_{4\pi}\Phi\left(\hat{s}^{l'},\hat{s}^{l}\right)d\Omega^{l'}=\sum_{l'=1}^{M}\Phi^{l'l}\Delta\Omega^{l'} \tag{5.3}$$

where $\Phi^{l'l}$ is average energy scattered from control angle *l'* to the control angle *l*.

The scattering phase function can be represented as a series in terms of Legendre's polynomial as follows:

$$\Phi\left(\hat{s}',\hat{s}\right)=1+\sum_{m=1}^{M}a_m P_m\left(\hat{s}',\hat{s}\right) \tag{5.4}$$

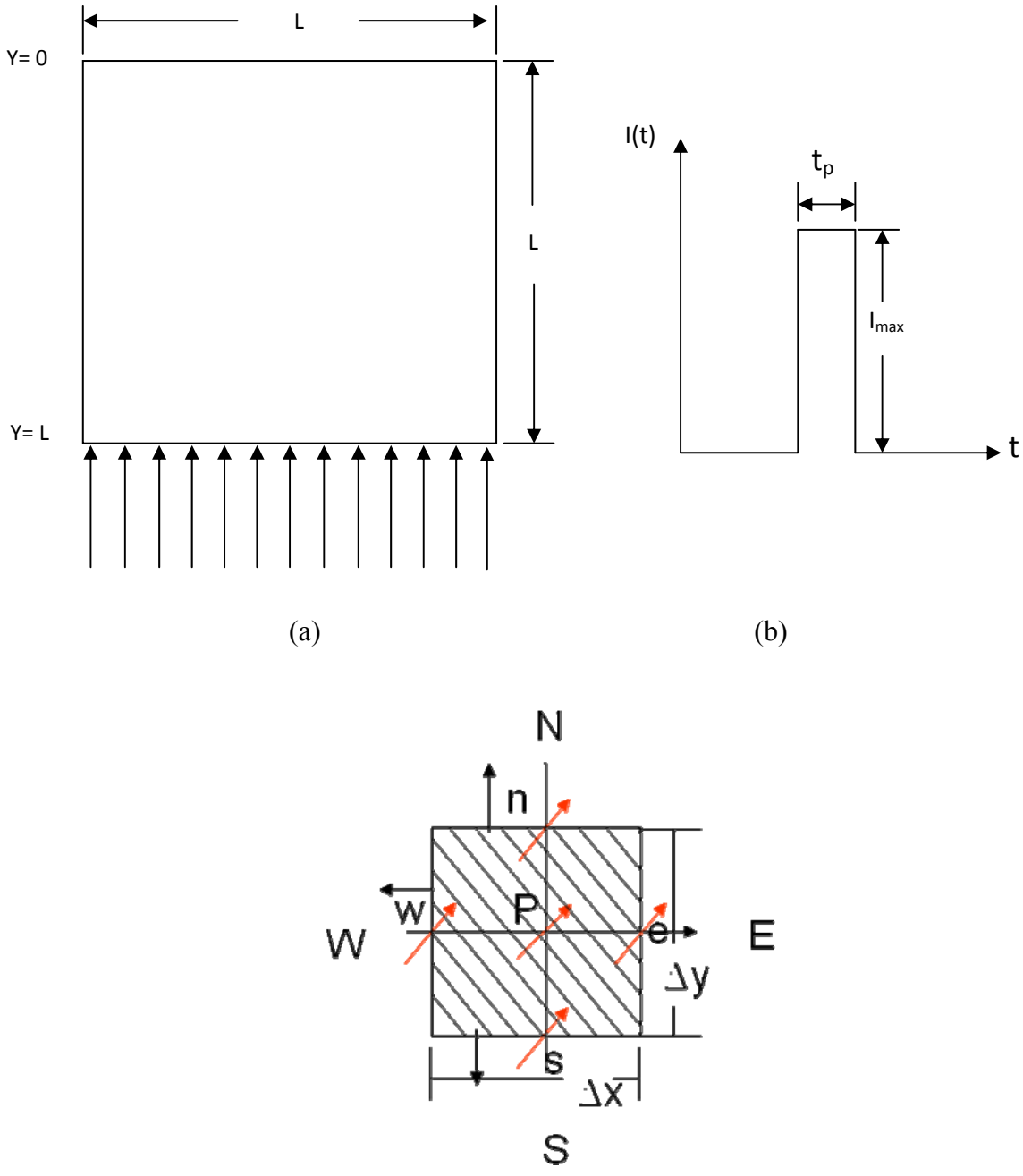

Fig. 5.1(a) Computational domain (b) Pulse profile (c) Control volume.

For linear anisotropic condition $M = 1$. Hence, the above equation becomes

$$\Phi(\hat{s}', \hat{s}) = 1 + a_1 P_1(\hat{s}' \cdot \hat{s}) = 1 + a_1(\hat{s}' \cdot \hat{s}) \tag{5.5}$$

$$\text{Also,} \quad P_1(\hat{s}' \cdot \hat{s}) = (\hat{s}' \cdot \hat{s}) \tag{5.6}$$

Therefore, the linear anisotropic scattering phase function for two-dimensional problem can be expressed as

$$\Phi(\hat{s}^{l'} \to \hat{s}^{l}) = 1 + a(\cos\theta^{l} \cos\theta^{l'} + \sin\theta^{l} \sin\theta^{l'} \cos(\phi^{l'} - \phi^{l}) \tag{5.7}$$

since, $\hat{s}' = \sin\theta'(\cos\phi' \hat{i} + \sin\phi' \hat{j}) + \cos\theta' \hat{k}$

and, $\hat{s} = \sin\theta(\cos\phi \hat{i} + \sin\phi \hat{j}) + \cos\theta \hat{k}$

The average scattering phase function is given by

$$\Phi^{l'l} = \frac{\int \Phi(\hat{s}', \hat{s}) d\Omega^{l'}}{\Delta\Omega^{l'}} \tag{5.8}$$

Hence

$$\Phi^{l'l} = \frac{\int_{\phi_1^{l'}}^{\phi_2^{l'}} \int_{\theta_1^{l'}}^{\theta_2^{l'}} \{1 + a\cos\theta^{l} \cos\theta^{l'} + a\sin\theta^{l} \sin\theta^{l'} \cos(\phi^{l} - \phi^{l'})\} \sin\theta^{l'} d\phi^{l'} d\theta^{l'}}{\Delta\Omega^{l'}} \tag{5.9}$$

Expanding the integral, Eq. (5.9) becomes

$$\Phi^{l'l} = \frac{\begin{aligned}&\Delta\Omega^{l'} + \frac{a\cos\theta}{4}\left(\cos 2\theta_1^{l'} - \cos 2\theta_2^{l'}\right)\left(\phi_2^{l'} - \phi_1^{l'}\right) + \left(\frac{a\sin\theta\cos\phi}{2}\right)\\ &\left(\theta_2^{l'} - \theta_1^{l'} + \left(\frac{\sin 2\theta_1^{l'} - \sin 2\theta_2^{l'}}{2}\right)\right)\left(\sin\phi_2^{l'} - \sin\phi_1^{l'}\right)\\ &+\left(\frac{a\sin\theta\sin\phi}{2}\right)\left(\theta_2^{l'} - \theta_1^{l'} + \left(\frac{\sin 2\theta_1^{l'} - \sin 2\theta_2^{l'}}{2}\right)\right)\left(\cos\phi_1^{l'} - \cos\phi_2^{l'}\right)\end{aligned}}{\Delta\Omega^{l'}} \tag{5.10}$$

5.2. Formulation of the Discretization Equation

Equation (5.1) in non-dimensional form can be written (with linear anisotropy) as

$$\frac{1}{\beta c}\frac{\partial I^l}{\partial t} + \frac{1}{\beta}\frac{\partial I^l}{\partial s} = -I^l + (1-\omega)I_b + \frac{\omega}{4\pi}\sum_{l'=l}^{M} I^l \Phi^{l'l}\Delta\Omega^{l'} \tag{5.11}$$

Now the linearised TRTE can be written as, $\frac{1}{\beta c}\frac{\partial I^l}{\partial t} + \frac{1}{\beta}\frac{\partial I^l}{\partial s} = -\beta_m^l I^l + S_m^l$ (5.12)

where the modified extinction coefficient is

$$\beta_m^l = \left(1 - \frac{\omega}{4\pi}\Delta\Omega^l\right) - \frac{\omega}{4\pi}a\cos\theta^l\cos\theta^l\Delta\Omega^l - a\sin\theta^l\sin\theta^l\Delta\Omega^l \tag{5.13}$$

and the modified source function is

$$S_m^l = (1-\omega)I_b + \left\{ \begin{array}{l} \dfrac{\omega}{4\pi}\sum\limits_{\substack{l'=1 \\ l'\neq l}}^{M} I^{l'}\Delta\Omega^{l'} + a\cos\theta\sum\limits_{\substack{l'=1 \\ l'\neq l}}^{M} I^{l'}\cos\theta^{l'}\Delta\Omega^{l'} + \\ a\sin\theta^l\sum\limits_{\substack{l'=1 \\ l'\neq l}}^{M} I^{l'}\sin\theta^{l'}\cos\left(\phi^{l'}-\phi^l\right)\Delta\Omega^{l'} \end{array} \right\} \tag{5.14}$$

Upon integration over a typical control volume and a control angle within a specified time step, the TRTE becomes

$$\begin{aligned} &\int_{\Delta\Omega^l}\int_{\Delta V}\int_{\Delta t^*}\frac{\partial I^l}{\partial t^*}dt^*dV\,d\Omega + \frac{1}{\beta}\int_{\Delta\Omega^l}\int_{\Delta V}\int_{\Delta t^*}\frac{\partial I^l}{\partial s}dt^*dV\,d\Omega \\ &= \int_{\Delta\Omega^l}\int_{\Delta V}\int_{\Delta t^*}\left(-\beta_m^l I^l + S_m^l\right)dt^*dV\,d\Omega \end{aligned} \tag{5.15}$$

Applying divergence theorem to the 2nd term of the Eq. (5.15), the TRTE simplifies to

$$\begin{aligned} &\int_{\Delta\Omega^l}\int_{\Delta V}\int_{\Delta t^*}\frac{\partial I^l}{\partial t^*}dt^*dV\,d\Omega + \frac{1}{\beta}\int_{\Delta\Omega^l}\int_{\Delta t^*}\int_{\Delta A} I^l\left(s^l\cdot\hat{n}\right)dA dt^*d\Omega \\ &= \int_{\Delta\Omega^l}\int_{\Delta V}\int_{\Delta t^*}\left(-\beta_m^l I^l + S_m^l\right)dt^*dV\,d\Omega \end{aligned} \tag{5.16}$$

where $\hat{n}$ is the unit outward normal vector. The first term in the left hand side of Eq. (5.16) represents the change of radiation intensity with time; the second term represents the inflow and outflow of radiant energy across the faces of the control volume. The term on the right side accounts for the attenuation and augmentation of energy within a control volume and control angle. In the finite volume method, the magnitude of intensity is assumed to be constant over the control volume and a control angle. Under these assumptions and, using the fully implicit scheme, Eq. (5.16) can be written as

$$\left(I_P^l - I_P^{l0}\right)\Delta V\Delta\Omega^l + \frac{1}{\beta}\sum_{i=1}^{4} I_i^l \Delta A_i \Delta t^* \int_{\Delta\Omega^l}\left(\hat{s}\cdot\hat{n}\right)d\Omega^l = \left(-\beta_m^l I_P^l + S_m^l\right)\Delta V\Delta\Omega^l\Delta t^* \qquad (5.17)$$

where I_P^{l0} and I_P^l are the nodal intensities at the start and at the end of the time step respectively. On further simplification, for a control volume and a control angle Eq. (5.17) becomes

$$\begin{aligned}&\frac{\left(I_P^l - I_P^{l0}\right)\Delta V\Delta\Omega^l}{\Delta t^*} + \frac{\left(I_e^l - I_w^l\right)\Delta A_x D_{cx}^l}{\beta} + \\ &\frac{\left(I_n^l - I_s^l\right)\Delta A_y D_{cy}^l}{\beta} = \left(-\beta_{m,P}^l I_P^l + S_{m,P}^l\right)\Delta V\Delta\Omega^l\end{aligned} \qquad (5.18)$$

where, $D_{cyn}^l = \int\left(\hat{s}.\hat{n}_y\right)d\Omega^l = -D_{cys}^l = D_{cy}^l$, $\Delta\Omega^l = \int_{\Delta\Omega'} d\Omega$, $\Delta A_{yn} = \Delta A_{ys}$.

5.3. STEP Scheme

To relate the boundary intensities to the nodal intensities, the spatial difference scheme STEP is used. In the STEP or upwind scheme the downstream boundary intensities are set equal to the upstream nodal intensities (Fig.5.1 (c)).

$$I_e^l = I_n^l = I_P^l \ , \ I_s^l = I_S^l \ , \ I_w^l = I_W^l \qquad (5.19)$$

Applying the STEP scheme, Eq (5.18) becomes

$$\begin{aligned}&\left[\frac{\Delta A_x D_{cx}^l}{\beta} + \frac{\Delta A_y D_{cy}^l}{\beta} + \beta_{m,P}^l \Delta V\Delta\Omega^l + \frac{\Delta V\Delta\Omega^l}{\Delta t^*}\right] I_P^l = \left(\frac{\Delta V\Delta\Omega^l}{\Delta t^*}\right) I_P^{l0} \\ &+ \frac{\Delta A_x D_{cx}^l I_W^l}{\beta} + \frac{\Delta A_y D_{cy}^l I_S^l}{\beta} + S_{m,P}^l \Delta V\Delta\Omega^l\end{aligned} \qquad (5.20)$$

The standard form of the discretization equation in control volume formulation is

$$a_P I_P = a_P^0 I_P^0 + \sum a_{nb} I_{nb} + b \tag{5.21}$$

So the final discretization equation for the nodal intensities for the $D_{cx}^l > 0$ and $D_{cy}^l > 0$ conditions can be written as

$$a_P^l I_P^l = a_P^{l0} I_P^{l0} + a_w^l I_W^l + a_S^l I_S^l + b^l \tag{5.22}$$

where, $a_P^{l0} = \dfrac{\Delta V \Delta \Omega^l}{\Delta t^*}$, $a_S^l = \dfrac{\Delta A_y D_{cy}^l}{\beta}$, $a_w^l = \dfrac{\Delta A_x D_{cx}^l}{\beta}$, $\Delta t^* = \beta c \Delta t$

$$a_P^l = \left[\frac{\Delta A_x D_{cx}^l}{\beta} + \frac{\Delta A_y D_{cy}^l}{\beta} + \beta_{mP}^l \Delta V \Delta \Omega^l + \frac{\Delta V \Delta \Omega^l}{\Delta t^*} \right] , \qquad b^l = S_{mP}^l \Delta V \Delta \Omega^l$$

5.4. CLAM Scheme

Higher order resolution CLAM scheme (is of second order) expresses the dependent variables (the radiative intensity in the present case) at a cell face as a function of its values present at three neighboring grid nodes (two upstream and one downstream) from the cell face. In this formulation a normalized intensity and a normalized coordinate is defined as

$$\tilde{I} = \frac{I - I_U}{I_D - I_U} \tag{5.23}$$

$$\tilde{x} = \frac{x - x_U}{x_D - x_U} \tag{5.24}$$

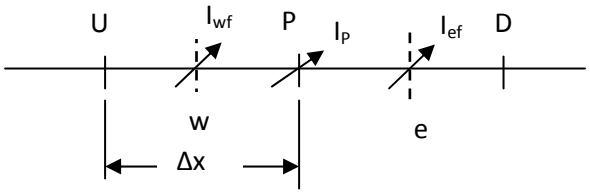

Fig.5.2 The control volume.

At face,

$$\tilde{I}_f = \frac{\left(\tilde{x}_C^2 - \tilde{x}_f\right)}{\tilde{x}_C\left(\tilde{x}_C - 1\right)}\tilde{I}_C + \frac{\left(\tilde{x}_f - \tilde{x}_C\right)}{\tilde{x}_C\left(\tilde{x}_C - 1\right)}\tilde{I}_C^2 \qquad \text{for } 0 < \tilde{I}_C < 1 \qquad (5.25)$$

$$\tilde{I}_f = \tilde{I}_C \qquad \text{elsewhere} \qquad (5.26)$$

For the east face

$$\tilde{I}_e = \frac{\left(\tilde{x}_P^2 - \tilde{x}_e\right)}{\tilde{x}_P\left(\tilde{x}_P - 1\right)}\tilde{I}_C + \frac{\left(\tilde{x}_e - \tilde{x}_P\right)}{\tilde{x}_P\left(\tilde{x}_P - 1\right)}\tilde{I}_C^2 \qquad (5.27)$$

$$I_e = I_P + S_{Ce^+} + S_{Pe^+} I_P \qquad (5.28)$$

where

$$\tilde{x}_P = \frac{x_P - x_W}{x_E - x_W} = 0.5 \qquad \tilde{x}_e = \frac{x_e - x_W}{x_E - x_W} = 0.75 \qquad (5.29)$$

$$S_{Ce^+} = I_E\left(\frac{I_P - I_W}{I_E - I_W}\right) \qquad S_{Pe^+} = -\left(\frac{I_P - I_W}{I_E - I_W}\right) \qquad (5.30)$$

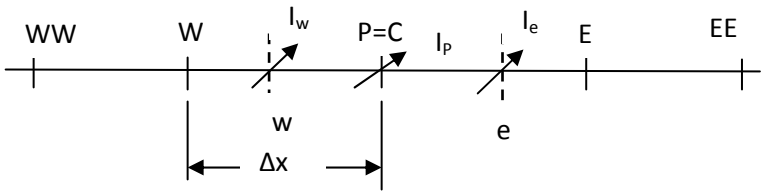

Fig.5.3 Control volume for CLAM scheme (from west to east).

For the west face,

$$\tilde{I}_w = \frac{\left(\tilde{x}_W^2 - \tilde{x}_w\right)}{\tilde{x}_W\left(\tilde{x}_W - 1\right)}\tilde{I}_W + \frac{\left(\tilde{x}_w - \tilde{x}_W\right)}{\tilde{x}_W\left(\tilde{x}_W - 1\right)}\tilde{I}_W^2 \tag{5.31}$$

$$I_w = I_W + S_{Cw^+} + S_{Pw^+} I_P \tag{5.32}$$

where,

$$\tilde{x}_W = \frac{x_W - x_{WW}}{x_P - x_{WW}} = 0.5 \qquad S_{Cw^+} = -I_W\left(\frac{I_W - I_{WW}}{I_P - I_{WW}}\right) \tag{5.33}$$

$$\tilde{x}_w = \frac{x_w - x_{WW}}{x_P - x_{WW}} = 0.75 \qquad S_{Pw^+} = \left(\frac{I_W - I_{WW}}{I_P - I_{WW}}\right) \tag{5.34}$$

For the north face

$$\tilde{I}_n = \frac{\left(\tilde{y}_P^2 - \tilde{y}_n\right)}{\tilde{y}_P\left(\tilde{y}_P - 1\right)}\tilde{I}_P + \frac{\left(\tilde{y}_n - \tilde{y}_P\right)}{\tilde{y}_P\left(\tilde{y}_P - 1\right)}\tilde{I}_P^2 \tag{5.35}$$

$$I_n = I_P + S_{Cn^+} + S_{Pn^+} I_P \tag{5.36}$$

where,

$$\tilde{y}_P = \frac{y_P - y_S}{y_N - y_S} = 0.5\,,\ \tilde{y}_n = \frac{y_n - y_S}{y_N - y_S} = 0.75 \tag{5.37}$$

$$S_{Cn^+} = I_N\left(\frac{I_P - I_S}{I_N - I_S}\right),\ S_{Pn^+} = -\left(\frac{I_P - I_S}{I_N - I_S}\right) \tag{5.38}$$

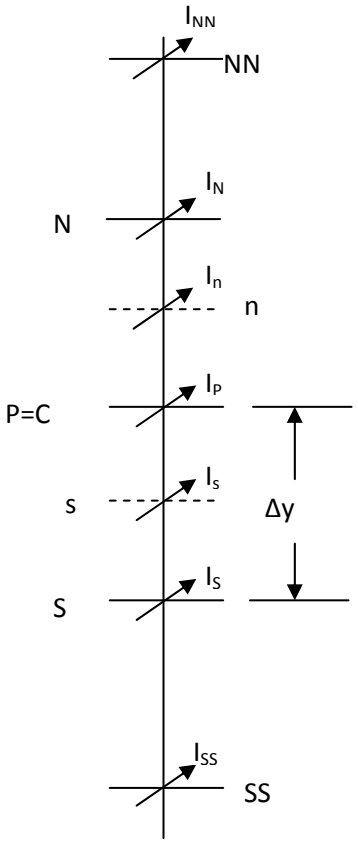

Fig.5.4 Control volume for CLAM scheme (from south to north).

For the south face,

$$\tilde{I}_s = \frac{\left(\tilde{y}_S^2 - \tilde{y}_s\right)}{\tilde{y}_S\left(\tilde{y}_S - 1\right)}\tilde{I}_S + \frac{\left(\tilde{y}_s - \tilde{y}_S\right)}{\tilde{y}_S\left(\tilde{y}_S - 1\right)}\tilde{I}_S^2 \tag{5.39}$$

$$I_s = I_S + S_{Cs^+} + S_{Ps^+} I_P \tag{5.40}$$

where

$$\widetilde{y}_S = \frac{y_S - y_{SS}}{y_P - y_{SS}} = 0.5 \ , \ S_{Cs^+} = -I_S\left(\frac{I_S - I_{SS}}{I_P - I_{SS}}\right) \tag{5.41}$$

$$\widetilde{y}_s = \frac{y_s - y_{SS}}{y_P - y_{SS}} = 0.75 \ , \ S_{Ps^+} = \left(\frac{I_S - I_{SS}}{I_P - I_{SS}}\right) \tag{5.42}$$

After substituting the boundary intensities in terms of nodal intensities, we may end up with negative intensity which is physically not acceptable. To avoid such unphysical situation during the iteration procedure an overall positive variable treatment from Patankar (1991) is adopted. After the treatment, the discretization equation becomes

$$\left[\left[D_{cy} + D_{cy}\left(\frac{S_{cn^+} - S_{cs^+}}{I^l_{P^*}}\right)\right]\times\left(\frac{1}{\beta}\right) + \beta_m \Delta V \Delta\Omega + \frac{\Delta V \Delta\Omega}{\Delta t^*}\right] I^l_P = D_{cy}\left(\frac{I_S}{\beta}\right) - D_{cy}\left(S_{Pn^+} - S_{Ps^+}\right) I^l_{P^*} + S_{mP}\Delta V\Delta\Omega + \frac{\Delta V\Delta\Omega}{\Delta t^*} I^{lo}_P \tag{5.43}$$

Similar procedure is adopted for the other two faces intensities.

The south boundary of the computational domain is subjected to a collimated irradiation with square as well as Gaussian pulse distribution. The radiation intensity incident on the south boundary is given by Eqs. (3.9-3.11).

Chapter-6

Results and Discussion

(Two-Dimensional Problem)

6.1. Introduction

In this chapter the numerical results for the transmitted flux and reflected flux for a two dimensional participating medium (Fig.5.1 (a) and Fig.6.1), subjected to short pulse collimated radiation, are discussed. The effects of different properties like optical and geometrical properties are also analyzed. Both isotropic scattering and linearly anisotropic scattering medium (with forward scattering and backward scattering) are considered. The transient radiative transfer equation has been solved using both STEP and CLAM schemes.

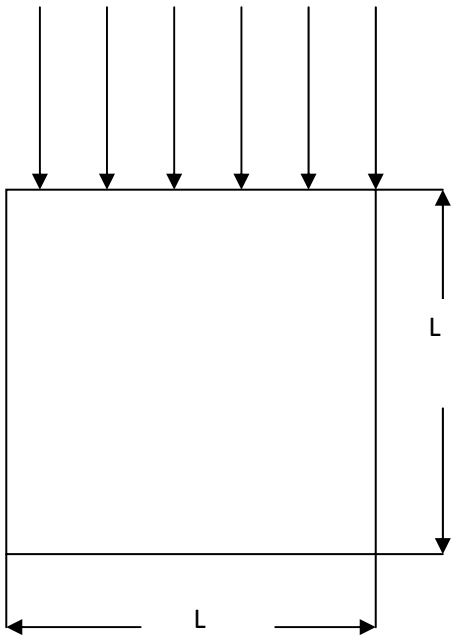

Fig.6.1 Computational domain.

6.2. Validation of the 2-D model for steady radiation

Figure 6.2 shows a schematic of a problem studied by Kim and Lee (1989), so chosen to show the ability of the present procedure to model problems with collimated incidence for steady radiation. The top wall of the black enclosure (Fig.6.1) is subjected to a normal collimated beam. The other walls are maintained at 0 K and the medium is considered to be isotropically scattering with a scattering albedo of unity. The domain is divided into 25 × 25 uniform control volumes and 9 × 5 control angles in θ and φ directions. The collimated radiation is captured by adjusting the control angle and the actual intensity is solved by using the STEP scheme. A good agreement is observed between the discrete ordinate solution of Kim and Lee (1989) and the present computation, as shown in Fig. 6.2.

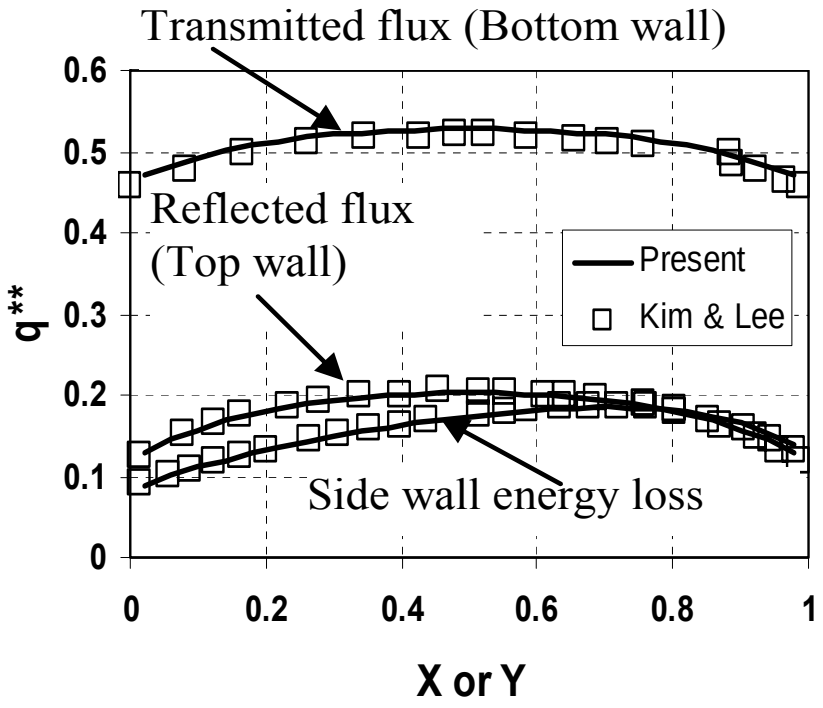

Fig.6.2 Comparison of dimensionless heat flux between the present method and Kim and Lee (1989).

6.3. Effect of incidence angle

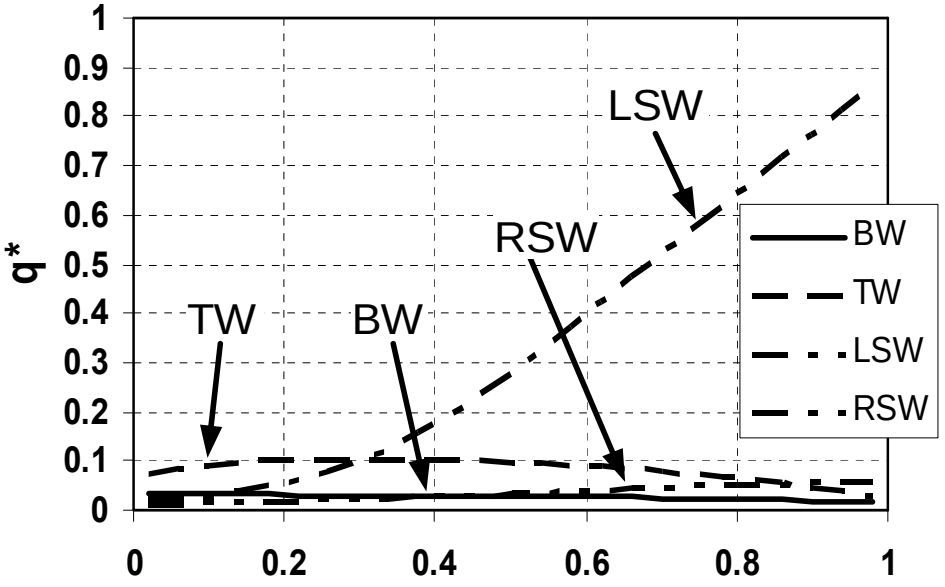

(a)

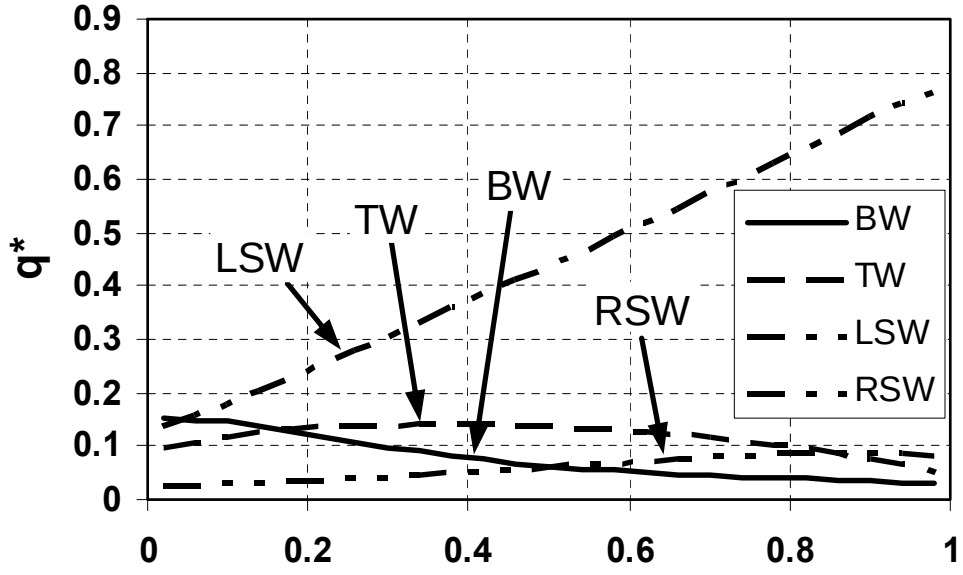

(b)

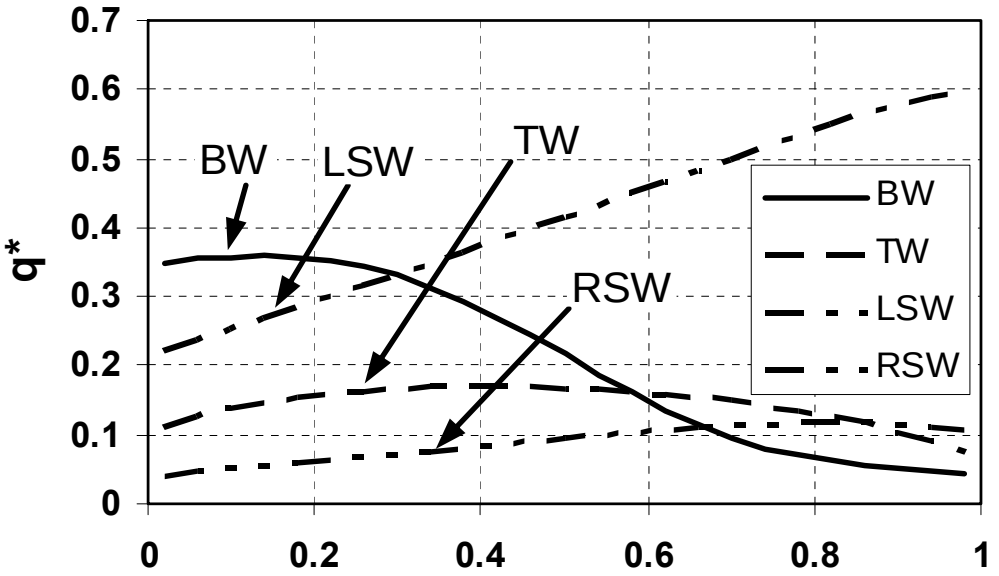

(c)

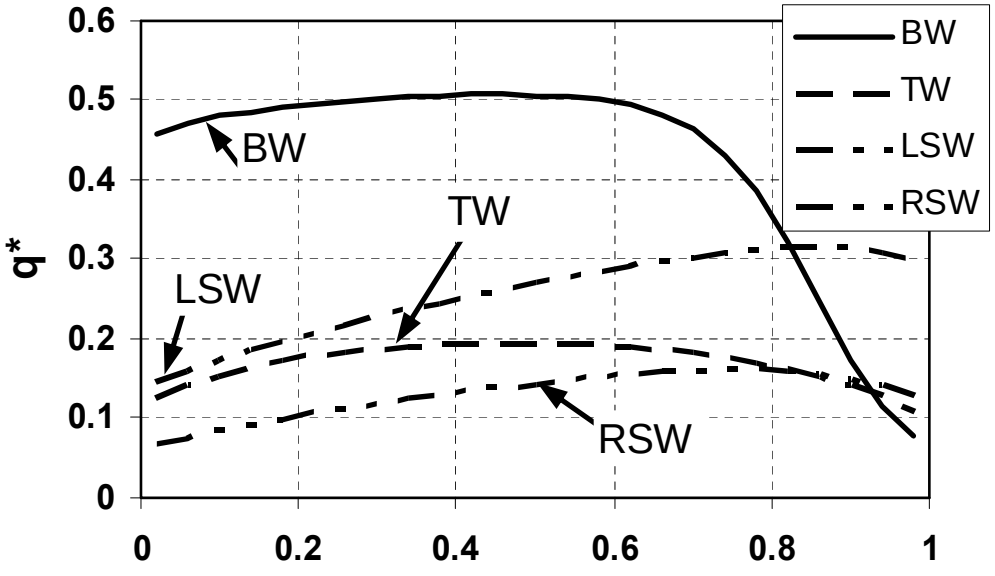

(d)

Fig.6.3 Reflected and Transmitted flux at top wall and bottom wall, the side wall energy loss at different incidence angles a) 210° b) 225° c) 240° d) 260°.

The variation of reflected flux, transmitted flux and side wall energy loss on different walls are shown in Figs. 6.3(a, b, c, d) for the collimated radiation at different incidence angles. As seen from the figure, the reflected flux changes a little with the incidence angle. The transmitted flux on the other hand, varies substantially with the incidence angle. The transmitted flux increases considerably with increase in incidence angle. The side energy loss curve however is of different nature. It shows that with the increase in incidence angle, the energy loss, which is accountably high towards the top, gradually reduces.

6.4. Effect of Transient radiation

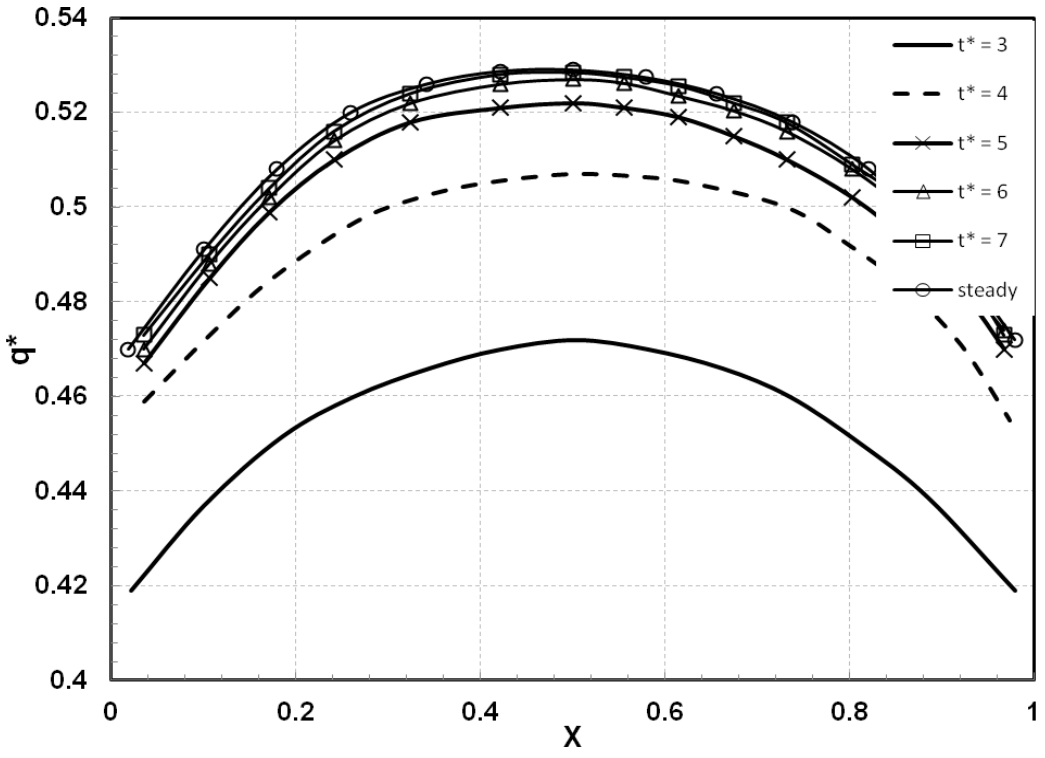

(a)Transmitted flux for Transient Radiation.

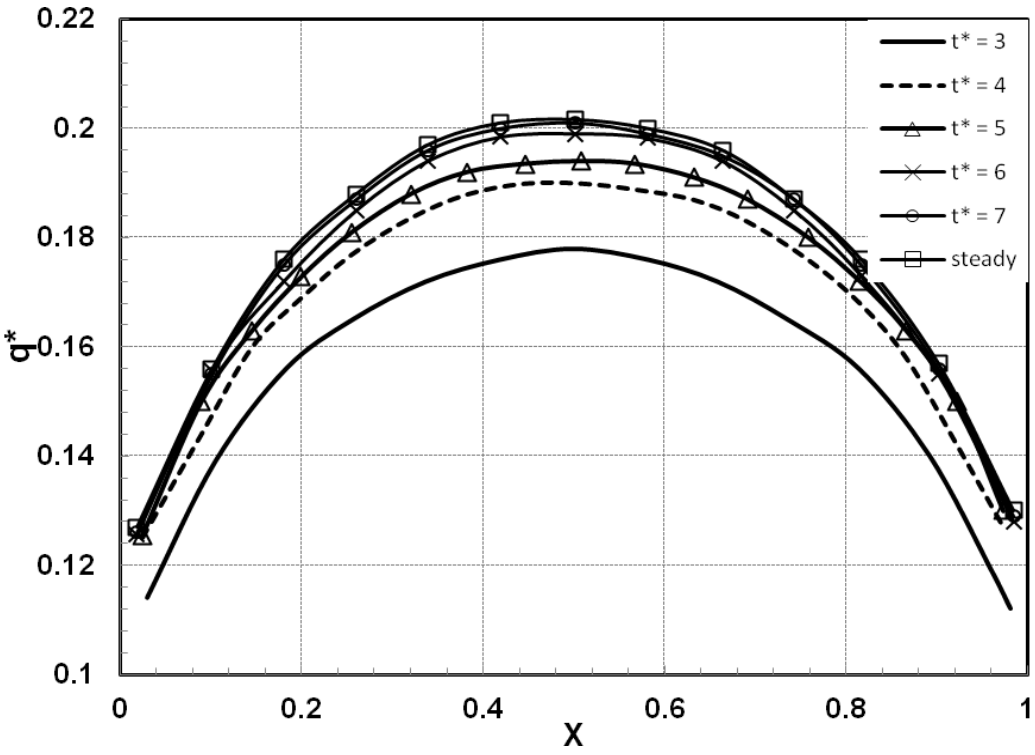

(b) Reflected flux for Transient Radiation.

Fig. 6.4 Validation of the two-dimensional model for transient radiation with all four black and cold walls with pure isotropic scattering.

Figures 6.4 (a) and (b) represent how the transmitted flux and reflected flux reach the steady state from transient state. As it is seen from the Figs. 6.4(a) and (b) that, when the non-dimensional time reaches to approximately 7, both transmitted flux and reflected flux gradually attain the steady state.

6.5. Validation for transient radiation

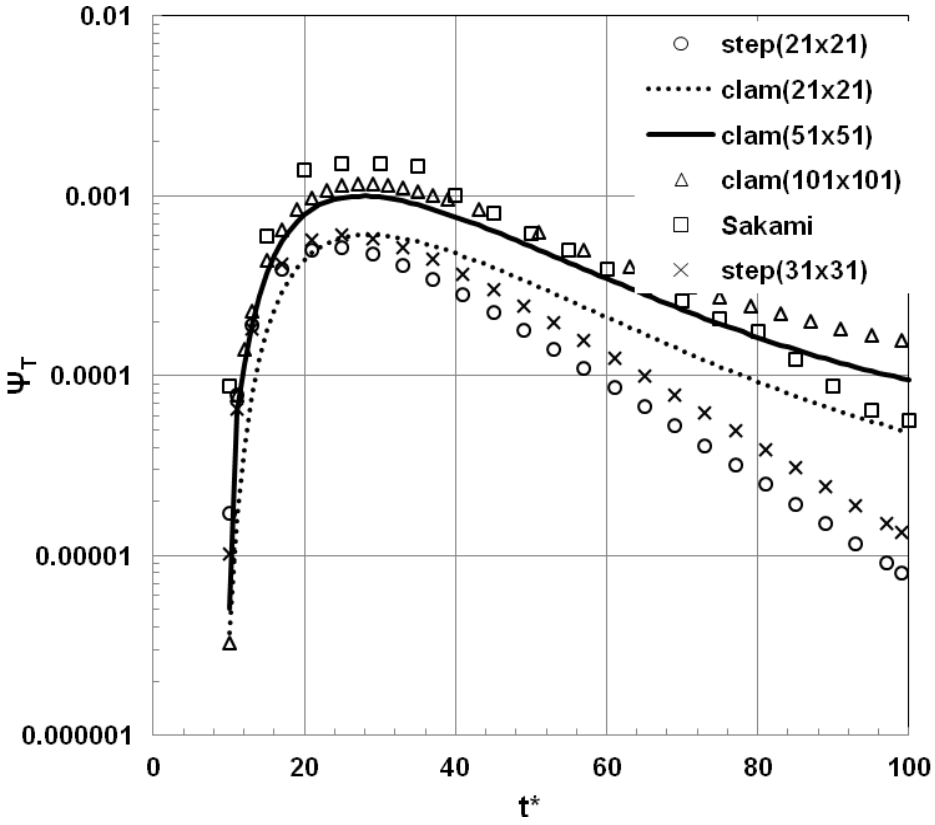

Fig.6.5 Grid Independence Test.

A grid independence test and comparison with available existing solution (Sakami et al., 2002) was performed with different spatial and angular grid sizes. It is observed that further refinement to the grid size of 51×51 control volumes and 9×5 control angles (polar and azimuthal angle) results in negligible change in the results as seen from Fig. 6.5, where the present method has been compared with the DOM used by Sakami et al. (2002) with optical thickness as 10, scattering albedo to be 0.998 and non-dimensional pulse width equals to 1. Although the grid test for non-dimensional time interval sizes is not shown, it is found that the time interval size of 0.01 is producing the optimum results

without any significant alteration. In grid independence test, it is found that there is about 38% change from grid size of 21×21 to 51×51 and about 11% change occurred from 51×51 to 101 × 101 grid sizes. Henceforth, the above grid size for space and time step are used for further presentation of results.

Table-6.1: Transmittance values at different grid sizes for STEP and CLAM schemes.

TIME STEP	TRANSMITTANCE			
	STEP (21×21)	CLAM (21×21)	CLAM (51×51)	CLAM (101×101)
1.00E+00	0.00E+00	0.00E+00	0.00E+00	0.00E+00
1.00E+01	1.73E-05	3.72E-06	5.08E-06	3.27E-06
2.00E+01	4.82E-04	4.41E-04	7.86E-04	9.13E-04
3.00E+01	4.61E-04	6.05E-04	9.84E-04	1.16E-03
4.00E+01	2.96E-04	4.80E-04	7.66E-04	9.22E-04
5.00E+01	1.69E-04	3.26E-04	5.23E-04	6.51E-04
6.00E+01	9.21E-05	2.12E-04	3.47E-04	4.51E-04
7.00E+01	4.95E-05	1.38E-04	2.33E-04	3.21E-04
8.00E+01	2.64E-05	9.25E-05	1.64E-04	2.39E-04
9.00E+01	1.41E-05	6.51E-05	1.21E-04	1.87E-04
1.00E+02	7.49E-06	4.86E-05	9.48E-05	1.55E-04

6.6. Performance of STEP and CLAM scheme

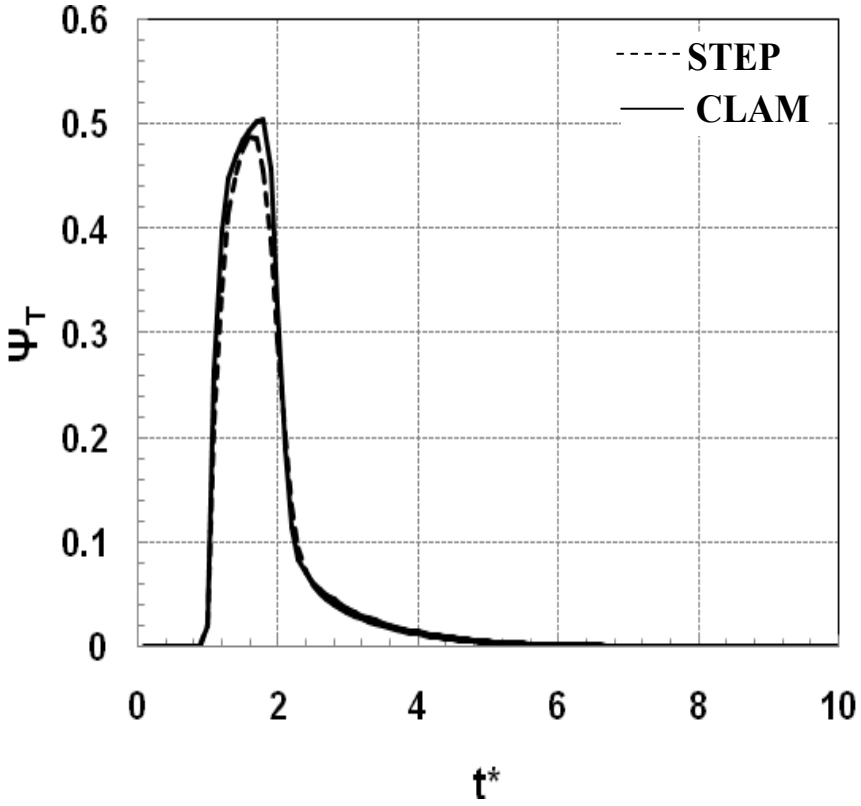

(a) Transmittance with $\tau = 1.0$, $a = 0.9$, $\omega = 1.0$, $\varepsilon_s = 0.25$.

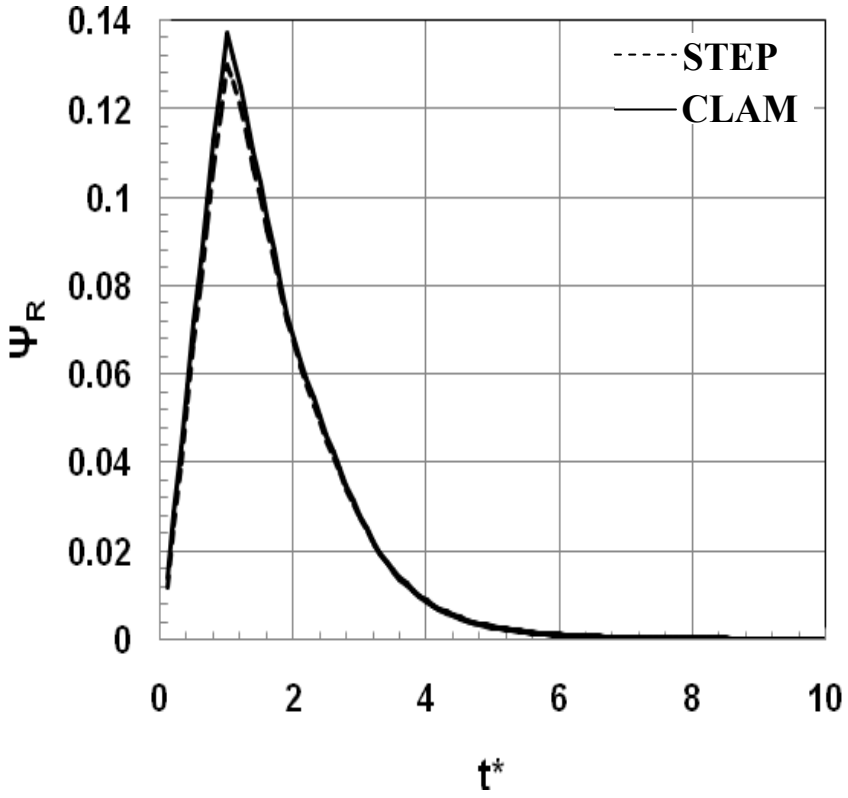

(b) Reflectance with $\tau = 1.0$, $a = 0.9$, $\omega = 1.0$, $\varepsilon_S = 0.25$.

Fig. 6.6 Performance of STEP and CLAM scheme.

For all the cases considered, effects are examined with two different spatial differencing schemes such as STEP and CLAM scheme. Figures 6.6(a) and (b) represent two particular cases examined for the performance of both the schemes taking the same optimized grid size of 51×51 control volumes and 9×5 control angles (polar and azimuthal angle) as concluded from section 6.5. From both the graphs it is observed that the CLAM scheme gives more accurate result as compared to the STEP scheme. Therefore, the results with CLAM scheme are presented.

6.7. Effect of reflective wall

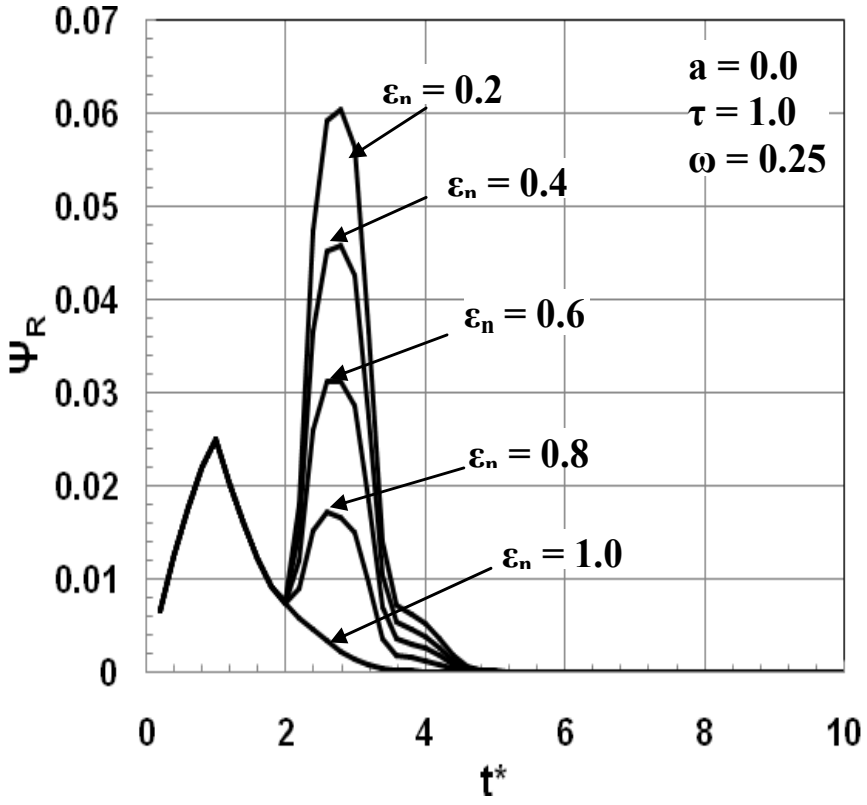

Fig. 6.7 (a) Effect of gray north wall and other black walls on Reflectance for *a* = 0.0 with τ = 1.0, ω = 0.25.

As seen from Fig. 6.7, for a given scattering albedo, as emissivity of the wall increases and approaches the value 1 (i.e. black wall), multiple maxima of reflectance curve gradually disappear. This indicates that as the north wall becomes more reflective, the peak value of secondary maxima is increasing because of the cumulative effect of reflected radiation from the wall as well as the scattering radiation from the medium. Comparing both the reflectance curve for isotropic and linearly anisotropic scattering medium as shown in Fig. 6.7 (a) and (b), there is a significant decrease in magnitude of peak value till the pulse reaches the opposite wall when the medium becomes strongly

forward scattering. This is due to more scattering in the direction of the collimated irradiation. After the pulse is switched off, the reflectance signal starts dying out from the medium for the black wall case. Again as a result of reflection from the wall and their scattering in the respective direction produces a small increase in the peak value of secondary maxima (Fig. 6.7 (b)) which broadens the reflectance curve.

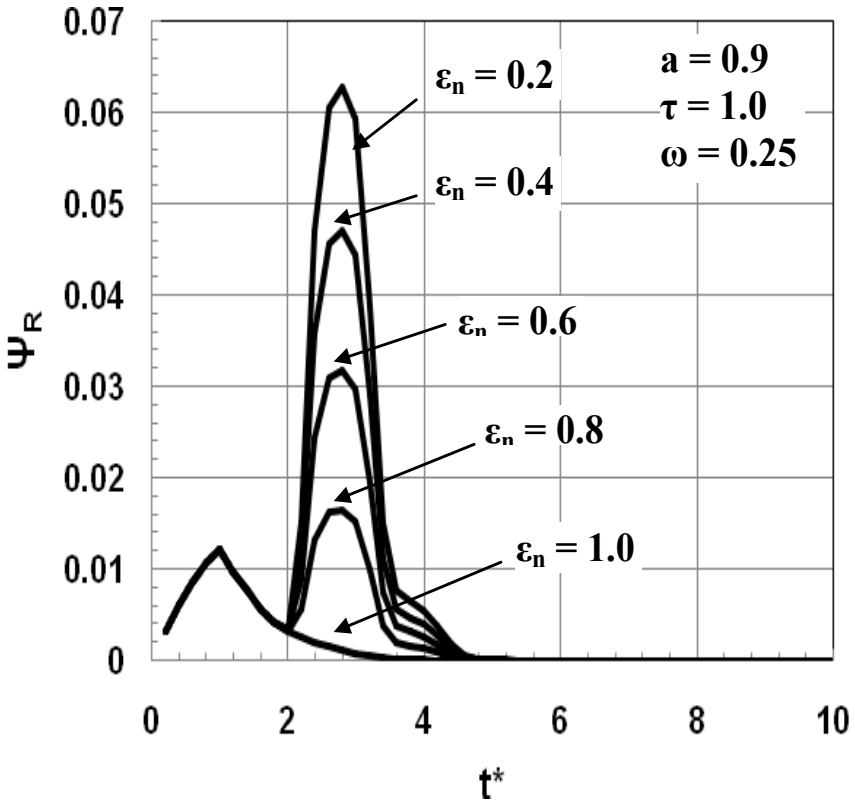

Fig. 6.7 (b) Effect of gray north wall and other black walls on Reflectance for a = 0.9 with τ = 1.0, ω = 0.25.

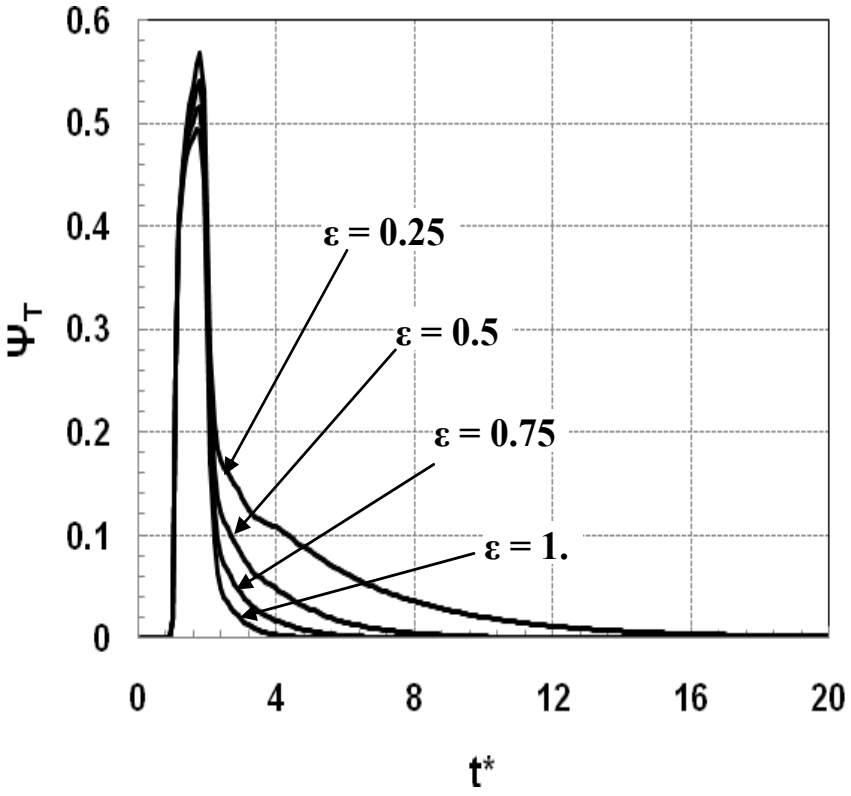

Fig.6.8 (a) Effect of all gray walls on transmittance for **τ = 1.0, *a* = 0.9, ω = 1.0.**

Figures 6.8 (a) and (b) represent how the wall emissivity affects the temporal variation of transmittance and reflectance in the presence of anisotropic scattering medium. As seen from Fig. 6.8 (a) the magnitude of transmittance increases with decrease in emissivity of the walls and also the transmittance signal remains for longer time as there is more radiative interaction in the medium. The rate of decrease of transmittance with time after the pulse leaves the medium gradually reduces, as a result of gray walls and forward scattering medium. A different feature is revealed from the reflectance curve (Fig. 6.8 b), as compared to the transmittance graph. There are multiple maxima appearing when the walls are increasingly reflective whereas the secondary maxima vanishes in case of the black walls. This is due to the interaction of the gray walls with the anisotropically scattering medium which causes multiple maxima to appear. The back scattered flux gets

added to the reflectance in case of gray wall and as a combined effect of the flux reflected from the gray wall and scattered medium flux, the reflected flux again reaches to the second maxima. The reflected flux starts reducing once the pulse is switched off.

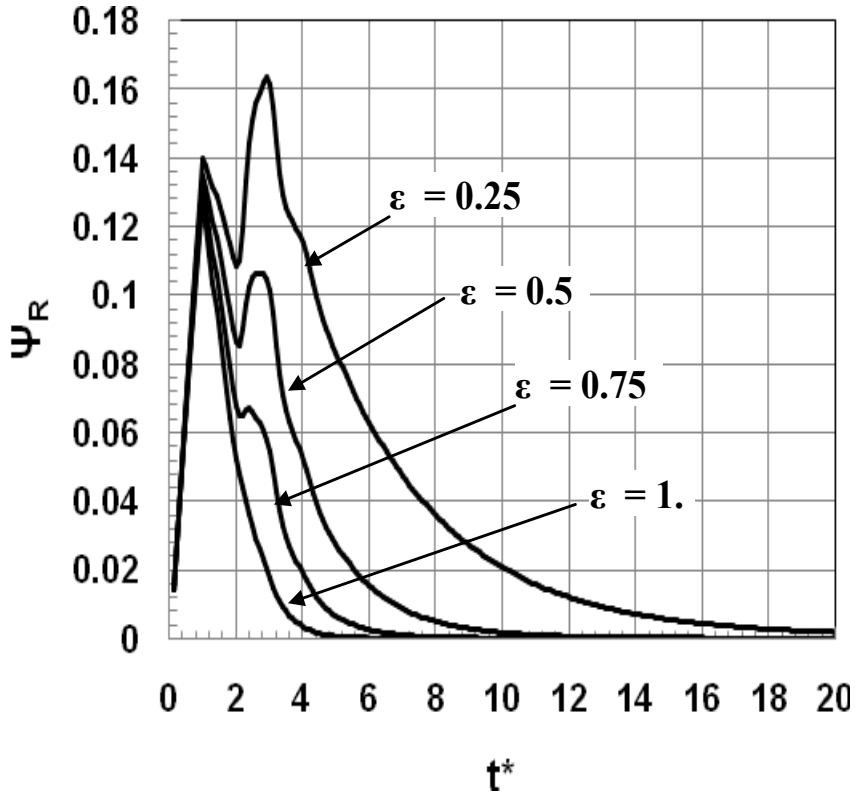

Fig.6.8 (b) Effect of all gray walls on reflectance for τ = 1.0, *a* = 0.9, ω = 1.0.

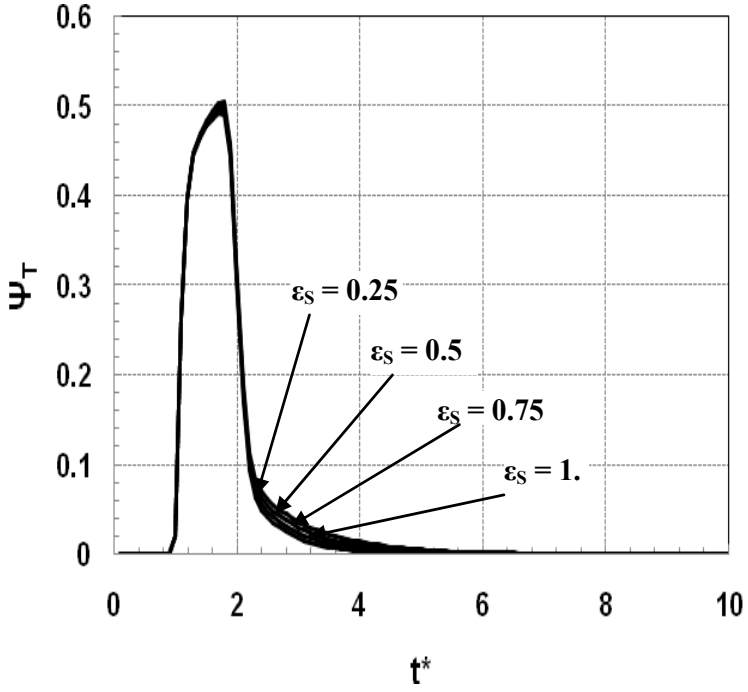

Fig.. 6.9 (a) Effect of gray south wall and other black walls on transmittance with τ = 1.0, a = 0.9, ω = 1.0.

Figures 6.9 (a) and (b) show the influence of anisotropic scattering and wall emissivity on the temporal variation of transmittance and reflectance when the south wall (the wall subjected to collimated radiation) becomes gray and all other walls are black. In case of smaller emissivity of wall, the transmittance signal remains for longer duration as there is more radiative interaction in the medium. This can be easily observed from the different time rate of decrease of transmittance after the pulse leaves the medium.

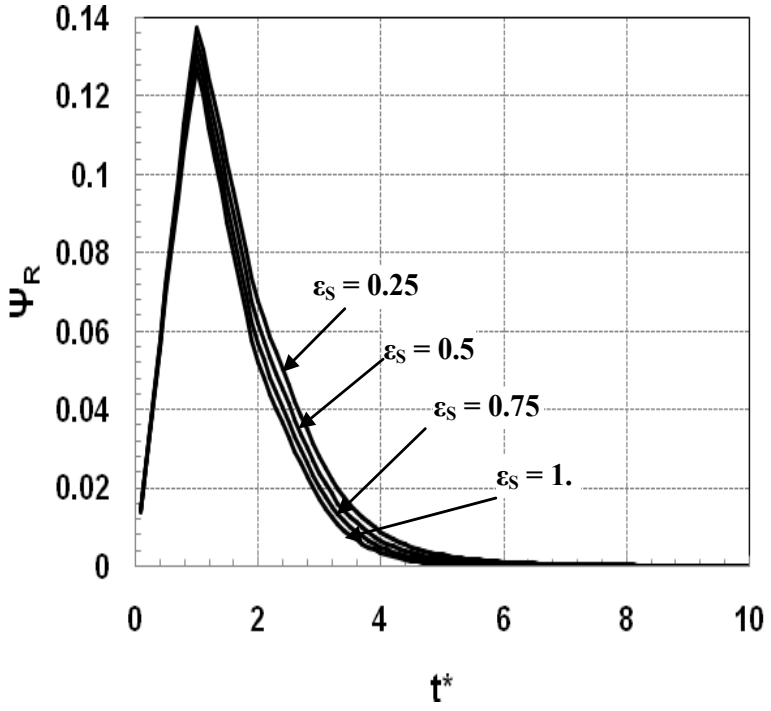

Fig.6.9 (b) Effect of gray south wall and other black walls on reflectance for with τ = 1.0, a = 0.9, ω = 1.0.

As seen from the reflectance curve (Fig. 6.9 b), there is a little variation in the peak value. The broadening of curve with decrease in wall emissivity indicates that the signal is relatively significant even after the pulse is switched off. This is due to the effect of the gray south wall and the forward scattering medium. Forward scattering increases the maximum value of the transmitted peaks, whereas there is no significant change in the maximum value of reflectance. The observations from the figures are in accordance with the isotropic scaling rule, which states that forward scattering can be scaled into isotropic scattering with a smaller scattering coefficient while backward scattering can be modeled by isotropic scattering with an increased scattering coefficient.

6.8. Effect of optical thickness

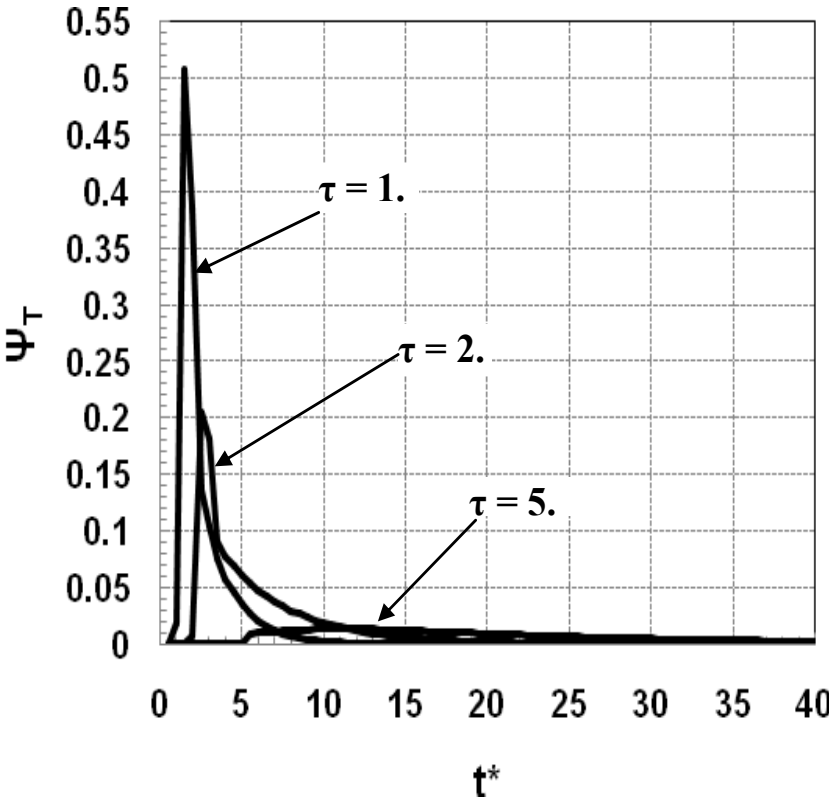

Fig. 6.10(a) Effect of optical thickness on transmittance for a = 0.0, $\varepsilon_e = \varepsilon_w = \varepsilon_n$ = 0.25, ε_s = 1.0 and ω = 1.0.

Figures 6.10 (a) and (b) present the influence of optical thickness on transmittance and reflectance when all the boundary walls are gray except the wall subjected to irradiation. As expected, the magnitude of transmitted signal goes on reducing with increased optical thickness. As the pulse leaves, transmittance signal will tend to leave the medium much faster when the optical thickness of the medium is less. As it is observed from Fig. 6.10 (b), there are multiple maxima disappearing with increased optical thickness which indicates the dominance of optical thickness over the wall emissivity. The interesting features observed here are that the magnitude of reflectance reduces sharply in case lower

optical thickness because higher optical thickness allows radiative interaction in the medium for a longer duration.

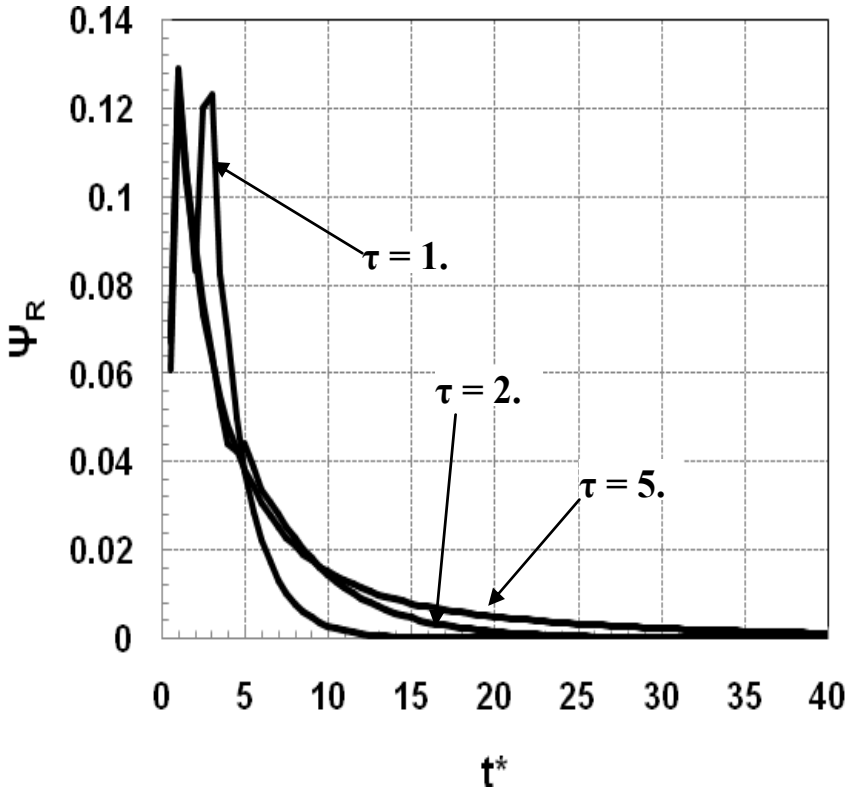

Fig. 6.10 (b) Effect of optical thickness on reflectance for a = 0.0, $\varepsilon_e = \varepsilon_w = \varepsilon_n$ = 0.25, ε_s = 1.0 and ω = 1.0

6.9. Effect of scattering albedo

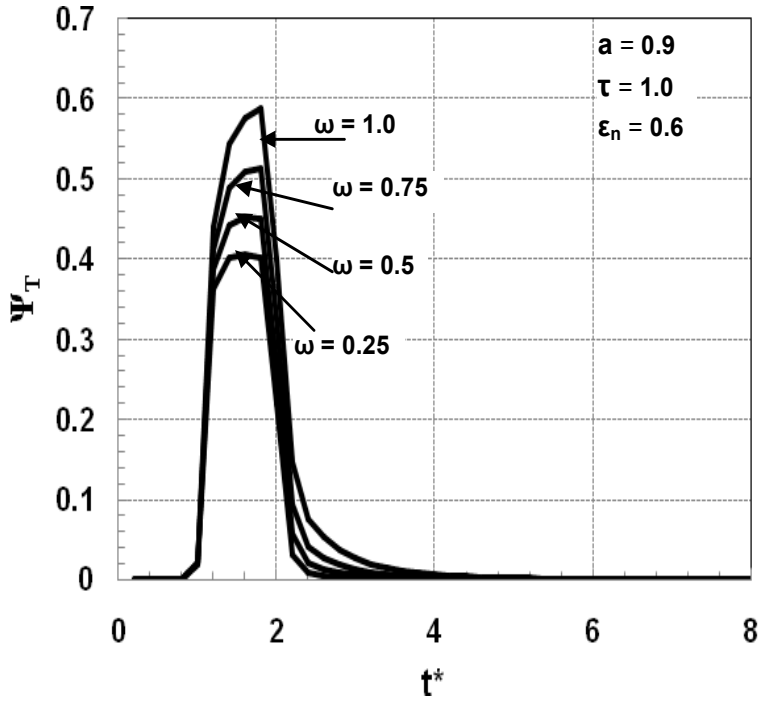

Fig. 6.11 (a) Effect of scattering albedo on transmittance for a = 0.9, $\varepsilon_e = \varepsilon_w = \varepsilon_s$ = 1.0, ε_n = 0.6.

Figure 6.11 represents the effect of scattering albedo on transmittance and reflectance with gray north wall. From Fig. 6.11 (a), it is observed that the magnitude of transmittance goes on increasing with the increased scattering albedo because of more and more scattering in the medium. Also as there is more radiative interaction in the medium, the transmittance signal continue to emerge out for longer duration for higher scattering albedo even after the pulse has left the medium. Figure 6.11 (b) indicates about the different features of reflectance curve as the irradiation passes through the anisotropically scattering medium. Multiple maxima seen in Fig. 6.11 (b) are due to the net result of strongly forward scattering medium and reflective wall. As the medium is

strongly forward scattering, the reflected radiation from the wall is scattered more in its direction of propagation. This is the cause for the magnitude of the peak of secondary maxima to continuously increase with large value of scattering albedo. The reason for the magnitude of primary maxima to be increased is due to the sole effect of scattering of collimated irradiation in the anisotropically scattering medium.

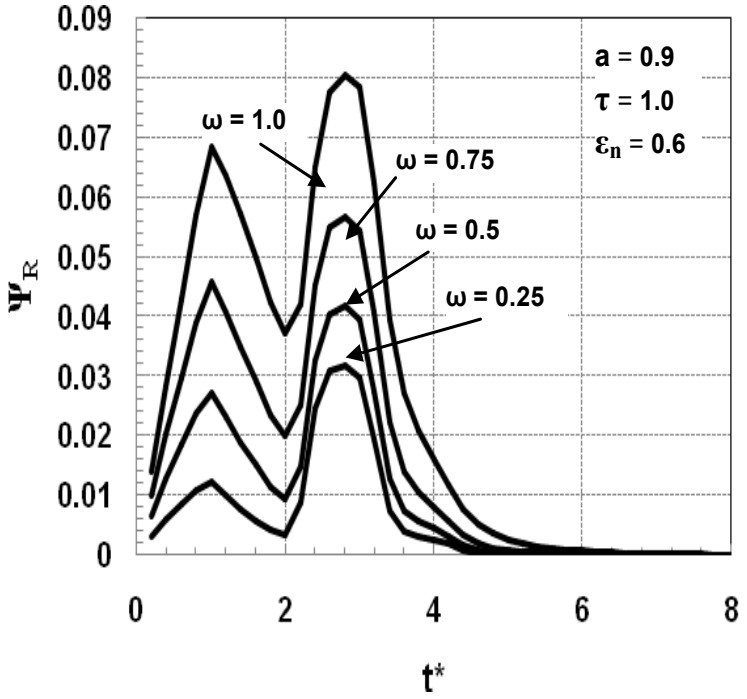

Fig. 6.11 (b) Effect of scattering albedo on reflectance for a = 0.9, $\varepsilon_e = \varepsilon_w = \varepsilon_s = 1.0$, $\varepsilon_n = 0.6$.

6.10. Effects of emissivity

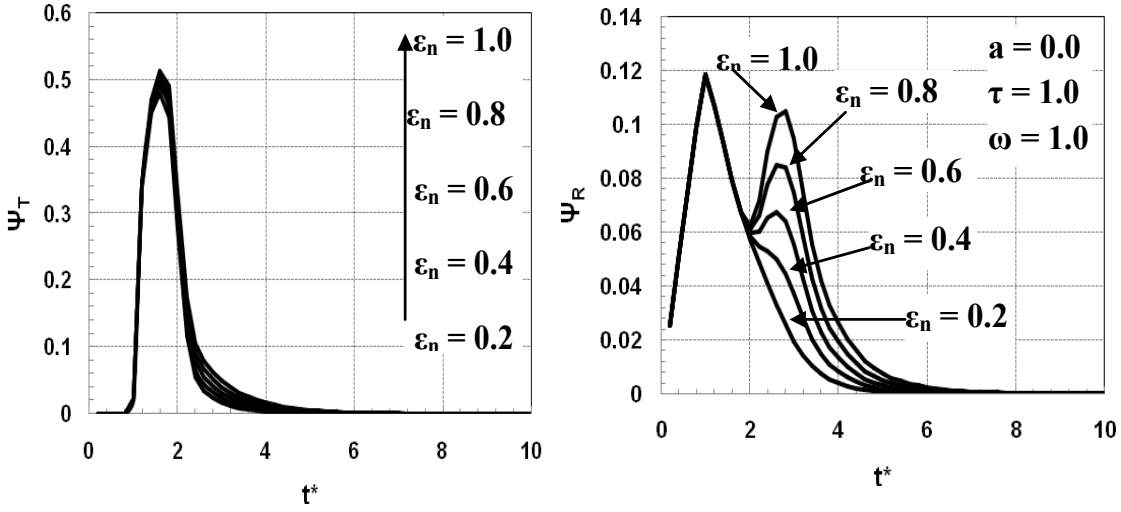

(a) **(b)**

Fig. 6.12 Effect of emissivity on (a) transmittance and (b) reflectance for $\tau = 1.0$, a = 0.0, $\omega = 1.0$.

Figures (6.12), (6.13), (6.14) and (6.15) represent the effects of emissivity on the transmittance and reflectance for different values of scattering albedo ranging from 1.0 to 0.25 when the media is isotropically scattering. There is a significant decrease in the peak value of reflectance curve as the scattering albedo decreases. This is due to the fact that, as scattering of the collimated radiation reduces, the amount of flux reaching the opposite wall also reduces. The first interesting feature observed here is that for increasing value of scattering albedo, the peak value of secondary maxima for reflectance goes on increasing even though there is a negligible change in the peak value of primary maxima. The second interesting feature is that the magnitude of peak value of primary maxima is reduced as compared to that of the secondary maxima. These two features observed are mostly due to the order of change of emissivity. Also an increase in

temporal broadening is noticed in the reflectance curve for increasing value of emissivity. The secondary maxima vanishes as the emissivity of the wall goes on decreasing. The change in the maximum value of transmittance is very marginal even though there is an increment in emissivity.

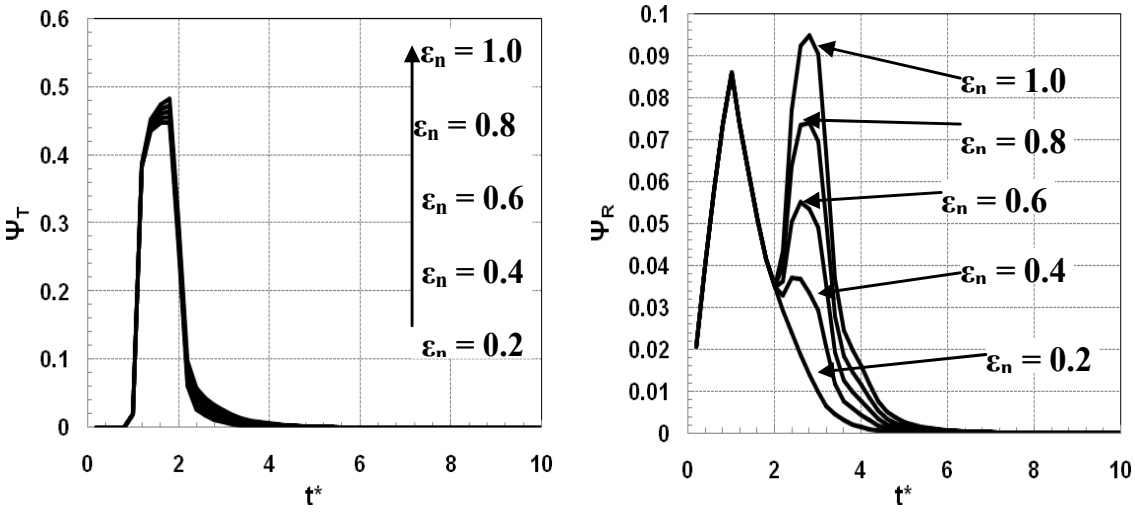

(a) **(b)**

Fig. 6.13 Effect of emissivity on (a) Transmittance and (b) Reflectance for $\tau = 1.0$, $a = 0.0$, $\omega = 0.75$.

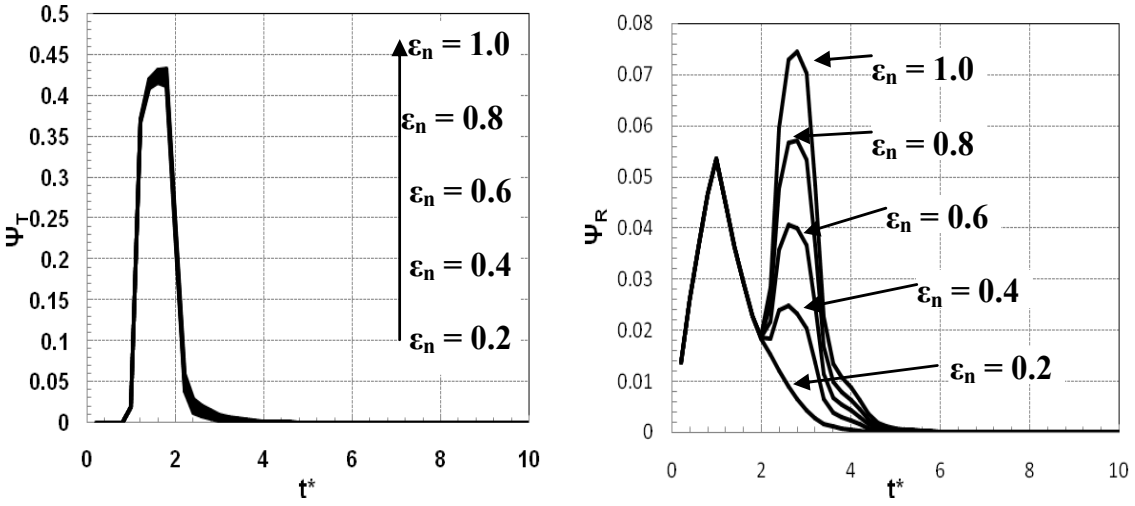

(a) **(b)**

Fig. 6.14. Effect of emissivity on (a) Transmittance and (b) Reflectance for $\tau = 1.0$, $a = 0.0$, $\omega = 0.5$.

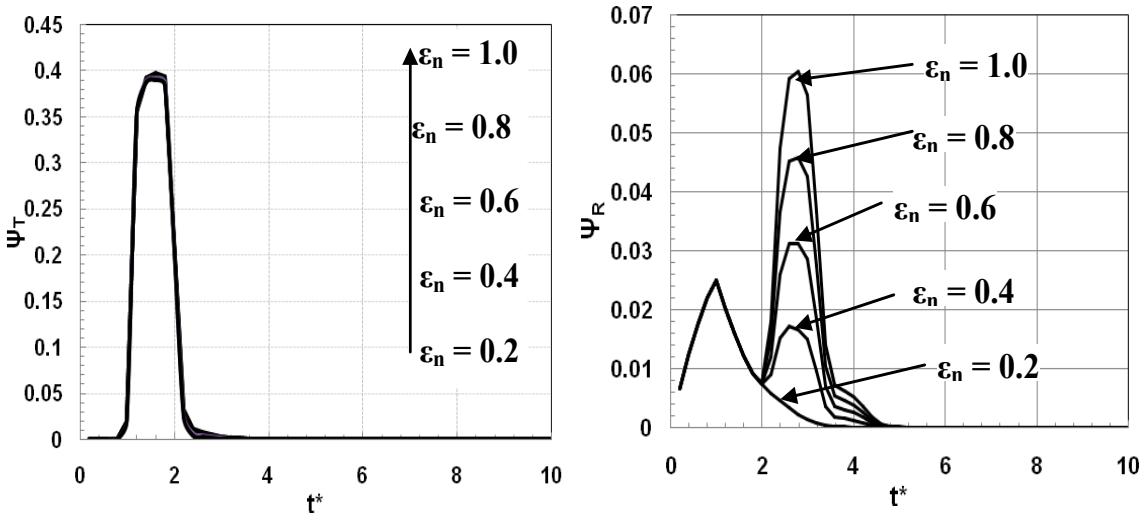

(a) **(b)**

Fig.6. 15. Effect of emissivity on (a) Transmittance and (b) Reflectance for $\tau = 1.0$, $a = 0.0$, $\omega = 0.25$.

Chapter-7

Conclusions and Scope for Future Work

Conclusions and Scope for Future Work

A numerical investigation on the collimated radiation passing through a participating medium has been successfully carried out to analyze the unique features of transient radiation involved in the process. General conclusions that stemmed from this analysis are presented here, together with a brief recapitulation of some of the important remarks made earlier.

7.1. Conclusions

From the present investigation, we can draw the conclusions as follows:

- In the proposed approach, one does not have to split the intensity of radiation into diffused and collimated part.
- Transmittance decreases with increase in optical thickness, whereas a reverse trend is observed with scattering albedo.
- As a result of forward scattering, transmitted pulse peak is enhanced but the pulse width is reduced whereas the backward scattering decreases the transmitted pulse peak but augments the pulse width.
- For a particular optical thickness, as the boundary emissivity decreases, two local maxima are appearing in reflectance variation due to reflective wall condition.

- However, the secondary maxima appeared vanishes as the scattering albedo is either increased or decreased.
- Moreover, transmittance signal is quite stronger even after the pulse is switched off, when the boundary becomes more gray.
- Both the schemes (STEP and CLAM) give almost similar predictions in case of one-dimensional problem although CLAM scheme gives more accurate results than the STEP scheme in case of the two-dimensional problem.

7.2. Scope for Future Work

The proposed formulation is believed to be capable of solving a class of radiative heat transfer problems in participating media and can be easily extended to more complicated problems. The suggested numerical method may be beneficial in solving three-dimensional homogeneous as well as non-homogeneous participating media. The finite volume method may also be extended to refine the solution taking other higher order schemes like SMART etc. The problem may also be solved with a series of pulses. The same can be extended to one, two and three-dimensional problems with temperature dependent optical properties.

Bibliography

Bibliography

1. Altac, Z., (2002), "The SK_N Approximation for Solving Radiative Transfer Problems in Absorbing, Emitting, and Linearly Anisotropically Scattering Plane-Parallel Medium: Part 2", ASME Journal of Heat Transfer, **124**, pp. 685-695.
2. Altaç, Z., (2002), "Radiative transfer in one-dimensional hollow cylindrical geometry with anisotropic scattering and variable medium properties", International Journal of Heat and Mass Transfer, **45**, pp. 5239-5242.
3. Altaç, Z., and Tekkalmaz, M., (2004), "Solution of the radiative integral transfer equations in rectangular participating and isotropically scattering inhomogeneous medium", International Journal of Heat and Mass Transfer, **47**, pp. 101-109.
4. An, W., Ruan, L. M., Tan, H P, Qi, H., and Lew, Y. M., (2007), "Finite element simulation for short pulse light radiative transfer in homogeneous and non-homogeneous media", ASME Journal of heat transfer-ASME, **129**, pp. 353-362.
5. An, W., Ruan, L. M., Tan, H. P., and Qi, H. (2006), "Least-Squares Finite Element Analysis for Transient Radiative Transfer in Absorbing and Scattering Media", ASME Journal of Heat Transfer, **128**, pp. 499-503.
6. An, W., Ruan, L., Qi, H., and Liu, L., (2005), "Finite element method for radiative heat transfer in absorbing and anisotropic scattering media", Journal of Quantitative Spectroscopy and Radiative Transfer, **96**, pp. 409-422.
7. Asllanaj, F., Parent, G., Jeandel, G., (2007), "Transient radiation and conduction heat transfer in a gray absorbing - emitting medium applied on two - dimensional complex shaped - domains", Numerical Heat Transfer, Part-B, Fundamentals, **52**, pp.179-200.
8. Baek, S. W., Byun, D. Y., and Kang, S. J., (2000), "The combined Monte-Carlo and finite-volume method for radiation in a two-dimensional irregular geometry", International Journal of Heat and Mass Transfer, **43**, pp. 2337-2344.
9. Beck, T. J., Beyer, W., Pongratz, T., Stummer, W., Waidelich, R., Stepp, H., et al. (2003). "Clinical determination of tissue optical properties in vivo by spatially resolved reflectance measurements", Proceedings of SPIE, **5138**, pp. 96-105.

10. Bianco, N, Manca, O., Naso, V I., (2001), "Transient conductive–radiative numerical analysis of multilayer thin films heated by different laser pulses", International Journal of Thermal Sciences, **40**, pp. 959-968.

11. Brewster, M. Q., and Yamada, Y., (1995), "Optical properties of thick, turbid media from picosecond time-resolved light scattering measurements", Science, **38**, pp. 2569-2581.

12. Byun, D., (2004), "Radiative heat transfer in discretely heated irregular geometry with an absorbing, emitting, and anisotropically scattering medium using combined Monte-Carlo and finite volume method", International Journal of Heat and Mass Transfer, **47**, pp. 4195-4203.

13. Cha, H., Song, T.-H., (2000), "Discrete Ordinates Interpolation Method Applied to Irregular Three-Dimensional Geometries", ASME Journal of Heat Transfer, **122**, pp. 823-827.

14. Chai, J. C. (2003), "One-dimensional transient radiation heat transfer modeling using a finite-volume method", Numerical Heat Transfer, Part B, **44**, pp. 187-208.

15. Chai, J. C., Lee, H. S., and Patankar, S. V., (1994), "Finite volume method for Radiation Heat Transfer", Journal of Thermophysics and Heat Transfer, **8**, pp. 419-425.

16. Chai, J. C., Parthasarathy, G., Lee, H. S., and Patankar, S. V. (1994). A Finite-Volume "Radiation Heat Transfer Procedure for Irregular Geometries", 6th AIAA-JASME Joint Thermophysics and Heat Transfer Conference, June 20-23, 1994.

17. Chai, J., (2004), "Transient radiative transfer in irregular two-dimensional geometries", Journal of Quantitative Spectroscopy and Radiative Transfer, **84**, pp. 281-294.

18. Chai, J. C., and Rath, P. (2006). "Discrete-Ordinates and Finite-Volume Methods for Radiation Heat Transfer", Treatment of Thermal Radiation in Heat Transfer Problems, IIT, Guwahati, pp. 1-15.

19. Cheng, Q., Zhou, H-C., (2007), "The DRESOR Method for a Collimated Irradiation on an Isotropically Scattering Layer", ASME Journal of Heat Transfer, **129**, pp. 634-645.

20. Chui, E. H., Hughes, P. M., and Raithby, G. D., (1992), "Prediction of radiative transfer in cylindrical enclosures with the finite volume method", Journal of Thermophysics and Heat Transfer, **6**, pp. 605-611.

21. Coelho, P. J., (2002), "Bounded Skew High-Order Resolution Schemes for the Discrete Ordinates Method", Journal of Computational Physics, **175**, pp. 412-437.

22. Coelho, P. J., (2004), "A modified version of the discrete ordinates method for radiative heat transfer modeling", Computational Mechanics, **33**, pp. 375-388.

23. Coelho, P. J., and Carvalho, M. G., (1997), "A Conservative Formulation of the Discrete Transfer Method", ASME Journal of Heat Transfer, **119**, pp. 118-128.

24. Coelho, P., and Aelenei, D., (2008), "Application of high-order spatial resolution schemes to the hybrid finite volume/finite element method for radiative transfer in participating media", International Journal of Numerical Methods for Heat and Fluid Flow, **18**, pp. 173-184.

25. Condiff, D. W., (1987), "Anisotropic scattering in three-dimensional differential approximation for radiation heat transfer", International Journal of Heat and Mass Transfer, **30**, pp 1371-1380.

26. Crosbie, A. L., and Schrenker, R. G. (1984), "Radiative transfer in a two-dimensional rectangular medium exposed to diffused radiation", Journal of Quantitative Spectroscopy and Radiative Transfer, **31**, pp. 339-372.

27. Cui, X. Li, B. Q., (2005), "A Mixed-Mesh and New Angular Space Discretization Scheme of Discontinuous Finite Element Method for Three-Dimensional Radiative Transfer in Participating Media", Journal of Heat Transfer, **127**, pp.1236-1244

28. Darwish, M. S., Moukalled, F. H., (1994), "Normalized Variable and Space Formulation Methodology for High-Resolution Schemes", Numerical Heat Transfer, Part B: Fundamentals, **26**, pp. 79-96.

29. Das C., Trivedi A., Mitra K., Vo-Dinh T., (2003), "Experimental and numerical analysis of short pulse interaction with tissue phantoms containing inhomogeneities", Applied Optics, **42**, pp. 5173-5180.

30. Ferretti, G., (2010), "Wavelets and the Discrete Ordinate Method for Radiative Heat Transfer in a Two-Dimensional Rectangular Enclosure with a Nongray Medium", ASME Journal of Heat Transfer, **124**, pp. 971-975.

31. Flock, S. T., Wilson, B. C., and Patterson, M. S., (1989), "Monte Carlo modeling of light propagation in highly scattering tissues--II: Comparison with measurements in phantoms", IEEE transactions on bio-medical engineering, **36**, pp. 1169-1173.

32. Goyhénèche, J. M., Sacadura, J. F., (2002), "The Zone Method: A New Explicit Matrix Relation to Calculate the Total Exchange Areas in Anisotropically Scattering Medium Bounded by Anisotropically Reflecting Walls", ASME Journal of Heat Transfer, **124**, pp. 696-703.

33. Grissa, H, Askri, F, Bensalah, M, Bennasrallah, S., (2007), "Three-dimensional radiative transfer modeling using the control volume finite element method", Journal of Quantitative Spectroscopy and Radiative Transfer, **105**, pp. 388-404.

34. Guo, Z., and Kumar, S., (2000), "Equivalent isotropic scattering formulation for transient short-pulse radiative transfer in anisotropic." Applied Optics, **39**, pp. 4411-4417.

35. Guo, Z., and Kumar, S., (2001), "Radiation element method for transient hyperbolic radiative transfer in plane-parallel inhomogeneous media", Numerical Heat Transfer, Part B: Fundamentals, **39**, pp. 371-387.

36. Guo, Z., and Kumar, S., (2001), "Discrete-ordinates solution of short-pulsed laser transport in two-dimensional turbid media", Applied optics, **40**, pp. 3156-3163.

37. Guo, Z., Kumar, S., and San, K., (2000), "Multidimensional Monte Carlo Simulation of Short-Pulse Laser Transport in Scattering Media", Journal of Thermophysics and Heat Transfer, **14**, pp.504-511.

38. Guo, Z., and Maruyama, S., (2001), "Prediction of Radiative Heat Transfer in Industrial Equipment Using the Radiation Element Method", Journal of Pressure Vessel Technology, **123**, pp. 530-536.

39. Guo, Z., Maruyama, S., (1999), "Scaling anisotropic scattering in radiative transfer in three-dimensional nonhomogeneous media", International. Communications in Heat and Mass Transfer, **26**, pp. 997-1007.

40. Guo, Z., (2000), "Radiative heat transfer in inhomogeneous, nongray, and anisotropically scattering media", International Journal of Heat and Mass Transfer, **43**, pp. 2325-2336.

41. Guo, Z., (2002), "Monte Carlo simulation and experiments of pulsed radiative transfer", Journal of Quantitative Spectroscopy and Radiative Transfer, **73**, pp. 159-168.

42. Hasegawa, Y., Yamada, Y., Tamura, M., and Nomura, Y., (1991), "Monte Carlo simulation of light transmission through living tissues", Applied Optics, **30**, pp. 4515-4520.

43. Hassanzadeh, P., and Raithby, G. D., (2008), "Finite-Volume Solution of the Second-Order Radiative Transfer Equation: Accuracy and Solution Cost", Numerical Heat Transfer, Part B: Fundamentals, **53**, pp.374-382.

44. Henson, J. C., Malalasekera, W. M. G., (1997), "Comparison of the Discrete Transfer and Monte Carlo Methods for Radiative Heat Transfer in Three-Dimensional Nonhomogeneous Scattering Media", Numerical Heat Transfer, Part A: Applications, **32**, pp.19-36.

45. Hsu, P., Tan, Z., Wu, S., and Wu, C., (1999), "Radiative heat transfer in finite cylindrical homogeneous and exposed to collimated radiation". Numerical Heat Transfer, Part A, **35**, pp. 655-679.

46. Hsu, P., (2001), "Effects of multiple scattering and reflective boundary on the transient radiative transfer process", International Journal of thermal sciences, **40**, pp. 539-549.

47. Ismail, K., (2004), "Application of multidimensional scheme and the discrete ordinate method to radiative heat transfer in a two-dimensional enclosure with diffusely emitting and reflecting boundary walls", Journal of Quantitative Spectroscopy and Radiative Transfer, **88**, pp. 407-422.

48. Itaya, Y., Arai, N., and Hasatani, M., (1985), "Unsteady heat transfer characteristics in a semitransparent medium heated by diffuse and collimated radiation", Journal of chemical engineering of Japan, **18**, pp. 87-91.

49. Jaunich, M., Raje, S., Kim, K., Mitra, K., and Guo, Z., (2008), "Bio-heat transfer analysis during short pulse laser irradiation of tissues", International Journal of Heat and Mass Transfer, **51**, pp. 5511-5521.

50. Jiang, Y. Y., (2009), "A Vector Form Exchange-Area-Based Method for Computation of Anisotropic Radiative Transfer", ASME Journal of Heat Transfer, **131**, pp.1-7.

51. Jiao, J., and Guo, Z., (2009), "Thermal interaction of short-pulsed laser focused beams with skin tissues", Physics in medicine and biology, **54**, pp. 4225-4241.

52. Jiang, Y. Y., (2008), "A two-step strategy for numerical simulation of radiative transfer with anisotropic scattering and reflection", Journal of Quantitative Spectroscopy and Radiative Transfer, **109**, pp. 636-649.

53. Jinbo, H., Liming, R., and Heping, T., (2003), "Effect of anisotropic scattering on radiative heat transfer in two-dimensional rectangular media", Journal of Quantitative Spectroscopy and Radiative Transfer, **78**, pp. 151-161.

54. Jeong, S. W., Liu, H., Chen, W. R., (2003), "Temperature control in deep tumor treatment", Proceedings of SPIE, **5068**, pp. 210-216.

55. Joseph, D., Coelho, P.J., Cuenot, B., and Hafi, M. El., (2003), "Application of the discrete ordinates method to grey media in complex geometries using unstructured meshes", Proceedings of Eurotherm73 on Computational Thermal Radiation in Participating Media, 15-17 April 2003, Mons, Belgium.

56. Katika, K. M., and Pilon, L., (2006), "Modified method of characteristics in transient radiation transfer", Journal of Quantitative Spectroscopy and Radiative Transfer, **98**, pp. 220-237.

57. Kim, T. K., Menart, J. A., and Lee, H. S., (1991), "Nongray Radiative Gas Analyses Using the S-N Discrete Ordinates Method", ASME Journal of Heat Transfer, **113**, pp. 946-952.

58. Kim, S., Huh, K., (1999), "Assessment of the Finite-Volume Method and the Discrete Ordinate Method for Radiative Heat Transfer in a Three-Dimensional Rectangular Enclosure", Numerical Heat Transfer, Part B: Fundamentals, **35**, pp. 85-112.

59. Kim, S., (2000), "A new angular discretization scheme of the finite volume method for three-dimensional radiative heat transfer in absorbing, emitting and anisotropically scattering media", International Journal of Heat and Mass Transfer, **43**, pp. 1233-1242.

60. Kim, T., and Lee, H., (1988), "Effect of anisotropic scattering on radiative heat transfer in two-dimensional rectangular enclosures", International Journal of Heat and Mass Transfer, **31**, pp.1711-1721.

61. Kim T. K., and Lee H S., (1989), "Radiative transfer in two-dimensional anisotropic scattering media with collimated incidence", Journal of Quantitative Spectroscopy and Radiative Transfer, **42**, pp.225-238.

62. Kim, T., and Lee, H. S., (1990), "Scaled Isotropic Results for Two-Dimensional Anisotropic Scattering Media". ASME Journal of Heat Transfer, **112**, pp. 721-727.

63. Kowsary, F., and Mahan, J. R., (2006), "Radiative Characteristic of Spherical Cavities with Specular Reflectivity Component", ASME Journal of Heat Transfer, **128**, pp.261-268.

64. Krishnaprakas C. K., (1998), "Radiation Heat Transfer in a participating medium bounded by specular reflectors", International Communications in Heat and mass Transfer, **25**, pp. 1181-1188.

65. Krishnaprakas C. K, Narayana, K. B., and Dutta, P., (2001), "Combined conduction and radiation heat transfer in a gray anisotropically scattering planar medium with diffuse-specular boundaries", International Communications in Heat and mass Transfer, **28**, pp.77-86.

66. Li, J., and Kumar, S., (2003), "Radiation heat transfer in tissue welding and soldering with ultrafast lasers". 2003 IEEE 29th Annual Proceedings of Bioengineering Conference, pp.185-186.

67. Liu, L., (2005), "Finite element solution of radiative transfer across a slab with variable spatial refractive index", International Journal of Heat and Mass Transfer, **48**, pp. 2260-2265.

68. Liu, L, Ruan, L, Tan, H., (2002), "On the discrete ordinates method for radiative heat transfer in anisotropically scattering media", International Journal of Heat and Mass Transfer, **45**, pp. 3259-3262.

69. Liu, L. H., and Liu, L. J., (2007), "Discontinuous Finite Element Approach for Transient Radiative Transfer Equation", Journal of Heat Transfer, **129**, pp. 1069-1074.

70. Liu, F., Garbett, E. S., and Swithenbank, J., (1992), "Effects of anisotropic scattering on radiative transfer using the P_1-approximation", International Journal of Heat and Mass Transfer, **35**, pp. 2491-2499.

71. Liu, L. H., and Liu, L. J., (2007), "Discontinuous Finite Element Approach for Transient Radiative Transfer Equation", Journal of Heat Transfer, **129**, pp. 1069-1074.

72. Liu, L., Ruan, L., and Tan, H., (2003), "On the treatment of open boundary condition for radiative transfer equation", International Journal of Heat and Mass Transfer, **46**, pp. 181-183.

73. Lu, X., and Hsu, P., (2004), "Reverse Monte Carlo Method for Transient Radiative Transfer in participating media", ASME Journal of Heat Transfer, **126**, pp. 621-627.

74. Maruyama, S., and Aihara, T., (1997), "Radiation Heat Transfer of Arbitrary Three–Dimensional Absorbing, Emitting and Scattering Media and Specular and Diffuse Surfaces", ASME Journal of Heat Transfer, **119**, pp.129-136.

75. Mishra, S. C., Kuar, N., and Roy, H. K., (2006), "The DOM approach to the collapsed dimension method for solving radiative transport problems with participating media", International Journal of Heat and Mass Transfer, **49**, pp. 30-41.

76. Mishra, S. C., Chugh, P., Kumar, P., and Mitra, K., (2006), "Development and comparison of the DTM, the DOM and the FVM formulations for the short-pulse laser transport through a participating medium", International Journal of Heat and Mass Transfer, **49**, pp. 1820-1832.

77. Mishra, S. C., and Prasad, M., (2002), "Radiative heat transfer in absorbing - emitting - scattering gray medium inside 1-D gray Cartesian enclosure using the collapsed dimension method", International Journal of Heat and Mass Transfer, **45**, pp. 697-700.

78. Mitra, K., and Churnside, J. H., (1999), "Transient radiative transfer equation applied to oceanographic lidar", Applied Optics, **38**, pp.889-895.

79. Mitra, K., and Kumar, S., (1999), "Development and comparison of models for light-pulse transport through scattering–absorbing media", Applied Optics, **38**, pp. 188-196.

80. Mitra, K., Kumar, S., and Lai, M., (1997), "Transient Radiation Transport in Participating Media Within a Rectangular Enclosure", Journal of Thermophysics and Heat Transfer, **11**, pp. 409-414.

81. Modest, M. F., (2003), "Backward Monte Carlo Simulations in Radiative Heat Transfer", ASME Journal of Heat Transfer, **125**, pp 57-62.

82. Mondal B, and Mishra S C., (2008), "Lattice Boltzmann Method applied to the solution of the energy equations of the transient conduction and radiation problems on non-uniform lattices", International Journal of Heat and Mass Transfer, **51**, pp. 68–82.

83. Muthukumaran, R., and Mishra, S., (2008), "Thermal signatures of a localized inhomogeneity in a two-dimensional participating medium subjected to an ultra-fast step-pulse laser wave", Journal of Quantitative Spectroscopy and Radiative Transfer, **109**, pp.705-726.

84. Okutucu, T., and Yener, Y., (2006), "Radiative transfer in participating media with collimated short-pulse Gaussian irradiation", Journal of physics D; Applied physics, **39**, pp. 1976-1983.

85. Okutucu, T., and Yener, Y., (2007), "Participating media exposed to collimated short-pulse irradiation – A Laguerre – Galerkin solution. International Journal of Heat and Mass Transfer, **50**, pp. 4352-4359.

86. Okutucu, T., Yener, Y., and Busnaina, A. A., (2007), "Transient radiative transfer in participating media with pulse-laser irradiation — an approximate Galerkin solution", Journal of Quantitative Spectroscopy and Radiative Transfer, **103**, pp. 118-130.

87. Patankar S. V., (1991), "Computation of conduction and duct flow heat transfer", Ed-1, Taylor and Francis.

88. Patterson, M. S., Wilson, B. C., and Wyman, and D. R., (1991), "The propagation of optical radiation in tissue I. Models of radiation transport and their application", Lasers in Medical Science, **6**, pp. 155-168.

89. Pfefer, T. J., Choi, B., Vargas, G., McNally, K. M., and Welch, A. J., (2000), "Pulsed laser-induced thermal damage in whole blood", Journal of biomechanical engineering, **122**, pp.196-202.

90. Pourshaghaghy, A., Pooladvand, K., Kowsary, F., and Karimizand, K., (2006), "An inverse radiation boundary design problem for an enclosure filled with an emitting,

absorbing, and scattering media", International Communications in Heat and Mass Transfer, **33**, pp. 381-390.

91. Rath, P., Mishra, S. C., Mahanta, P., Saha, U. K., and Mitra, K., (2003). "Discrete transfer method applied to transient radiative transfer problems in participating medium", Numerical Heat Transfer: Part A: Applications, **44**, pp. 183-197.
92. Sakami, M., El Kasmi, A., and Charette, A., (2001), "Analysis of Radiative Heat Transfer in Complex Two-Dimensional Enclosures with Obstacles Using the Modified Discrete Ordinates Method", Journal of Heat Transfer, **123**, pp. 892-900.
93. Sakami M, Mitra K, Hsu P. F., (2002), "Analysis of light pulse transport through two-dimensional scattering and absorbing media", Journal of Quantitative Spectroscopy and Radiative Transfer, **73**, pp.169-179.
94. Santarelli F., Stramioioli C., and Spiga G., (1980), "Rigorous and simplified approach to the radiative transfer in an absorbing and anisotropically scattering slab with a reflecting boundary", International Journal of Heat and Mass Transfer. **23**, pp.853-860.
95. Sarma, D., Mishra, S. C., Mahanta, P., (2005), "Analysis of collimated radiation in participating media using the discrete transfer method", Journal of Quantitative Spectroscopy and Radiative Transfer, **96**, pp. 123-135.
96. Singh, R., Mishra, S. C., (2007), "Analysis of Radiative Heat Transfer in a Planar Participating Medium Subjected to Diffuse and/or Collimated Radiation - A Comparison of the DTM, the DOM, and the FVM", Numerical Heat Transfer, Part A: Applications, **52**, pp. 481-496.
97. Spiga G., Santarelli F., and Stramigioli C., (1980), "Radiative transfer in an absorbing and anisotropically scattering slab with a reflecting boundary", International Journal of Heat and Mass Transfer, **23**, pp. 841-852.
98. Spiga G., Spiga M., (1985), "Effects of Boundary Reflection on radiative heat transfer in participating media", International Journal of Heat and Fluid Flow, **6**, pp.235-240.
99. Talukdar, P., (2006), "Radiative heat transfer for irregular geometries with the collapsed dimension method", International Journal of Thermal Sciences, **45**, pp. 103-109.

100. Talukdar, P., Steven, M., Issendorff, F., and Trimis, D., (2005), "Finite volume method in three-dimensional curvilinear coordinates with multiblocking procedure for radiative transport problems", International Journal of Heat and Mass Transfer, **48**, pp. 4657-4666.

101. Talukdar, P., Issendorff, F. V., Trimis, D., and Simonson, C. J., (2007), "Conduction–radiation interaction in 3D irregular enclosures using the finite volume method", Heat and Mass Transfer, **44**, pp. 695-704.

102. Tan, Z. M., and Hsu, P. F., (2002), "Transient radiative transfer in three-dimensional homogeneous and non-homogeneous participating media, Journal of Quantitative Spectroscopy and Radiative Transfer,**73**, pp. 181-194.

103. Tan, Z., and Hsu, P., (2001), "An Integral Formulation of Transient Radiative Transfer, Transactions of ASME, **123**, pp. 466-475.

104. Tan, H., Huang, Y., and Xia, X-L., (2003), "Solution of radiative heat transfer in a semitransparent slab with an arbitrary refractive index distribution and diffuse gray boundaries", **46**, pp. 2005-2014.

105. Tan, H., Yi, H-L., Wang, P-Y., Ruan, L-M., and Tong, T. W., (2004), "Ray tracing method for transient coupled heat transfer in an anisotropic scattering layer", International Journal of Heat and Mass Transfer, **47**, pp. 4045-4059.

106. Tan, H., Ruan, L., and Tong, T. W., (2000), "Temperature Response in Absorbing, Isotropic Scattering Medium Caused by Laser Pulse", International Journal of Heat and Mass Transfer, **43**, pp.311-320.

107. Tan H., Ruan, L., Xia, X., Yu, Q., and Tong, T. W., (1999), "Transient coupled radiative and conductive heat transfer in an absorbing, emitting and scattering medium", International Journal of Heat And Mass Transfer, **42**, pp.2967-2980.

108. Tan, H-P., and Yi, H-L., (2004), "Temperature response in participating media with anisotropic scattering caused by pulsed lasers", Journal of Quantitative Spectroscopy and Radiative Transfer, **87**, pp.175–192.

109. Thomson, D. L., Meade, A. J., and Bayazitoglu, Y., (2001), "Solution of the radiative transfer equation in discrete ordinate form by sequential function approximation", International Journal of Thermal Sciences, **40**, pp. 517-527.

110. Tian, W., and Chiu, W., (2005), "A Two-Dimensional Scheme for Axisymmetric Radiative Heat Transfer Using the Finite-Volume Method", Numerical Heat Transfer, Part B: Fundamentals, **47**, pp. 199-211.

111. Trivedi, a., Basu, S., and Mitra, K., (2005), "Temporal analysis of reflected optical signals for short pulse laser interaction with nonhomogeneous tissue phantoms", Journal of Quantitative Spectroscopy and Radiative Transfer, **93**, pp. 337-348.

112. Trivic, D., Amon, C., (2008), "Modeling the three-dimensional radiation of anisotropically scattering media by two different numerical methods", International Journal of Heat and Mass Transfer, **51**, pp. 2711-2732.

113. Trivic, D. N., Obrien, T. J., and Amon, C. H., (2004), "Modeling the radiation of anisotropically scattering media by coupling Mie theory with finite volume method", International Journal of Heat and Mass Transfer, **47**, pp. 5765-5780.

114. Tzou, D. Y., Beraun, J. E., and Chen, J. K., (2002), "Ultrafast Deformation in Femtosecond Laser Heating", ASME Journal of Heat Transfer, **124**, pp. 284-292.

115. Wang, F., Liu, D., Cen, K., Yan, J., and Huang, Q., (2008), "Efficient inverse radiation analysis of temperature distribution in participating medium based on backward Monte Carlo method", Journal of Quantitative Spectroscopy and Radiative Transfer, **109**, pp. 2171-2181.

116. Wong, B. T., Mengüç, M. P., and Mengu, M. P., (2002), "Comparison of monte carlo techniques to predict the propagation of a collimated beam in participating media", Numerical Heat Transfer, Part B: Fundamentals, **42**, pp. 119-140.

117. Wu, C., (2000), "Propagation of scattered radiation in a participating planar medium with pulse irradiation", Journal of Quantitative Spectroscopy and Radiative transfer, **64**, pp. 537-548.

118. Wu, C. Y., Chiang, J Y., (1990), "Linearly anisotropic scattering in a rectangular medium exposed to collimated radiation". International Journal of Heat and Mass Transfer, **33**, pp.1032-1034.

119. Wu, C. Y., and Ou, N. R., (2002), "Differential approximations for transient radiative transfer through a participating medium exposed to collimated irradiation", Journal of Quantitative spectroscopy and Radiative transfer, **73**, pp.111-120.

120. Wu C.-Y., Ou N.-R., (1994), "Transient Two-Dimensional Radiative and Conductive Heat Transfer in a Scattering Medium", International Journal of Heat and Mass Transfer, **31**, pp.2675-2686.

121. Wu C-Y., Wu S-H., (2000), "Integral equation formulation for transient radiative transfer in an anisotropically scattering medium", International Journal of Heat and Mass Transfer, **43**, pp. 2009-2020.

122. Wu, S., (2001), "Time-resolved spatial distribution of scattered radiative energy in a two-dimensional cylindrical medium with a large mean free path for scattering", International Journal of Heat and Mass Transfer, **44**, pp. 2611-2619.

123. Wu, S., and Wu, C., (1997), "Radiative heat transfer in a two-dimensional cylindrical medium exposed to collimated radiation", International Communications in Heat Mass Transfer, **24,** pp.475-484.

124. Yi H-L., Zhen B., Tan, H. P., and Tong, T. W., (2009), "Radiative heat transfer in a participating medium with specular–diffuse surfaces", International Journal of Heat and Mass Transfer, **52**, pp. 4229–4235.

125. Yi, H-L, Tan, H-P., Lu, Y-P., (2005), "Effect of reflecting modes on combined heat transfer within an anisotropic scattering slab", Journal of Quantitative Spectroscopy and Radiative Transfer, **95**, pp.1–20.

126. Yilmazer, A., and Kocar, C., (2008), "Ultraspherical-polynomials approximation to the radiative heat transfer in a slab with reflective boundaries", International Journal of Thermal Sciences, **47**, pp. 112-125.

127. Yuen, W. W., and Ho, C. F., (1985), "Analysis of two-dimensional radiative heat transfer in a gray medium with internal heat generation", International Journal of Heat and Mass Transfer, **28**, pp.17-23.

128. Alves M. A., Oliveira P. J., and Pinho F. T., (2003), " A convergent and universally bounded interpolation scheme for the treatment of advection", International Journal For Numerical Methods In Fluids, **41**, pp.47–75.

List of Publications

1. **B. N. Padhi**, P. Rath, S. K. Mahapatra and A. K. Satapathy, "Short Pulse Collimated Radiation with Diffusely Reflecting Boundaries." *Heat Transfer Research, Begell House Inc, Publishers, vol.42, No.3, 2011.*
2. **B. N. Padhi**, P. Rath, S. K. Mahapatra and A. K. Satapathy, "Radiative heat transfer in a participating medium bounded by diffusely reflecting boundaries with Short-pulse collimated irradiation." Communicated to *International Journal of Numerical Methods in Heat and Fluid flow*.
3. **B. N. Padhi,** P. Rath and S. K. Mahapatra**,** "Interaction of a short-pulse laser with a participating medium bounded by diffusely reflecting boundaries." *Proceedings of Eurotherm83-Computational Thermal Radiation in Participating Media III, 15-17 April 2009, Lisboa, Portugal.*
4. **B.N.Padhi**, S.Choudhury, P.Rath and S.K.Mahapatra "Radiation modeling of participating medium in a 2-D enclosure", Paper No.TF 13 ,pp.60-64, *Proceedings of International Conference on Advances in Mechanical Engineering ICAME-2010,January 4-6, 2010, SVNIT,Surat-395007, Gujarat, India.*
5. **B. N. Padhi**, P. Rath and S. K. Mahapatra, **"**Effects of radiative heat transfer in a planar participating medium**."** *National Conference on Modelling and Simulation in Heat Transfer and Fluid Flow, June 11-12, 2010, NIT, Jamshedpur*.
6. **B. N. Padhi**, P. Rath, S. K. Mahapatra and A K Satapathy, **"**Radiative heat transfer in a participating medium bounded by diffusely reflecting boundaries with short-pulse collimated irradiation**."** *7th International Conference on Computational Heat and Mass Transfer, July 18-22, 2011, Istanbul, Turkey.*
7. **B N Padhi**, P Rath, S K Mahapatra and A K Satapathy, "Short-pulse collimated radiation in a participating medium bounded by diffusely reflecting boundaries." *3rd International Conference on Mechanical and Electrical Technology, Dalian, China, August 26-27, 2011*.

APPENDIX-1:
BACKGROUND OF CURVED LINE ADVECTION METHOD (CLAM)

In this scheme, the normalized face value is approximated by a combination of linear and parabolic characteristics passing through the points, *O*, *Q*, and *R* in the Normalized Variable Diagram given in Fig. A1.1. The advected variable at face passing through *Q* in the shaded region is necessary and sufficient condition for second-order accuracy (Alves et al., 2003).

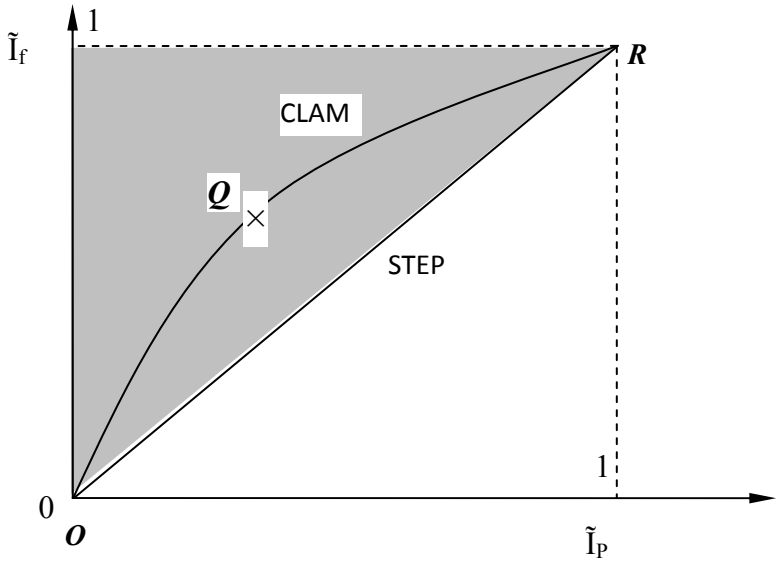

Fig.A1.1: Normalised Variable Diagram

In this formulation the advected variable *I* is normalized as

$$\tilde{I} = \frac{I - I_U}{I_D - I_U} \tag{A1.1}$$

and the normalized coordinates can be given as

$$\tilde{x} = \frac{x - x_U}{x_D - x_U} \tag{A1.2}$$

where the subscripts U and D refer to the upstream and downstream cells to cell P which is, itself, upstream of the cell face f under consideration, as shown in Fig. A1.2.

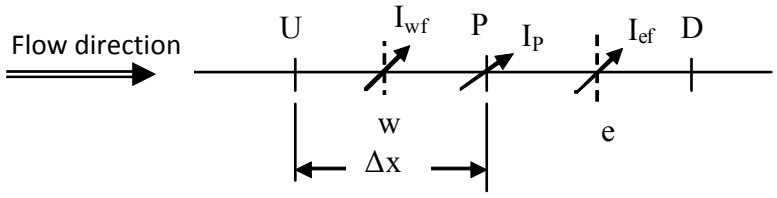

Fig.A1.2 : The control volume.

In general, any differencing scheme (of third-order or less) that evaluates a cell face value "f" as a function of the neighbor cell values (U, P and D) can be written under a simplified functional form, $\tilde{I}_f = f(\tilde{I}_P)$, where the normalization defined by Equation (A1.1 and A1.2) is employed.

Normalized variables for CLAM scheme can be written as

$$\tilde{I}_f = a + b\,\tilde{I}_P + c\,\tilde{I}_P^2 \qquad \text{for} \quad 0 < \tilde{I}_P < 1 \tag{A1.3a}$$

$$\tilde{I}_f = \tilde{I}_P \qquad \text{elsewhere} \tag{A1.3b}$$

Equation A1.3 can be solved with following boundary conditions.

$$Y = 0 \qquad \text{at} \qquad X = 0, \tag{A1.4a}$$

$$Y = 1 \qquad \text{at} \qquad X = 1 \tag{A1.4b}$$

$$Y = Y_Q \qquad \text{at} \qquad X = X_Q \tag{A1.4c}$$

The above boundary conditions (A1.3a and A1.3b) gives,

$$a = 0 \quad \text{and} \quad b + c = 1.$$

Now at point "Q",

$$Y_Q = b\,X_Q + c\,X_Q^2 = (1-c)X_Q + c\,X_Q^2 \tag{A1.5}$$

The above equation gives, $c = \dfrac{(Y_Q - X_Q)}{(X_Q^2 - X_Q)}$

such that, $b = (1-c) = 1 - \left(\dfrac{Y_Q - X_Q}{X_Q^2 - X_Q}\right)$, or $b = \dfrac{(Y_Q - X_Q^2)}{(X_Q - X_Q^2)}$.

Substituting the above values for the respective faces the following statements can be reached.

For the east face

$$\tilde{I}_e = \frac{\left(\tilde{x}_P^2 - \tilde{x}_e\right)}{\tilde{x}_P\left(\tilde{x}_P - 1\right)}\tilde{I}_C + \frac{\left(\tilde{x}_e - \tilde{x}_P\right)}{\tilde{x}_P\left(\tilde{x}_P - 1\right)}\tilde{I}_C^2 \qquad \text{(A1.6)}$$

where

$$\tilde{x}_P = \frac{x_P - x_W}{x_E - x_W} = 0.5 \qquad \text{and}$$

$$\tilde{x}_e = \frac{x_e - x_W}{x_E - x_W} = 0.75 \qquad \text{uniformly spaced grids.} \qquad \text{(A1.7)}$$

Substituting the above values in Eqn.(3)

$$\frac{I_e - I_W}{I_E - I_W} = \frac{0.5^2 - 0.75}{0.5(0.5-1)}\left(\frac{I_P - I_W}{I_E - I_W}\right) + \frac{0.75 - 0.5}{0.5(0.5-1)}\left(\frac{I_P - I_W}{I_E - I_W}\right)^2$$

$$= \frac{-0.5}{-0.25}\left(\frac{I_P - I_W}{I_E - I_W}\right) + \frac{0.25}{-0.25}\left(\frac{I_P - I_W}{I_E - I_W}\right)^2 \qquad \text{(A1.8)}$$

After simplifying the above equation, the following argument will be obtained:

$$I_e = I_P + S_{Ce^+} + S_{Pe^+} I_P$$

where $$S_{Ce^+} = I_E\left(\frac{I_P - I_W}{I_E - I_W}\right) \qquad S_{Pe^+} = -\left(\frac{I_P - I_W}{I_E - I_W}\right) \qquad \text{(A1.9)}$$

Similarly the intensities at other faces of the control volume can be determined. Finally all the face values and nodal values of intensities are substituted in the basic equation of radiative intensity.